Hamiltonian Thermostatting Techniques for Molecular Dynamics Simulation.

Thesis submitted for the degree of

Doctor of Philosophy

at the University of Leicester

by

Christopher Richard Sweet BSc (Leicester)

Department of Mathematics

University of Leicester

June 14, 2004

ProQuest LLC
789 East Eisenhower Parkway
P.O. Box 1346
Ann Arbor, MI 48106-1346

Abstract

Hamiltonian Thermostatting Techniques for Molecular Dynamics Simulation.

by

Christopher Richard Sweet.

Molecular dynamics trajectories that sample from a Gibbs, or canonical, distribution can be generated by introducing a modified Hamiltonian with additional degrees of freedom as described by Nosé [50] and, although this method has found widespread use in its time re-parameterized Nosé-Hoover form, the lack of a Hamiltonian structure coupled with the need to 'tune' thermostatting parameters has limited its use compared to stochastic methods. In addition, thermostatting small or stiff systems often does not give the correct distributions unless the Nosé-Hoover chains [47] method is used, which inherits the Nosé-Hoover deficiencies noted above. More recently the introduction of the Hamiltonian Nosé-Poincaré method [8] has renewed interest in the possibility of Hamiltonian methods which can improve dynamical sampling.

In this Thesis multiple thermostat Hamiltonian methods are proposed, from which a better understanding of Nosé type schemes has been obtained by experimentation. This has allowed an accurate mathematical model of a thermostatted oscillator to be proposed, which in turn has led to the construction of two important new Hamiltonian methods, Nosé-Poincaré chains (NPC) and Recursive Multiple Thermostats (RMT). The NPC method provides the advantages of Nosé-Hoover chains but with a Hamiltonian structure, where symplectic integrators can be used for improved long term stability. The RMT method, while retaining the advantages of the NPC method, obtains canonical sampling without the stability problems encountered with chains and has the additional advantage that the choice of Nosé mass is essentially independent of the underlying system. The methods proposed here, although applicable to small systems, have applications in large scale models with complex structure, such as protein-bath, quantum-classical and systems which are difficult to thermostat such as Butane molecules.

Preface

"A light, once cast, illuminates beyond its immediate boundary." Unknown.

This thesis concerns the thermostatting of Molecular Dynamics simulations and, as such, is at the applied end of applied maths. During my recent undergraduate degree I studied all of the pure maths modules available, which reflected my interests during the 1970's when I should have been studying. In my second year I took a numerical linear algebra course taught by Ben Leimkuhler to fill a gap in my timetable which ignited my enthusiasm for applied maths and numerical methods, no doubt influenced by working as an electronics engineer for many years. Upon the completion of my degree, with little or no experience of differential equations and some trepidation, I embarked on a PhD at the suggestion of Ben, who became my supervisor. This proved to be something of a roller-coaster ride through Geometric Integrators, N-body systems and Statistical Mechanics, but throughout this time Ben was prepared to spend a great deal of time discussing these matters, dispelling the often held belief that PhD supervisors are both unapproachable and often unavailable. I would like to acknowledge Ben for his support and guidance leading to the completion of this thesis, and thank him for imparting a large part of the knowledge that I have gained.

My weapon of choice for gaining an understanding of these problems has been computation and I have spent many hours running simulations. Looking at my most used code I notice that is based on some Fortran code which I converted to C++, originally written by Brian Laird. I would like to thank Brian for the use of the code, and also the knowledge I gained from him while running simulations for the Generalized Thermostatting Bath paper which he wrote with Ben. I would also like to thank Zhidong Jia for the many discussions we had, and the comments he made on early versions of the thesis, which were an invaluable contribution. Thanks must also go to EPSRC for funding my research.

The transition from having a successful career to being a student was difficult, but perhaps more so for my family. I would like to thank my wife Fiona and my sons James and Charles for their support and tolerance of this long project, especially during the times when the research was not going well when their encouragement was the only thing keeping me going.

Chris Sweet
June 2004

Contents

Chapter 1

Introduction

In this chapter we look at the general framework of modern thermostating techniques and give an overview of the objectives of this Thesis in Section 1.1. In Section 1.2 a brief introduction to molecular dynamics is provided, followed by a discussion of the microcanonical and canonical ensembles from statistical mechanics in Section 1.3. Section 1.4 looks at the commonly available constant temperature methods and Section 1.5 looks at symplectic integrators as a motivation for the development of fully Hamiltonian methods. Section 1.6 reviews the open problems for thermostatting using extended system methods based on Nosé's scheme. The final section, 1.7, details the contribution to the literature from this Thesis.

1.1 Thesis overview.

Molecular dynamics simulations are generally based on the classical equations of motion of particles derived from a Hamiltonian, $H(q,p)$, where $q = (q_1, q_2, \cdots, q_N)$ represents the N particles positions and $p = (p_1, p_2, \cdots, p_N)$ their momenta. The total energy for a classical mechanical system, free from external force, is conserved and hence any macroscopic properties obtained from the simulation are at constant energy E, number of particles N, and generally volume V. This corresponds to the microcanonical ensemble in statistical mechanics where only the phase-space points which satisfy $H(q,p) = E$ are allowed for a phase-space $\Gamma = (q,p)$. The temperature T of the system is related to the average kinetic energy by the equipartition theorem (see Appendix D),

$$\left\langle \sum_{i=1}^{N} \frac{p_i^2}{2m_i} \right\rangle = \frac{3NkT}{2}, \tag{1.1}$$

where k is the Boltzmann constant and m_i the mass of the i^{th} particle. For many laboratory experiments T would be constant and in addition the macroscopic properties of interest are from the canonical ensemble, where the statistical mechanical expression is well known. Although other methods, such as the Monte Carlo method, sample from the canonical ensemble they cannot determine dynamical properties, making it desirable to obtain molecular dynamics methods which sample from the canonical ensemble.

Several deterministic methods have been proposed using non-reversible temperature controls and isokinetic constraints but, although smooth trajectories result, they fail to produce the canonical fluctuations in kinetic energy. More recent work concerns the idea of adding some form of 'heat bath' with which the simulated system can exchange energy,

giving a constant average temperature. These ideas began with the work of Andersen [4] who was studying constant volume simulations, this led to the ground breaking work of Nosé [50] where a single thermostating variable was added to the equations of motion to act as the heat bath. For this method it can be shown analytically that sampling from the canonical ensemble occurs under an ergodicity assumption, but an artificial scaling of the time variable is introduced which makes computation of time-correlation functions cumbersome. While correcting this deficiency, Hoover's coordinate and time transformations [30] destroy the Hamiltonian structure, which is undesirable since it precludes the use of geometric integrators [42, 22, 23], which have excellent long term behavior. More recent work by Bond, Laird and Leimkuhler [8] introduced the Nosé-Poincaré method wherein the desired rescaling of time is accomplished through transformation of the Hamiltonian itself.

A feature associated with these methods is the introduction of a parameter, Q, the Nosé mass. The selection of this mass is critical if the correct sampling is to be obtained, and it is generally calculated so that the thermostatting variable has a self-resonant frequency, estimated by linearization, coincident with some natural frequency within the original system. For complex systems, where several frequencies exist, the correct method of choosing of Q is less clear and is dependent on the coupling between sub-systems and modes. For systems such as liquids with a Lennard-Jones potential, where the coupling between different parts of the system is good and they display a broad frequency spectrum, a very wide choice of Q is applicable. By contrast, for simulations of Butane molecules, having poor coupling between modes and discreet frequency spectra, the choice of Q is critical and generally determined empirically. It is desirable to develop a method which improves

the dynamical sampling for systems which display the problems that are seen in simulating Butane molecules. This motivates the study of thermostatted multiple harmonic oscillators to determine the relationship between Q and the system to be simulated.

Since sampling from the canonical ensemble is dependent on an assumption of ergodicity many systems fail to give the correct distributions when modified by these schemes, particulary small and stiff systems. A method was proposed by Martyna, Klein and Tuckerman [47] to improve the ergodicity in these systems by arranging that each thermostat is controlled by another thermostat, forming a thermostat chain. This is reasonable successful but has no Hamiltonian since it is based on the Nosé-Hoover method, and requires the selection of additional parameters, or Nosé masses, Q_i. There is also a question of stability since the time reparametrization is only applied through the first thermostat.

The object of this Thesis is to develop a thermostatting scheme with the following properties:

- Real-time evolution, with all parts of system evolving in a common timescale.
- Hamiltonian based.
- Interaction with multiple frequencies within the original system.
- Stability levels equivalent to the underlying Nosé-Poincaré method.
- Ergodicity enhanced in a similar manner to that observed for chains.
- The choice of Nosé masses should be essentially independent of the underlying system.
- Can be shown analytically to sample from the canonical ensemble, assuming ergodic-

ity.

Since a Hamiltonian formulation is required, and is not presently available for chains methods, the task was undertaken in two stages:

- The development of a Hamiltonian chains method based on the Nosé-Poincaré scheme.
- The introduction of multiple thermostats which interact directly with the system to be thermostatted.

In Chapter 2 the thermostatting schemes currently available are introduced and the proofs of the correct sampling given. To gain a better understanding of the basic methods we examine the role of the Nosé mass in providing ergodic behavior in Chapter 3. A frequency domain analysis of the real-time Nosé-Poincaré method when applied to harmonic models is introduced, which offers a useful insight into the role of the Nosé mass with particular reference to the thermostatting variable phase-space. Chapter 4 extends the Generalized Thermostatting Bath of Laird and Leimkuhler [38] to include multiple thermostats which interact directly with the system to be thermostatted. The Hamiltonian Nosé and Nosé-Poincaré chains are then described as special cases of this class of methods. In Chapter 5 the Recursive Multiple Thermostat (RMT) method is introduced, a method which encompasses the thermostatting scheme requirements given above in addition to having other desirable properties. Chapter 6 summarizes this work and looks at further work that should be undertaken to apply these methods to a wider range of problems, such as protein modelling. An important feature of the formalism presented here is that the methods always remain within the class of Hamiltonian dynamical models, for which symplectic

integrators, having superior long-term stability properties, are possible. Construction of efficient schemes suitable for molecular dynamics applications is an important task, in Sections 4.9 and 5.4 it is shown that this is possible by designing efficient Hamiltonian splitting methods for both Nosé-Poincaré chains and RMTs.

An electronic aid to understanding the thermostatting methods described in this Thesis is available at the URL http://www.recursivethermostat.info.

1.2 Molecular Dynamics simulations.

Molecular dynamics (MD) simulations form one of the main methods used in the theoretical study of chemical and biological molecules, wherein the time dependent behavior of a molecular system is computed. These MD simulations can provide detailed information on molecular fluctuations and conformational changes and are used routinely to investigate the thermodynamics, dynamics and structure of chemical and biological molecules. MD methods date back to the 1950's, when Alder and Wainwright [1, 2, 3] studied the interactions of hard and elastic spheres leading to important insights into the behavior of simple liquids, and have been refined to the point where realistic simulations of solvated proteins, and the folding of small proteins, is possible.

MD simulations solve the equations of motion of the particles within the system and hence the information generated is at the microscopic level, such as atomic positions and velocities, which can be converted to macroscopic quantities, such as pressure, energy and heat capacity, by the use of statistical mechanics as shown in Section 1.3. Statistical mechanics provides the mathematical expressions that relate these macroscopic quantities to

the distribution and motion of the atoms and molecules of an N-body system. One of the main advantages of MD simulations over other schemes, such as the Monte-Carlo method, is that it is possible to study both thermodynamic and time dependent properties.

When considering macroscopic quantities, an ensemble is a collection of all possible systems which have different microscopic states but have an identical macroscopic or thermodynamic state. Examples of a number of ensembles with different characteristics are,

- Microcanonical ensemble (NVE) : The thermodynamic state characterized by a fixed number of atoms, N, a fixed volume, V, and a fixed energy, E. This corresponds to an isolated system.
- Canonical Ensemble (NVT): This is a collection of all systems whose thermodynamic state is characterized by a fixed number of atoms, N, a fixed volume, V, and a fixed temperature, T.
- Isobaric-Isothermal Ensemble (NPT): This ensemble is characterized by a fixed number of atoms, N, a fixed pressure, P, and a fixed temperature, T.
- Grand canonical Ensemble (mVT): The thermodynamic state for this ensemble is characterized by a fixed chemical potential, m, a fixed volume, V, and a fixed temperature, T.

The ensemble average of some quantity $A(q,p)$ is then defined as,

$$\langle A(q,p)\rangle_{Ensemble} = \int A(q,p)\rho(q,p)dqdp, \tag{1.2}$$

where $\rho(q,p)$ is the probability density of the ensemble. This integral is generally difficult to evaluate as it is necessary to calculate all possible states of the system, and a molecular

dynamics simulation calculates the points in the ensemble sequentially in time. For MD simulations we instead determine a time average of $A(q,p)$ which is expressed as, for time $\mathcal{T}$,

$$\langle A(q,p)\rangle_{Time} = \lim_{\mathcal{T}\to\infty} \frac{1}{\mathcal{T}} \int_0^{\mathcal{T}} A(q(t),p(t))\ dt \approx \frac{1}{M} \sum_{i=1}^{M} A(q_i,p_i), \tag{1.3}$$

where M is the number of steps of time Δt and $A(q_i,p_i)$ is the value of $A(q,p)$ at the discreet points $q_i = q(i\Delta t), p_i = p(i\Delta t)$. From this it is possible to calculate time averages by molecular dynamics simulations, but these experimental averages are then assumed to be ensemble averages. This apparent problem is resolved by the ergodic hypothesis, one of the most fundamental axioms of statistical mechanics, which states that the ensemble average equals the time average i.e.,

$$\langle A(q,p)\rangle_{Ensemble} = \langle A(q,p)\rangle_{Time}. \tag{1.4}$$

The basic concept here is that if the system is allowed to evolve in time indefinitely it will eventually pass through all possible states. Because of this it is important in MD simulations to generate enough representative conformations such that this equality is satisfied and, since the simulations are of fixed duration, a sufficient amount of phase space must be sampled. We will see in Chapter 2 that the proof of sampling from the correct ensemble, for systems thermostatted by Nosé's method, is dependent on the system being ergodic, which is not always true particularly for small or stiff systems. The definition of ergodic as time average being equal to ensemble average is used throughout this Thesis.

The MD simulation method is generally based on Newtons second law or the equation of motion $F = ma$, where F is the force exerted on the particle, m its mass and a its acceleration. From a knowledge of the forces acting within the system it is possible to

determine the acceleration of each atom or particle. The equations of motion are then integrated to give a trajectory that describes the positions, velocities and accelerations of the particles as they vary with time, allowing the average values of properties to be determined. The method is deterministic, once the positions and velocities of each atom are known the state of the system can be predicted at any time in the future or the past. Due to the complicated nature of the potential energy functions found in all but the simplest of systems there will be no analytical solution to the equations of motion and they must be solved numerically. Many numerical methods have been developed for integrating these equations but the most effective for use in MD simulations should conserve energy and momentum and permit a large integration time step. A class of integrators which meet these requirements are Geometric integrators which preserve geometric properties of the original system. The most common of these are time-reversible, a property found in Newtonian mechanics, and symplectic which are applicable for Hamiltonian systems and are discussed in Section 1.5.

Molecular dynamics simulations are generally computationally expensive, mitigated to some extent by the availability of increasingly faster and cheaper computers. Despite this, simulations of solvated proteins are routinely calculated up to the nanosecond time scale, with simulations into the millisecond time scale reported. Since a significant part of the simulation can be taken up by equilibration, which must be completed before averages can be taken, methods which converge quickly to the correct ensemble are desirable.

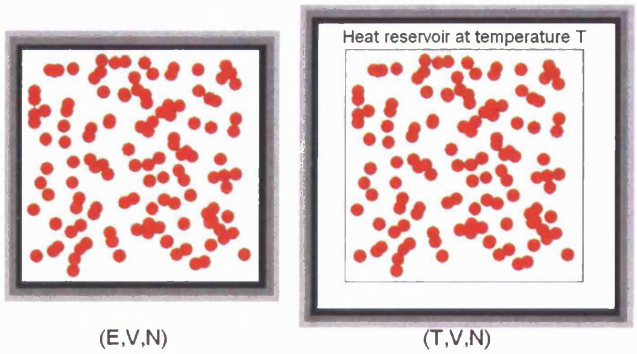

Figure 1.1: Systems in the microcanonical (left) and canonical (right) ensembles. The shaded outlines represent heat insulating walls.

1.3 Microcanonical and canonical ensembles.

Although constant energy simulations are straightforward it is not as convenient to derive statistical mechanical formulae from the microcanonical ensemble as it is from the canonical ensemble, as considered by Lebowitz, Percus and Verlet [40]. As a motivation for developing methods which sample from the canonical ensemble both ensembles are studied, and are shown schematically in Figure 1.1.

1.3.1 Microcanonical ensemble.

As stated in Section 1.1 the microcanonical ensemble in statistical mechanics is equivalent to constant energy conditions, the external control parameters being number of particles N, total energy, E, and the volume V. For a single harmonic oscillator, with angular frequency $\omega = 1$, sampling from the microcanonical ensemble, the q histogram and q, p phase space are shown in Figure 1.2. For a Hamiltonian,

$$H(q,p) = \sum_{i=1}^{N} \frac{p_i^2}{2m_i} + V(q), \tag{1.5}$$

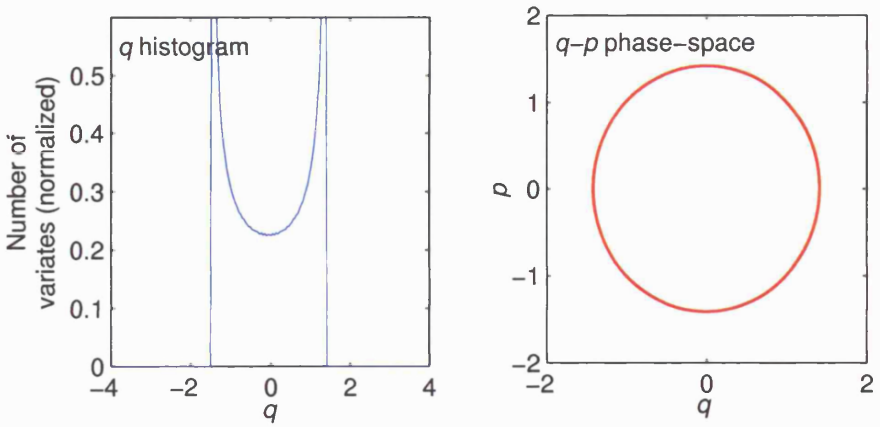

Figure 1.2: Harmonic oscillator for angular frequency $\omega = 1$, q histogram and q, p phase-space for the microcanonical ensemble.

where $V(q)$ is the potential energy, the equations of motion,

$$\dot{q}_i = \frac{p_i}{m_i}, \quad \dot{p}_i = -\nabla_{q_i} V(q), \tag{1.6}$$

conserve the total energy $H(q,p)$, the only phase-space points (q,p) allowed are those on the constant energy hypersurface satisfying $H(q,p) = E$. It is assumed that that every allowed point in phase-space has equal weight in microcanonical ensemble averages, the principle of of equal a priori probability in statistical mechanics. This is closely related to the assumption of ergodicity, where the trajectory of a phase-space vector (q,p) will pass through almost all points within the allowed portion of phase-space, which is integral to the proof of the correct sampling for Nosé schemes. The probability that a phase-space point (q,p) appears in an average is defined by the equilibrium density function $f(q,p)$ and, for the microcanonical ensemble,

$$f_{mc}(q,p) \propto \delta[H(q,p) - E]. \tag{1.7}$$

The Dirac Delta function δ form reflecting the constraint $H(q,p) = E$ with $\delta(x-a) = 0,\ x \neq a$ and $\int_{a-\epsilon}^{a+\epsilon} \delta(x-a)dx = 1,\ \forall \epsilon > 0$. The ensemble average for some quantity $A(q,p)$

is then defined as,

$$\langle A(q,p)\rangle = \frac{\int A(q,p)f(q,p)dqdp}{\int f(q,p)dqdp}. \tag{1.8}$$

By using thermodynamic relations the macroscopic properties of the system can be derived. The Boltzmann relation for entropy is,

$$S = k \ln W, \tag{1.9}$$

where W is the number of microscopic states which, for the microcanonical ensemble, is given by,

$$\begin{aligned} W &= \frac{1}{N!h^{N_f}} \int^{E} dE' \int f_{mc}(q,p)dqdp \\ &= \frac{C_1}{N!h^{N_f}} \int \theta(E - H(q,p))dqdp, \end{aligned} \tag{1.10}$$

for constant C_1 and Planck's constant h. Here $\theta(x)$ is the Heaviside function with $\theta(x) = 1,\ x > 0$, $\theta(x) = 0,\ x < 0$ and $\delta(x) = d\theta(x)/dx$.

The statistical mechanical expressions can then be derived using the methods of Pearson, Halicioglu and Tiller [55]. For systems where the kinetic energy is given by a quadratic form of the momenta, where it is possible to perform the integration in $3N$ dimensional momentum space, (1.10) simplifies to,

$$W = C_2 \int \frac{2}{3N}(E - V(q))^{(3/2)N} dq, \tag{1.11}$$

for constant C_2. Substituting (1.11) into (1.9),

$$S = k \ln \left(C_2 \int \frac{2}{3N}(E - V(q))^{(3/2)N} dq \right). \tag{1.12}$$

From (1.8) the average of a quantity $A(q)$, where $\langle\ \rangle_{mc}$ is the average in the microcanonical

ensemble is,

$$\langle A(q)\rangle_{mc} = \frac{\int A(q)(E-V(q))^{(3/2)N-1}dq}{\int (E-V(q))^{(3/2)N-1}dq}. \tag{1.13}$$

Temperature is defined by the thermodynamical relationship,

$$\frac{1}{T} = \left(\frac{\partial S}{\partial E}\right)_V = k\frac{\int \frac{3N}{2}(E-V(q))^{(3/2)N-1}dq}{\int (E-V(q))^{(3/2)N}dq} = \frac{3Nk}{2\langle K\rangle}, \tag{1.14}$$

for kinetic energy $K = E - V(q)$. Then the temperature is related to the average kinetic energy by the equipartition theorem (see Appendix D),

$$T = \frac{2}{3Nk}\langle K\rangle_{mc}. \tag{1.15}$$

The heat capacity is,

$$C_V = \left(\frac{\partial E}{\partial T}\right)_V = \left(\frac{\partial T}{\partial E}\right)_V^{-1} = k\left(1-\left(1-\frac{2}{3N}\right)\langle K\rangle_{mc}\left\langle\frac{1}{K}\right\rangle_{mc}\right)^{-1}. \tag{1.16}$$

The average of the inverse of the kinetic energy in the thermodynamical limit is approximated by,

$$\left\langle\frac{1}{K}\right\rangle_{mc} = \frac{1}{\langle K\rangle}\left(1+\frac{\langle(\delta K)^2\rangle}{\langle K\rangle^2}\right), \tag{1.17}$$

where $K = \langle K\rangle + \delta K$ and $\langle(\delta K)^2\rangle = \langle K^2\rangle - \langle K\rangle^2$. Substituting (1.17) into (1.16) we get,

$$C_V \approx k\left(\frac{2}{3N} - \frac{\langle(\delta K)^2\rangle}{\langle K\rangle^2}\right)^{-1}, \tag{1.18}$$

an equation obtained by Lebowitz, Percus and Verlet [40]. The fluctuation of the kinetic energy in the microcanonical ensemble is then,

$$\langle(\delta K)^2\rangle_{mc} = \frac{2}{3N}\langle K\rangle^2\left(1-\frac{3Nk}{2C_V}\right). \tag{1.19}$$

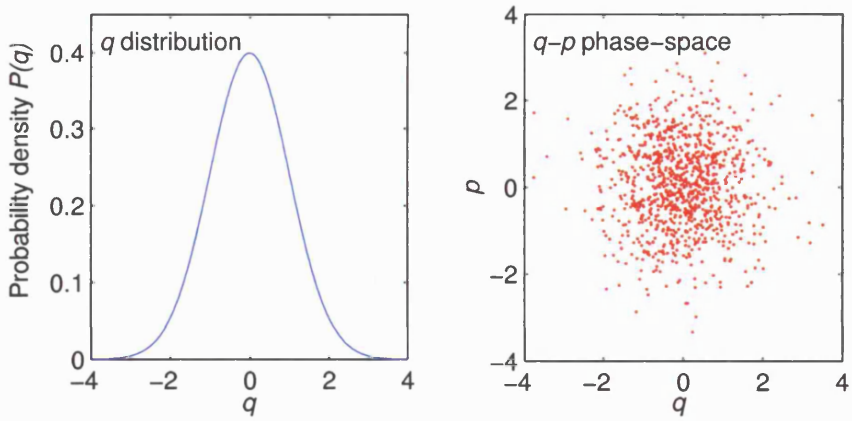

Figure 1.3: Harmonic oscillator with $\omega = 1$, q distribution and q, p phase-space for the canonical ensemble.

1.3.2 Canonical ensemble.

The canonical ensemble relates to simulations where temperature T is fixed instead of total energy E. This ensemble is shown schematically in Figure 1.1 where the original system is surrounded by large external system and energy, but not particles, can be exchanged between them. The external system, or heat bath, must be large in relation to the original system so that temperature changes caused by any energy transfer will be negligible. If we define the temperature of the original system by the average total kinetic energy (1.15), the temperature will be maintained at a constant value by thermal contact with the heat bath. Since temperature is now constant the total energy of the system fluctuates and the distribution is now the canonical distribution,

$$f_c(q,p) = \frac{1}{\sqrt{2\pi kT}} \exp\left(-\frac{H(q,p)}{kT}\right). \tag{1.20}$$

For a single harmonic oscillator, with $\omega = 1$, sampling from the canonical ensemble the q distribution and q, p phase space are shown in Figure 1.3. The relationship between the

distribution functions (1.7) and (1.20) is given by the Laplace transformation, with energy E,

$$f_c(q,p;T) = \int dE \exp\left(-\frac{E}{kT}\right) f_{mc}(q,p;E). \tag{1.21}$$

The thermodynamical potential in the canonical ensemble is the Helmholtz energy $F(T,V,N)$ given by,

$$\begin{aligned} F(T,V,N) &= -kT \ln\left(\int f_c(q,p) dqdp\right) \\ &= -kT \ln\left(\frac{1}{\sqrt{2\pi kT}} \int \exp\left(-\frac{H(q,p)}{kT}\right) dqdp\right). \end{aligned} \tag{1.22}$$

The heat capacity is then expressed as a fluctuation of the total energy,

$$C_V = \frac{\langle H^2 \rangle_c - \langle H \rangle_c^2}{kT^2}. \tag{1.23}$$

The average and fluctuation of kinetic energy are then,

$$\langle K \rangle_c = \frac{3N}{2} kT, \tag{1.24}$$

and,

$$\langle (\delta K)^2 \rangle_c = \frac{2}{3N} \langle K \rangle^2 = \frac{3N}{2} (kT)^2. \tag{1.25}$$

It is noted that quantities which are first order derivative of the thermodynamical potential, such as total energy E and pressure P, are independent of the ensemble but second or higher order derivatives, as we see with heat capacity, are not.

The fluctuation of kinetic energy in the canonical ensemble (1.25) is greater than that in the microcanonical ensemble (1.19), and this inequality can be used to confirm that the sampling is correct for constant temperature simulations.

1.4 Constant temperature methods.

The most common constant temperature methods, required for sampling from the canonical ensemble, are: the constraint method, the stochastic method and the extended system method. Brief descriptions of these methods follow.

1.4.1 Constraint method.

This method works by imposing a constraint on the total kinetic energy as the average kinetic energy is related to the temperature (1.1). Since the relative amplitude of the fluctuations in kinetic energy becomes small for large systems this form of constraint does not seriously affect the resulting dynamic and static quantities. An early method of this type was proposed by Woodcock [68] using a velocity scaling algorithm where, after the temperature is adjusted to be near its target, the simulation is continued without the velocity scaling to calculate the required statistical mechanical averages. Since the scaling contravenes energy conservation the phase-space trajectories are discontinuous at the point of scaling and it is unclear if the correct distribution is obtained.

By studying nonequilibrium states a new constraint method is obtained by calculating the transport properties as a response to an external perturbation [19, 20]. For constant temperature dynamics a constraint of a constant kinetic energy is applied to the equations of motion [31, 16]. Gauss's principle of least constraint states that a constraint force added to restrict the particle motion on a constraint hypersurface should be normal to the surface in realistic constraint dynamics. The equations of motion (1.6) can be modified in this

manner [18] to give,

$$\dot{q}_i = \frac{p_i}{m_i}, \quad \dot{p}_i = -\nabla_{q_i} V(q) - \zeta p_i, \tag{1.26}$$

where ζ is the coefficient of the constraint force. This is known as the Gaussian thermostat method and ζ is a Lagrangian multiplier which satisfies the constant kinetic energy constraint when,

$$\zeta = -\left(\sum_{i=0}^{N} \frac{p_i}{m_i} . \nabla_{q_i} V(q)\right) \left(\sum_{i=0}^{N} \frac{p_i^2}{m_i}\right)^{-1}. \tag{1.27}$$

For these methods it can be shown that, in position q, the canonical distribution is realized.

1.4.2 Stochastic method.

The thermal motion of a particle, in a macroscopic scale, appears to be driven by a random force and hence stochastic methods, such as Monte Carlo and Brownian dynamics, are applicable. Equations similar to Langevin's equation for Brownian dynamics were proposed by Schneider and Stoll [59],

$$m_i \frac{d^2 q_i}{dt^2} = -\nabla_{q_i} V(q) - \gamma \dot{q}_i + R_i(t), \tag{1.28}$$

where a friction force, with coefficient γ, and a random force $R_i(t)$ are added. The random force, temperature T and friction coefficient γ are related by the second fluctuation dissipation theorem,

$$\langle R_i(t_1) R_j(t_2) \rangle = \delta_{ij} 2kT\gamma\delta(t_1 - t_2). \tag{1.29}$$

Thermal agitation due to the random force and slowing due to the friction force balance to keep the temperature constant.

Andersen [4] has proposed a more direct method where occasional collisions between a

particle and hypothetical particles cause the particle to lose its memory, the velocity is reset to a value randomly selected from a Maxwell distribution at temperature T.

Both of these approaches provide sampling from the canonical ensemble for position q, however care needs to be exercised in their use. For example if the frequency of the random collisions in Andersen's method is too high the particle loss of memory occurs in too short a time, leading to the velocity autocorrelation function damping quickly [65].

1.4.3 Extended system method.

Extended system schemes introduce additional degrees of freedom, corresponding to the heat bath, which allow the total energy of the original system to fluctuate. This family of methods was proposed by Nosé [50, 51] and, in its basic form with one additional degree of freedom, is a Hamiltonian formulation that can be shown analytically to sample from the canonical ensemble if the system is assumed to be ergodic. This scheme forms the basis for the majority of current research into thermostatting using deterministic methods, and has found its way into many diverse areas including the combination with constant pressure methods [57, 49, 54, 13] with more recent work by Laird and Sturgeon [39]. For a Hamiltonian of the form (1.5) the corresponding Nosé formulation with additional variable s and its momentum p_s would be,

$$H_{NOSÉ}(q,p,s,p_s) = \sum_{i=1}^{N} \frac{p_i^2}{2m_i s^2} + V(q) + \frac{p_s^2}{2Q} + gkT \ln s, \tag{1.30}$$

where Q and g are constants. If we look at the equation of motion for p_s,

$$\dot{p}_s = \frac{1}{s}\left(\sum_{i=1}^{N} \frac{p_i^2}{m_i s^2} - gkT\right). \tag{1.31}$$

Taking averages and assuming that time averages of time derivatives vanish suggests that the average kinetic energy coincides with the temperature T.

Since the variable s effectively scales the momentum this can be interpreted as a rescaling of time by a factor s^{-1}, which makes quantities such as autocorrelation functions difficult to calculate. To overcome this Nosé [51] proposed a transformation from these virtual variables into real variables, with further simplification by Hoover [30]. The equations of motion take on the form of the constrained dynamics (1.26) but with the friction coefficient ζ now a variable in the extended system method,

$$\dot{\zeta} = \frac{1}{Q}\left(\sum_{i=1}^{N} \frac{p_i^2}{m_i} - gkT\right), \tag{1.32}$$

where g is now the number of degrees of freedom and Q, the Nosé mass, a parameter which determines the speed of temperature control. The equations (1.26) and (1.32) are now known as the Nosé-Hoover thermostat [17]. Since this method has no Hamiltonian the volume in (q, p, ζ) phase-space is not conserved, changing in proportion to the Boltzmann factor $\exp(-H(q,p)/kT)$. It can be shown that the canonical distribution is a steady equilibrium solution for the equations expressing the conservative flow of probability with time for this method.

An alternative to the Nosé-Hoover method was proposed more recently by Bond, Laird and Leimkuhler in [8] where it is possible to obtain real-time results while remaining within a Hamiltonian formulation by applying a Poincaré time transformation to Nosé's original approach. For this Nosé-Poincaré method it is possible to show that sampling is from the canonical ensemble under an ergodic assumption.

Work by Bulgac and Kusnezov [9] has shown that Nosé-Hoover schemes can be extended

to classical spin systems, where there is no kinetic energy term. In this paper it is shown that the only requirement for obtaining the canonical distribution is to control a pair of quantities such that the ratio of their canonical ensemble averages is kT.

Ergodic properties are important for these methods and as a consequence the model consisting of a harmonic oscillator connected to the heat bath is often used [30, 56, 24, 37]. This has led to the work of Martyna, Klein and Tuckerman [47] where additional degrees of freedom were introduced into the Nosé-Hoover method to overcome the lack of ergodicity in small and stiff systems. Each additional degree of freedom thermostats the previous thermostat creating a thermostatting chain and this scheme is now known as the Nosé-Hoover chains method. Attempts at applying this concept to the Nosé-Poincaré method in a straightforward manner, in order to obtain the advantages of both chains and a Hamiltonian formulation, does not give the correct sampling.

Additional studies by Hoover and Holian [26, 27, 25, 29] have looked into the behavior of Nosé and Nosé-Hoover methods.

1.5 Symplectic integrators.

The thermostatting methods in the preceding section will require a numerical integrator as a mapping which approximates the flow-map of the system of differential equations. There are many numerical integrators discussed in the literature but the class of Geometric integrators have attracted attention for their ability to preserve geometric properties of the original system, the most common being time-reversibility, applicable to Newtonian mechanics, and symplecticness for Hamiltonian systems. The application of these methods

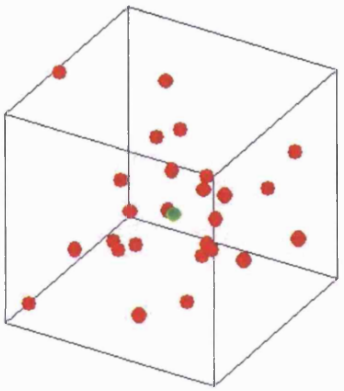

Figure 1.4: 27 particle simulation using a Lennard-Jones potential and periodic boundary conditions.

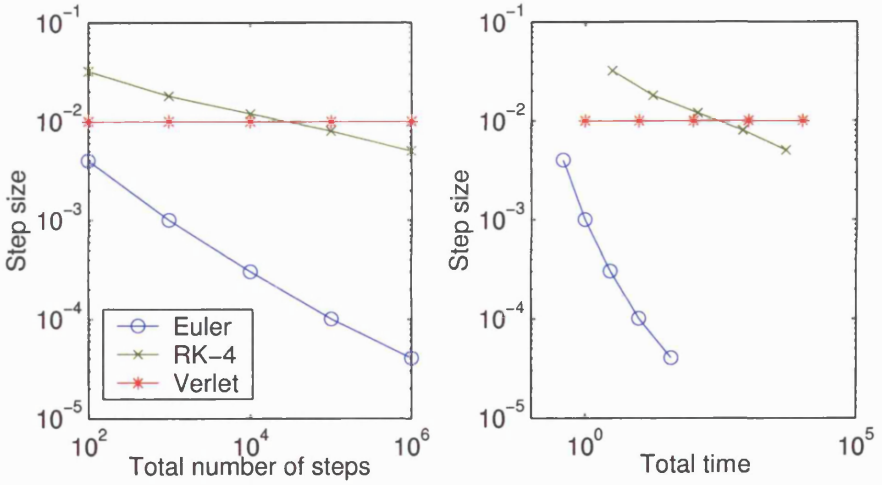

Figure 1.5: Maximum possible step size for Euler, 4^{th} order Runge-Kutta and Verlet methods for a given number of integration steps and simulation time.

is shown to provide excellent long-term stability and preservation of quantities such as first integrals, an example of which is energy in the Hamiltonian case.

Since thermostating methods generally introduce an undesirable mixing of the variables, leading to implicit integration schemes, Hamiltonian systems have an additional advantage as this limitation can be overcome by splitting the Hamiltonian to formulate explicit symplectic methods [22, 64]. This provides the motivation to develop Hamiltonian thermostatting methods.

To illustrate the importance of symplectic integrators for MD simulations a system consisting of 27 particles, using a Lennard-Jones potential and periodic boundary conditions as shown in Figure 1.4, was simulated using three different integrators; 1^{st} order Euler, 4^{th} order Runge-Kutta and the 2^{nd} order Verlet (symplectic) method. For a given number of integration steps the maximum possible step size was determined for each method as seen in Figure 1.5, from this it is clear that for the non-symplectic methods the number of integration steps determines the maximum step size that can be used. Since very long integration times are required for MD simulations, methods where the step size is independent of the number of integration steps are the only practical approach.

A Hamiltonian $H(z)$, $z = (q, p)$, can be written in the compact form,

$$\dot{z} = \mathbf{J}\nabla_z H(z), \tag{1.33}$$

where $\mathbf{J}$ is an invertible skew-symmetric matrix ($\mathbf{J}^T = -\mathbf{J}$). A smooth map ψ is called a symplectic map if its Jacobian $\psi_z(z)$ satisfies,

$$[\psi_z(z)]^T \mathbf{J}^{-1} \psi_z(z) = \mathbf{J}^{-1}. \tag{1.34}$$

Symplectic maps, time-reversibility and Hamiltonian splitting methods are discussed further in Appendix B.

Symplectic integrators have another important feature, the possibility of Backward Error Analysis. It can be shown that the approximate solution provided by a symplectic integrator is the exact solution of a modified Hamiltonian, which can be derived by the application of the backward error analysis. This is discussed further in Appendix C.

Anther important consideration for numerical integrators is the order of the method where, for a step size of h and order p, the global error will be $O(h^p)$. For N-body systems considerable computational advantage can be gained by employing high order methods since exact trajectories for the bodies are required. It is possible to construct higher order methods while remaining in the class of explicit and time-reversible integrators by using composition methods as described by Yoshida [69]. Further enhancements for N-body integrators can be produced by utilizing variable step-size techniques such as the Adaptive Verlet method proposed by Huang and Leimkuhler [32], but problems occur when combining this method with composition methods, leading to lower than expected order. This limitation has been overcome by Leimkuhler and Sweet [45] where a backward error analysis is used to develop a modified framework such that higher orders are obtained. An overview of [45] appears in Appendix E.

For molecular dynamics simulations low order methods are generally considered, such as the Verlet method, since exact trajectories are not required to generate ensemble averages. The Verlet method is also symplectic and hence applicable to Hamiltonian formulations, but not to schemes such as the Nosé-Hoover method.

1.6 Thermostatting open problems.

Despite the attention that schemes based on Nosé's method have attracted, there remain a number of unresolved issues which limit their usefulness when compared to stochastic methods.

With the methods in Section 1.4.3, the choice of Nosé mass or masses in the case of thermostatting chains have to be tailored to the system to be simulated. It has been generally accepted that the self-oscillation frequency of the thermostatting variable should coincide with some frequency within the original system, but this can be problematic in real systems where several such frequencies exist. Even in idealized systems the self-oscillation frequency has been found to be a poor guide, requiring the tedious tuning of parameters during several simulations, to determine the optimum values.

The correct sampling for extended systems relies on the system being ergodic which, especially for small or stiff systems, may not be true. The introduction of thermostatting chains alleviates this problem but the small dimensional sub-system that each additional thermostat is required to control can introduce the same problems experienced by the harmonic oscillator when thermostatted by Nosé's method. This can lead to stability problems in the numerical integrator and a lack of ergodicity in the thermostatting chain, so that the expected average values for the additional thermostats 'kinetic' terms may not be achieved. The lack of a Hamiltonian thermostatting chain method also prevents the use of symplectic integrators.

1.7 Thesis results.

The main results obtained in this Thesis are to published as two papers [43, 44], the important points of which are detailed below.

1) The Canonical Ensemble via Symplectic Integrators using Nosé and Nosé-Poincaré chains.

- The construction of a general family of fully Hamiltonian multiple thermostat methods, from which the chains methods are derived.
- The implementation of fully Hamiltonian Nosé/Nosé-Poincaré chains as an alternative to the non-Hamiltonian Nosé-Hoover chains.
- Construction of a Hamiltonian splitting method to implement explicit integrators for Nosé-Poincaré chains.
- Proof of the correct ensemble sampling for these methods, under an ergodic assumption.
- Experimental evidence for the broader choice of Nosé mass provided by chains methods.
- Experimental results showing the successful thermostatting of difficult systems such as the harmonic oscillator.

2) A Hamiltonian Formulation for Recursive Multiple Thermostats in a Common Timescale.

- The extension of the fully Hamiltonian multiple thermostat methods such that multiple thermostats can interact directly with the system to be thermostatted, from which the Recursive Multiple Thermostat method is derived.
- The implementation of the fully Hamiltonian Recursive Multiple Thermostat (RMT) method, overcoming the limitations of Nosé-Poincaré and chains methods.
- Construction of a Hamiltonian splitting method to implement explicit integrators for RMT.
- Proof of the correct ensemble sampling for this method, under an ergodic assumption.
- Special features of the thermostatting variable's phase-space, and their role in producing the correct sampling, are displayed.
- Construction of a frequency domain model of the Nosé-Poincaré thermostatting method to show that the correct choice of Nosé mass is determined by the requirement that the heat bath should be ergodic rather than that the thermostat should resonate with some frequency within the original system.
- Experimental evidence to show that the choice of Nosé mass is essentially independent of the underlying system.
- Experimental results showing the successful thermostatting of difficult systems such as the harmonic oscillator and multiple harmonic oscillators with large frequency difference.
- From the results obtained when applying the RMT method to multiple harmonic oscillators with large frequency difference it is expected that this method would be

applicable to systems which are difficult to thermostat, such as Butane molecules where there is poor coupling between modes.

Chapter 2

Nosé Dynamics

In this Chapter we examine Nosé's thermostatting scheme in detail, and consider the proof that the modified system samples from the canonical ensemble if ergodicity can be assumed. Since Nosé's method introduces an artificial scaling of the time variable, which makes computation of time-correlation functions cumbersome, we also consider methods which introduce time transformations to correct this deficiency. These include Hoover's coordinate and time transformations [30], which destroy the Hamiltonian structure, and more recent work by Bond, Laird and Leimkuhler [8] where the desired rescaling of time is accomplished through transformation of the Hamiltonian itself.

For small or stiff systems these methods are not ergodic and the correct distributions are not produced. To overcome this Martyna, Klein and Tuckerman [47] proposed a method, Nosé-Hoover chains, where each thermostat is controlled by another thermostat forming a thermostat chain. This scheme inherits the limitations of the Nosé-Hoover method, the lack of a Hamiltonian, and is described in Section 2.4.

2.1 Nosé Thermostats.

The paper of Nosé [50] introduced a family of extended dynamical systems, for which it can be shown analytically that sampling from the canonical ensemble occurs under an ergodicity assumption. We consider an N-body system with positions $q = (q_1, q_2, \cdots, q_N)$, momenta $p = (p_1, p_2, \cdots, p_N)$ with original Hamiltonian $H(q,p)$. The construction is based on one additional degree of freedom with an extended Hamiltonian,

$$H_N(q, s, p, p_s) = H\left(q, \frac{p}{s}\right) + \frac{p_s^2}{2Q} + (N_f + 1)kT \ln s, \tag{2.1}$$

where N_f is the number if degrees of freedom, s is the new thermostatting variable, p_s its corresponding momentum, T is temperature, Q the Nosé mass and k is the Boltzmann constant.

To illustrate how this method works we consider the equations of motion for the additional degree of freedom,

$$\dot{s} = \frac{p_s}{Q}, \quad \dot{p}_s = \sum_{i=1}^{N} \frac{p_i^2}{m_i s^3} - \frac{(N_f + 1)kT}{s}, \tag{2.2}$$

which can be rewritten as,

$$Q\ddot{s} = \sum_{i=1}^{N} \frac{p_i^2}{m_i s^3} - \frac{(N_f + 1)kT}{s}. \tag{2.3}$$

This can be interpreted as the application of negative feedback to control the kinetic energy. If the kinetic energy is greater than $(N_f + 1)kT$ then $\ddot{s}$ becomes positive, eventually increasing s and hence decreasing the kinetic energy. Conversely, if the kinetic energy is less than $(N_f + 1)kT$ then $\ddot{s}$ will become negative, eventually decreasing s and increasing the kinetic energy. Taking averages of (2.3) and assuming that time averages of time derivatives vanish we see that the average kinetic energy now coincides with the temperature T.

To show that sampling is from the canonical ensemble we consider the partition function which, for energy E and Planck's constant h, is defined as,

$$Z = \frac{1}{N!h^{N_f}} \int dp_s \int ds \int dp \int dq \; \delta \left[H\left(q, \frac{p}{s}\right) + \frac{p_s^2}{2Q} + (N_f + 1)kT \ln s - E \right].$$

We can substitute $p' = p/s$, the volume element then becomes $dp = s^{N_f} dp'$. There is no upper limit in momentum space so we can change the order of integration of dp' and ds giving,

$$Z = \frac{1}{N!h^{N_f}} \int dp_s \int dp' \int dq \int ds \; s^{N_f} \delta \left[H(q,p') + \frac{p_s^2}{2Q} + (N_f + 1)kT \ln s - E \right].$$

Using the equivalence relation for δ, $\delta[r(s)] = \delta[s - s_0]/r'(s)$, where s_0 is the zero of $r(s) = 0$ to get,

$$\begin{aligned} Z &= \frac{1}{N!h^{N_f}} \int dp_s \int dp' \int dq \int ds \frac{s^{N_f+1}}{(N_f+1)kT} \; \delta \left[s - \exp\left(\frac{-(H(q,p') + \frac{p_s^2}{2Q} - E)}{(N_f+1)kT} \right) \right] \\ &= \frac{1}{(N_f+1)kT} \frac{1}{N!h^{N_f}} \int dp_s \int dp' \int dq \; \exp\left(\frac{-(H(q,p') + \frac{p_s^2}{2Q} - E)}{kT} \right). \end{aligned}$$

Integrating with respect to p_s we get,

$$Z = \frac{1}{(N_f+1)} \left(\frac{2\pi Q}{kT} \right)^{\frac{1}{2}} \exp\left(\frac{E}{kT} \right) Z_c,$$

where Z_c is the partition function of the Canonical ensemble,

$$Z_c = \frac{1}{N!h^{N_f}} \int dp' \int dq \; \exp\left(\frac{-H(q,p')}{kT} \right).$$

This means that constant energy dynamics of the extended Hamiltonian $H_N(q, s, p, p_s)$ correspond to constant temperature dynamics of $H(q, p/s)$.

Since the momenta we are now using are $p' = p/s$, this is equivalent to re-scaling the time by s^{-1}, as can be illustrated by thermostatting a harmonic oscillator with angular

frequency ω and Hamiltonian $H_{ho} = p^2/2 + \omega^2 q^2/2$. If we modify this oscillator using Nosé's method the equations of motion for the real variables become,

$$\dot{q} = \frac{p}{s^2} \tag{2.4}$$

$$\dot{p} = -\omega^2 q. \tag{2.5}$$

From (2.4)-(2.5) the modified oscillator has a frequency of $s\omega$, equivalent to a rescaling of time by s^{-1}.

For the single harmonic oscillator this rescaling of time can introduce stability problems when using a numerical method, such as the Verlet method. If we consider (2.3) for $N = 1$ and small Q we see that,

$$\frac{p^2}{ms^2} \approx gkT, \tag{2.6}$$

and, in the limit of small Q, the oscillator moves between widely-separated turning points at velocity $\pm v$, for some v, as reported by Hoover [30] and depicted, for $Q = 0.03$, in the q, p phase-space diagram from Figure 2.1. From (2.6) the value of s is dependent on p and, even for reasonable values of Q, will be small when p makes the transition from $+v$ to $-v$ and viceversa. Given that the numerical method is stable up to a maximum step-size of h_{max} for this system, if the maximum value for the time rescaling is given by $tr_{max} = (\min s)^{-1}$ then the new maximum step-size is h_{max}/tr_{max}. By studying the auxiliary variable phase-space in Figure 2.1, p_s, s diagram, we see that $tr_{max} > 100$ for the optimum value of Q, leading to small maximum step-sizes of less than $h_{max}/100$. Clearly if the step-size is selected to be close to its maximum value for the original system, the procedure normally followed, the method will fail. An associated problem occurs in thermostatting chains, since the sub-system that each additional thermostat controls is of low dimension, and the time

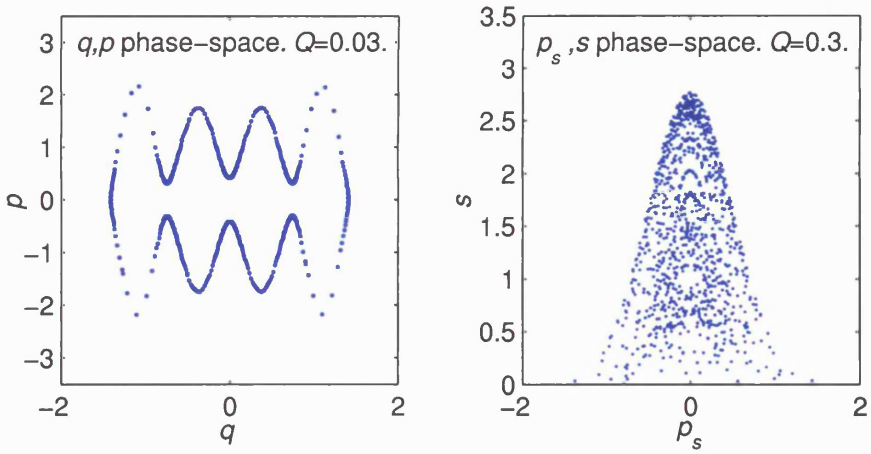

Figure 2.1: Phase-space diagrams for a Nosé thermostatted harmonic oscillator with $\omega = 1$. The q, p diagram was observed by Hoover in [30], the p_s, s diagram illustrates the minimum values obtained for s at the optimum value for Q.

reparametrization is only based on the first thermostat.

The choice of the constant Nosé mass, Q, is crucial to the effectiveness of this method and has been the subject of extensive discussion. When Q is too small the Nosé variable can become an isolated mode, it can oscillate independently of the simulated system, and the distribution of the total kinetic energy driven by the oscillator will deviate significantly from the Gaussian distribution. When Q is too large the situation is similar to that in the micro-canonical ensemble because the exchange of heat is slow. It has been generally accepted that the correct choice of Q occurs when the self-oscillation frequency of the thermostatting variable coincides with some frequency within the original system. As stated previously, for complex systems, where several frequencies exist, the correct method of choosing Q is less clear and is dependent on the coupling between sub-systems and modes. This can be illustrated by comparing two systems, liquids with a Lennard-Jones potential which have a very wide choice of Q and Butane molecules where the choice of Q is critical and generally

determined empirically.

Nosé showed [50], by a linearization method, that if the fluctuations of the thermostatting variable s are much faster than those of the bodies within the original system then it will have a self-oscillation frequency of,

$$\omega_N = \sqrt{\frac{2gkT}{Q}}, \tag{2.7}$$

where g is determined by the number of degrees of freedom of the system, generally $N_f + 1$ for Nosé's method. Since the frequency of self-oscillation is required, it is necessary to apply a time transformation to Nosé's scheme before the linearization method can be used. The first of these modified schemes is the Nosé-Hoover thermostat.

2.2 Nosé-Hoover Thermostats.

Nosé [51] proposed applying a time transformation to the extended system to correct for the rescaling of time, and this idea was developed further by Hoover [30] who applied both coordinate and time transformations to correct the dynamics, but these destroy the Hamiltonian structure so that symplectic methods are no longer applicable. To produce the Nosé-Hoover method for an underlying Hamiltonian of the form,

$$H(q,p) = \sum_{i=1}^{N} \frac{p_i^2}{2m_i} + V(q), \tag{2.8}$$

the equations of motion for Nosé's method (2.1) are then,

$$\begin{aligned} \dot{q}_i &= \frac{p_i}{m_i s^2}, \\ \dot{p}_i &= -\nabla_{q_i} V(q), \end{aligned}$$

$$\begin{aligned}\dot{s} &= \frac{p_s}{Q}, \\ \dot{p}_s &= \sum_{i=1}^{N} \frac{p_i^2}{m_i s^3} - \frac{gkT}{s}.\end{aligned}$$

Applying the Sundman transformation $\frac{dt}{dt'} = s$, and substituting $p' = p/s$, $t' = \int dt/s$, $p'_s = p_s/s$, we get:

$$\begin{aligned}\frac{dq_i}{dt'} &= \frac{p'_i}{m_i}, \\ \frac{dp'_i}{dt'} &= -\nabla_{q_i} V(q) - \frac{1}{s}\frac{ds}{dt'}p'_i, \\ \frac{ds}{dt'} &= s^2 \frac{p'_s}{Q}, \\ \frac{dp'_s}{dt'} &= \frac{1}{s}\left(\sum_{i=1}^{N} \frac{p_i'^2}{m_i} - gkT\right) - \frac{1}{s}\frac{ds}{dt'}p'_s.\end{aligned}$$

Hoover then made the coordinate transformations $p_\eta = Q(1/s)ds/dt' = s\ p'_s$, $\eta = \ln s$ to get:

$$\frac{dq_i}{dt'} = \frac{p'_i}{m_i}, \tag{2.9}$$

$$\frac{dp'_i}{dt'} = -\nabla_{q_i} V(q) - p'_i \frac{p_\eta}{Q}, \tag{2.10}$$

$$\frac{d\eta}{dt'} = \frac{p_\eta}{Q}, \tag{2.11}$$

$$\frac{dp_\eta}{dt'} = \sum_{i=1}^{N} \frac{p_i'^2}{m_i} - gkT. \tag{2.12}$$

Where $g = N_f$. This form is now known as the Nosé-Hoover thermostat [30].

It is now possible to consider the linearization methods [52] to determine the self-oscillation frequency of the thermostatting variable. If we consider the coordinate transformations with (2.12) then,

$$Q\frac{d}{dt'}\left(\frac{1}{s}\frac{ds}{dt'}\right) = \sum_{i=1}^{N} \frac{p_i^2}{m_i s^2} - gkT. \tag{2.13}$$

We will consider a fluctuation δs of s around an average $\langle s \rangle$ such that $s = \langle s \rangle + \delta s$. In addition we assume that the fluctuations of s are much faster than those of the original system, the constant temperature is then mainly maintained by s,

$$\sum_{i=1}^{N} \frac{p_i^2}{m_i \langle s \rangle^2} = gkT. \tag{2.14}$$

Linearizing (2.13) and substituting (2.14),

$$\begin{aligned} Q \frac{1}{\langle s \rangle} \frac{d^2 \delta s}{dt'^2} &= \sum_{i=1}^{N} \frac{p_i^2}{m_i \langle s \rangle^2} \left(1 - \frac{2\delta s}{\langle s \rangle} \right) - gkT \\ &= -\frac{2gkT}{\langle s \rangle} \delta s. \end{aligned}$$

This is equivalent to the equation for the harmonic oscillator given by (2.7).

Since this method has no Hamiltonian we cannot show that it samples from the canonical ensemble by employing the technique used for Nosé's method. Instead we can show that the canonical distribution is a steady equilibrium solution for the equations expressing the conservative flow of probability with time. Since q, p' and p_η are independent we can calculate the components of the flow of probability density $f(q, p', p_\eta)$ in (2N+1)-dimensional space. Since the equations of motion are not Hamiltonian the derivatives $\partial \dot{q}/\partial q$ and $\partial \dot{p}'/\partial p'$ do not generally sum to zero. The analog of Liouville's equation for the conservative flow of probability with time, including flow in the p_η direction, is,

$$\frac{\partial f}{\partial t} + \frac{\dot{q} \partial f}{\partial q} + \frac{\dot{p}' \partial f}{\partial p'} + \frac{\dot{p}_\eta \partial f}{\partial p_\eta} + f \left[\frac{\partial \dot{q}}{\partial q} + \frac{\partial \dot{p}'}{\partial p'} + \frac{\partial \dot{p}_\eta}{\partial p_\eta} \right] = 0. \tag{2.15}$$

For the canonical ensemble we have,

$$f(q, p', p_\eta) \propto \exp \left(- \frac{\sum_{i=1}^{N} p_i'^2/2m_i + V(q) + p_\eta^2/2Q}{kT} \right). \tag{2.16}$$

Using this density function the non-vanishing terms in (2.15) are,

$$\begin{aligned}
\frac{\dot{q}\partial f}{\partial q} &= \frac{f}{kT}\sum_{i=1}^{N}\frac{-\nabla_{q_i}V(q)p_i'}{m_i}, \\
\frac{\dot{p}'\partial f}{\partial p'} &= \frac{f}{kT}\sum_{i=1}^{N}\frac{(\nabla_{q_i}V(q)+\frac{p_\eta}{Q}p_i')p_i'}{m_i}, \\
\frac{\dot{p}_\eta\partial f}{\partial p_\eta} &= \frac{f}{kT}\frac{p_\eta}{Q}\left(-\sum_{i=1}^{N}\frac{p_i'^2}{m_i}+gkT\right), \\
\frac{f\partial\dot{p}'}{\partial p'} &= \frac{f}{kT}\left(-NkT\frac{p_\eta}{Q}\right),
\end{aligned}$$

These terms sum to zero, provided that g is chosen to be equal to the independent degrees of freedom in the original system.

2.3 Nosé-Poincaré Thermostats.

An alternative to the Nosé-Hoover method was proposed by Bond, Laird and Leimkuhler in [8] where it is possible to obtain real-time results without sacrificing the Hamiltonian by using a Poincaré transformation. The re-formulation for a Hamiltonian system with energy $H(q,p)$ is,

$$H_{NP}(q,s,p,p_s) = \left(H\left(q,\frac{p}{s}\right)+\frac{p_s^2}{2Q}+N_fkT\ln s - H_0\right)s. \tag{2.17}$$

Here N is the number of degrees of freedom of the real system and H_0 is chosen such that the Nosé-Poincaré Hamiltonian, H_{NP}, is zero when evaluated at the initial conditions.

This scheme can be shown to sample from the correct distribution in a similar manner to that used for Nosé's method, if the modified system is ergodic. The partition function for the canonical ensemble is defined as,

$$Z = \frac{1}{N!h^{N_f}}\int dp_s\int ds\int dp\int dq\;\delta\left[H_{NP}-0\right]. \tag{2.18}$$

Substituting (2.17) into (2.18) we get,

$$Z = \frac{1}{N!h^{N_f}} \int dp_s \int ds \int dp \int dq\ \delta\left[\left(H\left(q, \frac{p}{s}\right) + \frac{p_s^2}{2Q} + N_f kT \ln s - H_0\right) s\right].$$

We can substitute $p' = p/s$, the volume element then becomes $dp = s^{N_f} dp'$. There is no upper limit in momentum space so we can change the order of integration of dp' and ds giving,

$$Z = \frac{1}{N!h^{N_f}} \int dp_s \int dp' \int dq \int ds\ s^{N_f} \delta\left[\left(H(q,p') + \frac{p_s^2}{2Q} + N_f kT \ln s - H_0\right) s\right]. \quad (2.19)$$

Whenever a smooth function, $r(s)$, has a single simple root at $s = s_0$ we can write the equivalence relation for δ, $\delta[r(s)] = \delta[s - s_0]/|r'(s_0)|$, then,

$$\delta\left[\left(H(q,p') + \frac{p_s^2}{2Q} + N_f kT \ln s - H_0\right) s\right] =$$
$$\frac{1}{N_f kT}\ \delta\left[s - \exp\left(-\frac{1}{N_f kT}\left(H(q,p') + \frac{p_s^2}{2Q} - H_0\right)\right)\right]. \quad (2.20)$$

Substituting (2.20) into (2.19) we get,

$$Z = \frac{1}{N!h^{N_f}} \int dp_s \int dp' \int dq \int ds \frac{s^{N_f}}{N_f kT}\ \delta\left[s - \exp\left(-\frac{1}{N_f kT}\left(H(q,p') + \frac{p_s^2}{2Q} - H_0\right)\right)\right]$$
$$= \frac{1}{N_f kT} \frac{1}{N!h^{N_f}} \int dp_s \int dp' \int dq\ \exp\left(-\frac{1}{kT}\left(H(q,p') + \frac{p_s^2}{2Q} - H_0\right)\right)].$$

Integrating with respect to p_s we get,

$$Z = \left(\frac{2\pi Q}{N_f kT}\right)^{\frac{1}{2}} \exp\left(\frac{H_0}{kT}\right) Z_c,$$

where Z_c is the partition function of the Canonical ensemble,

$$Z_c = \frac{1}{N!h^{N_f}} \int dp' \int dq\ \exp\left(\frac{-H(q,p')}{kT}\right).$$

Again, it has been shown that sampling H_{NP} at constant energy is equivalent to sampling the original system at constant temperature T, but now in real-time. Quantities such

as velocity autocorrelations and diffusion constants can now be calculated in a straightforward manner. A symplectic numerical method is included in [8], which is reproduced in Section 4.9, and further research on integrators and applications [39, 53, 15] has helped to establish the Nosé-Poincaré framework.

2.4 Nosé-Hoover chains.

For ergodic systems thermostatted by Nosé's method it can be shown that $\langle p_s^2/Q \rangle = kT$ by the proof which appears in section 3.2, or by the equipartition theorem (see Appendix D). Motivated by this Martyna, Klein and Tuckerman [47] proposed a method to overcome the lack of ergodicity in small or stiff systems by regulating the thermostat's momentum such that its average achieves the ergodic value. Here each thermostat is controlled by another thermostat, forming a thermostat chain. The explantation provided in [47] is as follows; "In standard Nosé-Hoover dynamics the distribution has a Gaussian dependence on the particle momenta, p, as well as the thermostat momentum, p_η. The Gaussian fluctuations of p are driven by the thermostat but there is nothing to drive the fluctuations of p_η unless further thermostats are added as described above".

The Nosé-Hoover equations (2.9)-(2.12) are modified by adding the thermostat chain. The modified dynamics, for M thermostats, can then be expressed as,

$$\frac{dq_i}{dt'} = \frac{p_i'}{m_i}, \tag{2.21}$$

$$\frac{dp_i'}{dt'} = -\nabla_{q_i} V(q) - p_i' \frac{p_{\eta_1}}{Q_1}, \tag{2.22}$$

$$\frac{d\eta_i}{dt'} = \frac{p_{\eta_i}}{Q_i}, \tag{2.23}$$

$$\frac{dp_{\eta_1}}{dt'} = \left(\sum_{i=1}^{N}\frac{p_i'^2}{m_i} - N_f kT\right) - p_{\eta_1}\frac{p_{\eta_2}}{Q_2}, \tag{2.24}$$

$$\frac{dp_{\eta_j}}{dt'} = \left(\frac{p_{\eta_{j-1}}^2}{Q_{j-1}} - kT\right) - p_{\eta_j}\frac{p_{\eta_{j+1}}}{Q_{j+1}}, 1 < j < M, \tag{2.25}$$

$$\frac{dp_{\eta_M}}{dt'} = \left(\frac{p_{\eta_{M-1}}^2}{Q_{M-1}} - kT\right). \tag{2.26}$$

These equations can be shown to produce the correct phase-space distributions in a similar manner to that employed for the Nosé-Hoover method, but now $p_\eta = (p_{\eta_1}, \cdots, p_{\eta_M})$. For probability density f we have,

$$\frac{\partial f}{\partial t} + \frac{\dot{q}\partial f}{\partial q} + \frac{\dot{p}'\partial f}{\partial p'} + \frac{\dot{p}_\eta \partial f}{\partial p_\eta} + f\left[\frac{\partial \dot{q}}{\partial q} + \frac{\partial \dot{p}'}{\partial p'} + \frac{\partial \dot{p}_\eta}{\partial p_\eta}\right] = 0, \tag{2.27}$$

and for the canonical ensemble,

$$f(q, p', p_\eta) \propto \exp\left(-\frac{\sum_{i=1}^{N} p_i'^2/2m_i + V(q) + \sum_{j=1}^{M} p_{\eta_j}^2/2Q_j}{kT}\right). \tag{2.28}$$

Martyna, Klein and Tuckerman [47] estimated the required Q_i by generating second order equations of motion for each $\dot{\eta}_i$ from the time derivative of $\ddot{\eta}_i$. By considering that adjacent thermostats, η_{i-1} and η_{i+1}, are slow and η_{i+2} moves on the same timescale the resulting equations are,

$$\begin{aligned}
\frac{d^2\dot{\eta}_1}{dt^2} &= -\dot{\eta}_1\left(\frac{2N_f kT}{Q_1} - \frac{2kT}{Q_2}\right) - \frac{Q_1}{Q_2}\dot{\eta}_1^3, \\
\frac{d^2\dot{\eta}_j}{dt^2} &= -\dot{\eta}_j\left(\frac{2kT}{Q_j} - \frac{2kT}{Q_{j+1}}\right) - \frac{Q_{j-1}}{Q_{j+1}}\dot{\eta}_j^3, \\
\frac{d^2\dot{\eta}_M}{dt^2} &= -\dot{\eta}_M\left(\frac{2kT}{Q_M}\right).
\end{aligned}$$

Given an dominant frequency ω within the original system it was proposed that the choices $Q_1 = N_f kT/\omega^2$ and $Q_j = kT/\omega^2$ would give thermostats 1 to $M-1$ an average 'frequency' of ω. The M^{th} thermostat is then set to oscillate at 2ω.

It is noted that, for experiments using Nosé-Hoover chains, the choice of the Nosé mass for the first thermostat is less critical than in Nosé, Nosé-Hoover and Nosé-Poincaré methods

Chapter 3

Analysis of the Nosé-Poincaré Method.

In this chapter the behavior of the real time Nosé-Poincaré method is analyzed when applied to a single harmonic oscillator. Examining the auxiliary variable phase-space and modelling the system in the frequency domain provides a better understanding of the role of the Nosé mass parameter. It is anticipated that a very similar analysis would apply to Nosé-Hoover dynamics.

3.1 Auxiliary Variable Phase-Space.

If we consider the classical N-body problem (2.8) with potential bounded below, $V(q) \geq 0 \ \forall q$, and apply a thermostat using the Nosé-Poincaré method (2.17) we can see that, for

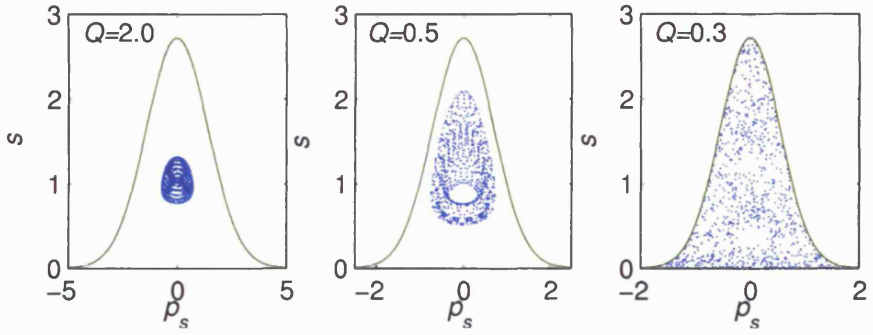

Figure 3.1: Auxiliary variable phase-space with Q=2.0, Q=0.5 and Q=0.3.

initial energy $E = H_0$,

$$\frac{p_s^2}{2Q} + N_f kT \ln s \leq E, \tag{3.1}$$

and hence the phase-space of the auxiliary variables is bounded by the equation,

$$s = \exp\left(\frac{E - \frac{p_s^2}{2Q}}{N_f kT}\right). \tag{3.2}$$

To illustrate the behavior of the auxiliary variables we consider a harmonic oscillator with underlying energy $H(q,p) = q^2/2 + \omega p^2/2$, thermostatted using the Nosé-Poincaré method, and examine, in Figure 3.1, the effect of a change in the Nosé mass on the auxiliary variable phase space. The parameters used were $E = 1$, $kT = 1$ and $\omega = 1$ for $Q = 0.3$, $Q = 0.5$ and $Q = 2$. As Q is reduced the phase-space occupied by the auxiliary variables (dots) increases and the bounding curve (solid line), given by (3.2), decreases. At $Q \approx 0.3$ the auxiliary variables reach the boundary and, at this point, although the system is not sufficiently ergodic to produce sampling from the canonical ensemble, the results are close in some sense as shown in Figure 3.2.

From Nosé's linearized equation in [50], $Q = 2gkT/\omega^2$, we would expect that the optimum $Q = 2$ whereas in practice we see that at this value the system is sampling from

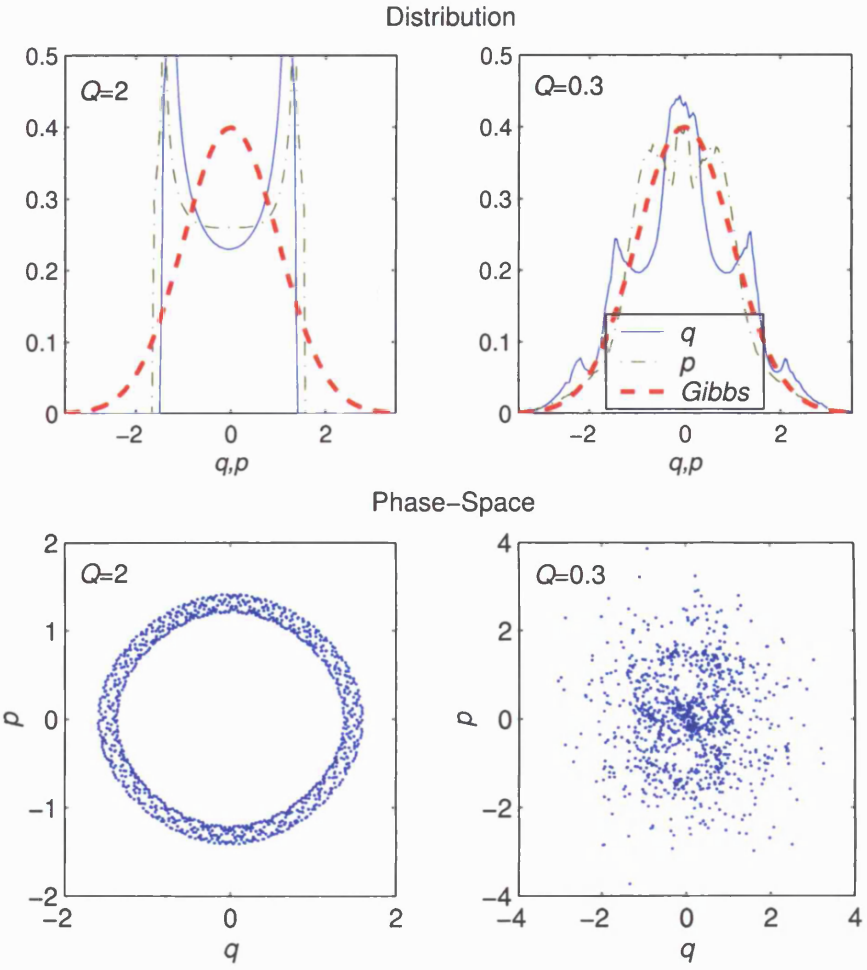

Figure 3.2: Harmonic oscillator q, p distributions and phase-space with Q=2 and Q=0.3.

the microcanonical ensemble. Since the oscillator is started at the correct temperature we expect that the average value of s will be 1 (as shown in Section 3.2.1).

Further experimental evidence for the correct choice of Q is found in the Generalized Dynamical Thermostatting Technique [38], here introducing ergodicity by coupling a box of soft spheres into the thermostatting momentum resulted in the correct distributions, but only where $Q \approx 0.4$ for a single harmonic oscillator with $\omega = 1$ and $kT = 1$. Details of this experiment can be found in Section 4.1.

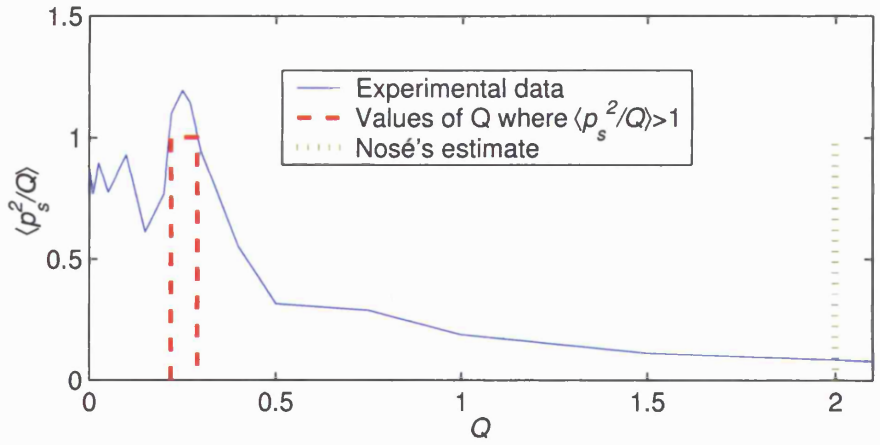

Figure 3.3: $\langle p_s^2/Q \rangle$ for Q in the range 0.001-2 with values of Q for $\langle p_s^2/Q \rangle > 1$ (thick dashed) and Nosé's estimate (thick dots).

In Figure 3.3 the relationship between the mean thermostat 'kinetic' energy $\langle p_s^2/Q \rangle$ and Q is shown for Q in the range 0.001-2. $\langle p_s^2/Q \rangle$ peaks after the point where the auxiliary variables reach the boundary of their phase-space, as given in (3.2), at a value of approximately $kT = 1$.

3.2 Average Values for the Auxiliary Variables.

As shown in Section 3.1, $\langle p_s^2/Q \rangle$ peaks at the optimum value for the Nosé mass Q. It is possible to calculate the average values for both the quantity p_s^2/Q and, for systems of harmonic oscillators, the auxiliary variable s if we assume that the system is ergodic. We consider the Nosé-Poincaré method (2.17) where it is possible to obtain real-time results without sacrificing the symplectic structure by using a Poincaré transformation.

THEOREM 3.2.1 *When thermostatting systems of harmonic oscillators with the Nosé-Poncaré method (2.17), if the system is ergodic, then the average of the auxiliary variable, s, will be*

given by,

$$\langle s \rangle = \exp\left(\frac{H_0}{N_f kT}\right)\left(\frac{N_f}{N_f+1}\right)^{\frac{2N_f+1}{2}} \tag{3.3}$$

Proof For an ergodic system the average of s is,

$$\langle s \rangle = \frac{\int dp_s \int ds \int dp \int dq \; s \; \delta\left[H_{NP} - 0\right]}{\int dp_s \int ds \int dp \int dq \; \delta\left[H_{NP} - 0\right]} = \frac{\mathcal{N}}{\mathcal{D}}. \tag{3.4}$$

Substituting (2.17) into the numerator of (3.4), $\mathcal{N}$, we get,

$$\mathcal{N} = \int dp_s \int ds \int dp \int dq \; s \; \delta\left[\left(H\left(q, \frac{p}{s}\right) + \frac{p_s^2}{2Q} + N_f kT \ln s - H_0\right) s\right]. \tag{3.5}$$

We can substitute $\tilde{p} = p/s$, the volume element then becomes $dp = s^{N_f} d\tilde{p}$. There is no upper limit in momentum space so we can change the order of integration of $d\tilde{p}$ and ds giving,

$$\mathcal{N} = \int dp_s \int d\tilde{p} \int dq \int ds \; s^{N_f+1} \delta\left[\left(H(q,\tilde{p}) + \frac{p_s^2}{2Q} + N_f kT \ln s - H_0\right) s\right]. \tag{3.6}$$

Whenever a smooth function, $h(s)$, has a single simple root at $s = s_0$ we can write the equivalence relation for δ, $\delta[h(s)] = \delta[s - s_0]/|h'(s_0)|$, then,

$$\begin{aligned} \delta\left[\left(H(q,\tilde{p}) + \frac{p_s^2}{2Q} + N_f kT \ln s - H_0\right) s\right] \; = \\ \frac{1}{N_f kT} \; \delta\left[s - \exp\left(\frac{-1}{N_f kT}\left(H(q,\tilde{p}) + \frac{p_s^2}{2Q} - H_0\right)\right)\right]. \end{aligned} \tag{3.7}$$

Substituting (3.7) into (3.6) and using the sifting property of δ we get,

$$\mathcal{N} = \frac{1}{N_f kT} \int dp_s \int d\tilde{p} \int dq \; \exp\left(\frac{-(N_f+1)}{N_f kT}\left(H(q,\tilde{p}) + \frac{p_s^2}{2Q} - H_0\right)\right). \tag{3.8}$$

Rescaling $\hat{p} = \tilde{p}\,\sqrt{N_f+1}$, $\hat{q} = q\,\sqrt{N_f+1}$ and $\hat{p_s} = p_s\,\sqrt{N_f+1}$ in (3.8),

$$\mathcal{N} = C_1 \int d\hat{p_s} \int d\hat{p} \int d\hat{q} \; \exp\left(\frac{-1}{N_f kT}\left(H(\hat{q},\hat{p}) + \frac{\hat{p_s}^2}{2Q}\right)\right), \tag{3.9}$$

where,

$$C_1 = \frac{1}{(N_f+1)^{\frac{2N_f+1}{2}} N_f kT} \exp\left(\frac{(N_f+1)H_0}{N_f kT}\right).$$

Similarly we can substitute $\tilde{p} = p/s$ into the denominator of (3.4), $\mathcal{D}$, use the equivalence relation for δ and define $\bar{p} = \tilde{p}\sqrt{N_f}$, $\bar{q} = q\sqrt{N_f}$ and $\bar{p}_s = p_s\sqrt{N_f}$ to get,

$$\mathcal{D} = C_2 \int d\bar{p}_s \int d\bar{p} \int d\bar{q}\ \exp\left(\frac{-1}{N_f kT}\left(H(\bar{q},\bar{p}) + \frac{\bar{p}_s{}^2}{2Q}\right)\right), \tag{3.10}$$

where,

$$C_2 = \frac{1}{N_f^{\frac{2N_f+1}{2}} N_f kT} \exp\left(\frac{N_f H_0}{N_f kT}\right).$$

Substituting (3.9) and (3.10) into (3.4) we get (3.3) as required. □

We note that $\exp(x) = \lim_{n\to\infty}(1+x/n)^n$. Then, in the limit $N_f \to \infty$,

$$\langle s \rangle = \exp\left(\frac{H_0}{N_f kT} - 1\right). \tag{3.11}$$

Substituting $N_f = 1$ into (3.3) gives $\langle s \rangle = \exp(H_0/kT - 1.04)$, a result close to (3.11). From this we conclude that (3.11) is a good approximation of $\langle s \rangle$ for all N_f.

We also have,

THEOREM 3.2.2 *When thermostatting with the Nosé-Poincaré method (2.17), if the system is ergodic, then the average of the quantity p_s^2/Q, will be given by,*

$$\left\langle \frac{p_s^2}{Q} \right\rangle = kT. \tag{3.12}$$

Proof If the system is ergodic, then the average of p_s^2/Q will be given by substituting p_s^2/Q for s in (3.4). In a method similar to that used above we can substitute $\tilde{p} = p/s$ and use

the equivalence relation for δ in both the denominator and numerator of the new equation. Noting that,

$$\int_{-\infty}^{\infty} \frac{p_s^2}{Q} \exp\left(-\frac{p_s^2}{2QkT}\right) dp_s = kT \int_{-\infty}^{\infty} \exp\left(-\frac{p_s^2}{2QkT}\right) dp_s, \tag{3.13}$$

the new equation reduces to (3.12). □

3.3 Frequency Domain Model of the Nosé-Poincaré method.

We would like to analyze Nosé's method to determine the optimum value of Q but, despite its apparent simplicity, Nosé's method is difficult to analyze dynamically. An alternative approach is to model the method in the frequency domain, and to do this it is necessary to use a method where the dynamics are in real time such as the Nosé-Poincaré method. By modelling the system for Q greater than its "optimum value", the value of Q at which the auxiliary variables intersect the boundary of their phase-space can be determined.

Consider a system with a Hamiltonian,

$$H_N(q,p) = \frac{p^2}{2m} + \frac{q^2}{2}. \tag{3.14}$$

The corresponding Nosé-Poincaré Hamiltonian is given by (2.17). We will assume that the fundamental frequency of the modified system is unchanged at $\omega = m^{-\frac{1}{2}}$ and that all other frequencies in p/s and q are of sufficiently small magnitude to be ignored. In addition we will assume that time averages of time derivatives vanish i.e. for $x(t)$ and time $\mathcal{T}$,

$$\langle \dot{x}(t) \rangle = \lim_{\mathcal{T}\to\infty} \frac{1}{\mathcal{T}} \int_0^{\mathcal{T}} \dot{x}(t)\, dt = \lim_{\mathcal{T}\to\infty} \left(\frac{x(\mathcal{T}) - x(0)}{\mathcal{T}}\right) = 0. \tag{3.15}$$

We can determine the average value of the oscillator kinetic term by considering the equations of motion for p_s,

$$\dot{p}_s = -\frac{\partial H_{NP}}{\partial s} = \frac{\tilde{p}^2}{m} - kT, \tag{3.16}$$

where $\tilde{p} = p/s$. Taking averages, and using our second assumption gives,

$$\left\langle \frac{\tilde{p}^2}{m} \right\rangle = kT, \tag{3.17}$$

These assumptions, and the predicted average kinetic energy, are generally observed in experiments.

We consider a harmonic oscillation and study the corresponding driven dynamics of the s, p_s variables. A harmonic vibration with average kinetic energy kT and frequency $\omega = m^{-\frac{1}{2}}$ takes the form,

$$\tilde{p} = \sqrt{2mkT}\cos(\omega t). \tag{3.18}$$

From the equation of motion for q,

$$\dot{q} = -\frac{\partial H_{NP}}{\partial p} = \frac{sp}{ms^2} = \frac{\tilde{p}}{m}, \tag{3.19}$$

we get,

$$q = \sqrt{2kT}\sin(\omega t), \tag{3.20}$$

the constant of integration being zero for the harmonic oscillator.

These equations, together with the equations of motion, can then be used to solve for p_s and s. From the equations of motion for p_s,

$$\dot{p}_s = -\frac{\partial H_{NP}}{\partial s} = \frac{\tilde{p}^2}{m} - kT = \frac{2mkT\cos^2(\omega t)}{m} - kT = kT\cos(2\omega t), \tag{3.21}$$

integrating with respect to t,

$$p_s = \int kT\cos(2\omega t)\ dt = \frac{kT\sin(2\omega t)}{2\omega} + C_1, \tag{3.22}$$

where C_1 is a constant, which can be determined as follows. From the equations of motion for s,

$$\dot{s} = \frac{\partial H_{NP}}{\partial p_s} = \frac{sp_s}{Q}, \tag{3.23}$$

which can be re-arranged as,

$$\frac{Q\dot{s}}{s} = p_s. \tag{3.24}$$

From this we can see that p_s is a time derivative and has an average of zero,

$$\langle p_s \rangle = \left\langle \frac{Q\dot{s}}{s} \right\rangle = Q\left\langle \frac{d\ln s}{dt} \right\rangle = 0, \tag{3.25}$$

from our second assumption. Hence $C_1 = 0$ giving,

$$p_s = \frac{kT\sin(2\omega t)}{2\omega}. \tag{3.26}$$

To obtain an expression for s we integrate both sides of (3.24) with respect to t to get,

$$Q\ln s = -\frac{kT\cos(2\omega t)}{4\omega^2} + C_2, \tag{3.27}$$

for constant C_2. Hence,

$$s = C_3\exp\left(-\frac{kT\cos(2\omega t)}{4Q\omega^2}\right), \tag{3.28}$$

where C_3 is a constant such that $\langle s \rangle$ satisfies (3.11). We can then show that,

$$s = A\exp\left(\frac{H_0}{kT} - 1\right)\exp\left(-\frac{kT\cos(2\omega t)}{4Q\omega^2}\right), \tag{3.29}$$

where,

$$A = \left\langle \exp\left(-\frac{kT\cos(2\omega t)}{4Q\omega^2}\right)\right\rangle^{-1}. \tag{3.30}$$

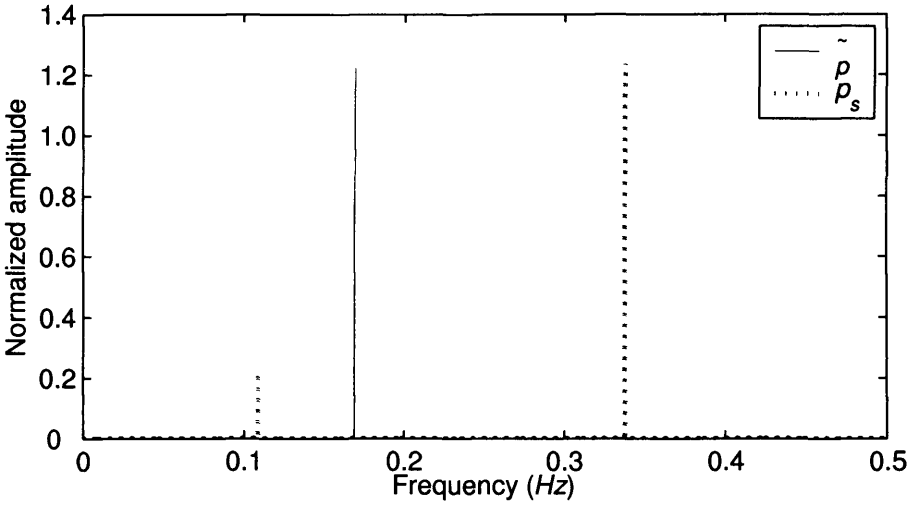

Figure 3.4: Frequency domain plot with Q=2.0. $\tilde{p}$ has a fundamental frequency of 0.167Hz as expected, and p_s has a fundamental frequency (at the 1^{st} harmonic) of 0.334Hz, as predicted in (3.26).

There is strong experimental evidence in support of this model when Q is greater than its optimum value. Figure 3.4 shows the Fourier analysis of a harmonic oscillator, with $kT = 1$, $\omega = 1$ and $Q = 2$, for $\tilde{p}$ and p_s. We note that $\tilde{p}$ has a fundamental frequency of 0.167Hz as expected, and p_s has a fundamental frequency (at the 1^{st} harmonic) of 0.334Hz as predicted by the model.

If we consider the quantity,

$$\langle |p_s| \rangle = \left\langle \left| \frac{kT sin(2\omega t)}{2\omega} \right| \right\rangle = \frac{\sqrt{2}kT}{4\omega}, \tag{3.31}$$

we get the results in Table 3.1 for simulations of 2 million steps of 0.02 which, again, shows good correlation with the predicted results.

ω	Q	Actual $\langle \lvert p_s \rvert \rangle$	Model $\langle \lvert p_s \rvert \rangle$
1	.5	.349	.354
1	1	.361	.354
$\sqrt{2}$	1	.493	.501
$\sqrt{2}$	2	.510	.501

Table 3.1: Average values for $|p_s|$ with varying Q and ω.

3.4 Estimating the Nosé Mass.

The model can be used to estimate the Nosé mass by calculating where the phase-space area occupied by the auxiliary variables interacts with the phase-space boundary, as shown in Section 3.1. For large Q we see that, from both Figure 3.1 and the model in the proceeding section (3.26)-(3.29), the maximum value of p_s occurs at the average value of s. Since the auxiliary variables phase-space is bounded by (3.2) substituting the average value of s, given by (3.11), has solutions for p_s^*, the value of p_s at the phase-space boundary,

$$p_s^* = \sqrt{2QkT}, \tag{3.32}$$

for the single harmonic oscillator ($N = 1$). To estimate the maximum value for p_s when $s = \langle s \rangle$ we will assume that p_s is scaled by some factor $a \geq 1$. Scaling (3.26) and following the methods in Section 3.3 yields the following equations for the scaled auxiliary variables,

$$p_s = \frac{akT \sin(2\omega t)}{2\omega}, \tag{3.33}$$

and,

$$s = A_a \exp\left(\frac{H_0}{kT} - 1\right) \exp\left(-\frac{akT\cos(2\omega t)}{4Q\omega^2}\right), \tag{3.34}$$

where,

$$A_a = \left\langle \exp\left(-\frac{akT\cos(2\omega t)}{4Q\omega^2}\right)\right\rangle^{-1}. \tag{3.35}$$

While the phase-space occupied by the auxiliary variables does not interact with the boundary some energy, say E_r, is retained by the system at all times and, from (3.2), the auxiliary variable phase-space is bounded by,

$$\frac{p_s^2}{2Q} + kT \ln s = E - E_r. \tag{3.36}$$

Substituting (3.33) and (3.34) into (3.36),

$$\frac{a^2(kT)^2 \sin^2(2\omega t)}{8Q\omega^2} + kT \ln A_a + E - kT - \frac{a(kT)^2 \cos(2\omega t)}{4Q\omega^2} = E - Er. \tag{3.37}$$

The $p_s^2/2Q$ term has maxima at $t = \pi/4\omega, 3\pi/4\omega, \cdots$ where the $\ln s$ term is at its average value and, conversely, the $\ln s$ term has maxima at $t = \pi/2\omega, 3\pi/2\omega, \cdots$ where $p_s^2/2Q = 0$.

From the model, where $a = 1$, (3.37) gives,

$$\max\left(\frac{p_s^2}{2Q}\right) < \max\left(kT \ln s\right). \tag{3.38}$$

As a is increased $\max\left(p_s^2/2Q\right)$ increases at a greater rate than $\max\left(kT \ln s\right)$ until it reaches the limit imposed by (3.36). The energy at the maximum points is now equal, substituting $t = \pi/4\omega$ and $t = \pi/2\omega$ into (3.37) and equating the results to find $\hat{a} = \max(a)$,

$$\frac{\hat{a}^2(kT)^2}{8Q\omega^2} = \frac{\hat{a}(kT)^2}{4Q\omega^2}, \tag{3.39}$$

with non-trivial solution,

$$\max(a) = \hat{a} = 2. \tag{3.40}$$

By examining Figure 3.5 we see that the value of E_r given by the model when $a = 2$ is correct, exactly enclosing the upper section of sampled auxiliary variable phase-space, and provides an upper bound for a. However examination of the auxiliary variable phase-space

trajectories for the model when $a = 2$ shows that for most of the trajectory the total energy would be greater than $E - E_r$, contravening (3.36). This discrepancy is related to the presence of different frequencies with small amplitude in both p_s and $\ln s$, as seen in Figure 3.4. An estimate for the upper bound, when only considering frequencies at the 2^{nd} harmonic, can be found by solving for trajectories with energy not exceeding $E - E_r$, where E_r is defined when $a = 2$. Differentiating (3.37) with respect to t to find maxima,

$$\frac{a^2(kT)^2 \sin(2\omega t)\cos(2\omega t)}{2Q\omega} + \frac{a(kT)^2 \sin(2\omega t)}{2Q\omega} = 0, \tag{3.41}$$

giving maxima at $t = \pi/2\omega, 2\pi/\omega, \cdots$ and $\cos(2\omega t) = -a^{-1}$. Substituting $\cos(2\omega t) = -a^{-1}$ into (3.37) for $\bar{a} = \max(a) < 2$ gives,

$$\frac{(\bar{a}^2 - 1)(kT)^2}{8Q\omega^2} + kT \ln A_{\bar{a}} + E - kT + \frac{(kT)^2}{4Q\omega^2} = E - E_r, \tag{3.42}$$

For this to be within the energy bound imposed by $a = 2$ we have,

$$\frac{(\bar{a}^2 - 1)(kT)^2}{8Q\omega^2} + \frac{(kT)^2}{4Q\omega^2} = \frac{(kT)^2}{2Q\omega^2}, \tag{3.43}$$

with solution,

$$\bar{a} = \sqrt{3} \approx 1.73. \tag{3.44}$$

This result provides the maximum value for a when $\ln s$ is equal to $\langle \ln s \rangle$ and, for large Q, is close to $\ln \langle s \rangle$ the point at which we require the maximum value for p_s. For smaller Q we need to correct for the additional $\ln A_a$ term. From (3.36) for $\tilde{a} = \max(a) < \sqrt{3}$,

$$\frac{\tilde{a}^2(kT)^2}{8Q\omega^2} = \frac{3(kT)^2}{8Q\omega^2} + kT \ln A_{\tilde{a}}, \tag{3.45}$$

giving,

$$\tilde{a} = \sqrt{3 + \frac{8Q\omega^2 \ln A_{\tilde{a}}}{kT}}. \tag{3.46}$$

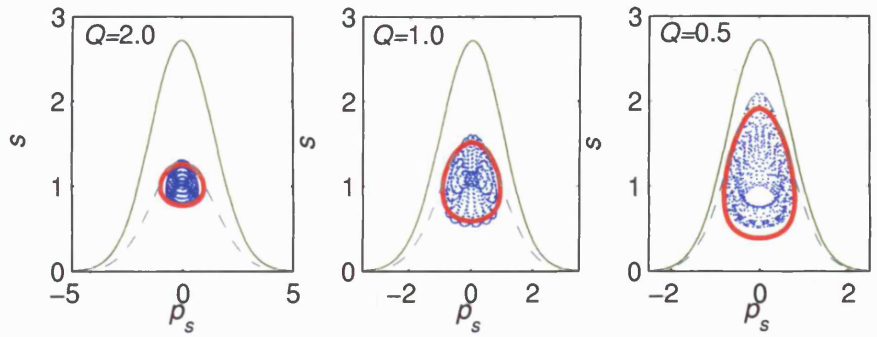

Figure 3.5: Auxiliary variable phase-space with Q=2.0, Q=1.0 and Q=0.5. Key: Actual phase-space=dots, predicted phase-space=thick solid, phase-space limit $E - E_r$=dashed, phase-space boundary=thin solid.

For $Q = 0.5$, $kT = 1$ and $\omega = 1$ we get $\tilde{a} \approx 1.54$.

Figure 3.5 shows the experimental results for a thermostatted harmonic oscillator where $kT = 1$, $\omega = 1$ and $Q = 0.5, 1.0, 2.0$, the actual measurements are the dots, the predicted phase-space is the thick solid line, the phase-space limit $E - E_r$ is the dashed line and the phase-space boundary is the thin solid line. This indicates that there is good correlation between the results predicted from the model and the actual experiments.

The maximum value of p_s from (3.44) and (3.33) is,

$$\max(p_s) \leq \frac{\bar{a}kT}{2\omega} \approx \frac{0.87kT}{\omega}. \tag{3.47}$$

The auxiliary variables will reach the boundary of phase-space when $\max p_s = p_s^*$ from (3.32),

$$Q \leq \frac{0.38kT}{\omega^2}. \tag{3.48}$$

This should be compared with Nosé's estimate in [50] of $Q = 2kT/\omega^2$. For the example of the harmonic oscillator, with $kT = 1$, $\omega = 1$, using the correction in (3.46) is $Q \approx 0.29$, which compares well with the experimentally obtained value of $Q = 0.3$ as shown in Figure

Q	$\sqrt{\frac{2gkT}{Q}}$ (Hz)	Actual (Hz)
0.005	3.3	2.8
0.01	2.3	2.0
0.02	1.7	1.4

Table 3.2: Auxiliary variable self oscillation frequency for small Q.

3.1.

3.5 Behavior of the Nosé-Poincaré method for small Q.

For small values of Q it has been observed by Hoover [30] and others that the auxiliary variables will oscillate independently of the system to be thermostatted. Under these conditions, where the frequency of the system is less than that of the auxiliary variable self oscillation frequency, Nosé's assumptions for the thermostat oscillation frequency now hold, as can be seen in Table 3.2 and Figure 3.6 for a thermostatted harmonic oscillator with $kT = 1$, $\omega = 1$. Experiments indicate that the onset of self-oscillation is typically around three times the fundamental frequency of the system, giving a very small band for the correct choice of Q, as seen in Figure 3.3. From this Figure we have $\langle p_s^2/Q \rangle \approx 0.8kT$ after the onset of self-oscillation, as Q decreases.

3.6 Thermostatting multiple oscillators.

Applying Nosé thermostats to multiple harmonic oscillators can be analyzed in a similar manner to the case of the single harmonic oscillator.

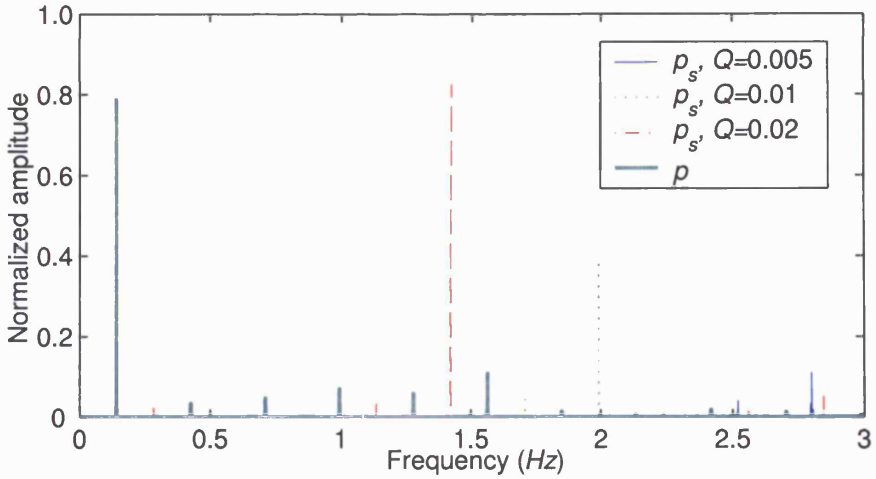

Figure 3.6: Frequency domain plot of a Nosé-Poincaré thermostatted harmonic oscillator with $\omega = 1$ (0.167Hz), for small values of Q.

It is generally assumed that the auxiliary variables will only interact with parts of the thermostatted system which have a fundamental frequency near to the self-oscillation frequency of the auxiliary variables. This is not generally the case as can be seen from Figure 3.7, a Fourier plot of the auxiliary variable when thermostatting 4 oscillators of frequencies $\omega_1 = 1.00$, $\omega_2 = 0.308$, $\omega_3 = 0.095$ and $\omega_4 = 0.052$, temperature $kT = 1$ and Nosé mass $Q = 2gkT/\omega_4^2 = 3200$ (which should resonate with oscillator 4). The magnitude of the position components for each oscillator are approximately the same, from (3.18) the magnitude of the oscillators momentum will be proportional to ω^{-1} and from (3.26) the magnitude of the component for each oscillator in the auxiliary variable momentum, p_s, will be proportional to an additional ω^{-1}, hence p_s has been scaled by ω^2. Note that, in this microcanonical experiment, each oscillator is represented by its first harmonic in the auxiliary variable momentum as predicted in the model of Section 3.3, and that the interaction with the auxiliary variables is similar for all of the oscillators.

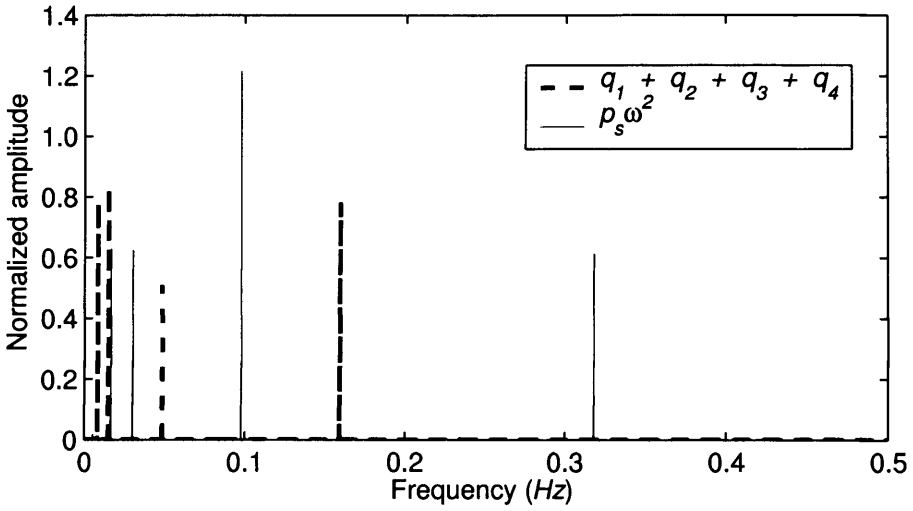

Figure 3.7: Frequency domain plot of position and scaled auxiliary variable momentum for 4 oscillators.

3.7 Extension of the model for multiple oscillators.

The model of Section 3.3 can easily be extended to multiple harmonic oscillators. Given a Hamiltonian for N oscillators,

$$\tilde{H}_{NO} = \sum_{i=1}^{N} \left(\frac{p_i^2}{2m_i} + \frac{q_i^2}{2} \right). \tag{3.49}$$

The corresponding Nosé-Poincaré Hamiltonian is given in (2.17). As before we will assume that the fundamental frequencies of the modified system are the same as those in the original system and that all other frequencies are of sufficiently small magnitude to be ignored. In addition we will assume that time averages of time derivatives vanish and that the initial energy is equally distributed between the oscillators, as expected by the equipartition theorem (see Appendix D). Then,

$$\left\langle \frac{\tilde{p}_i^{\,2}}{m_i} \right\rangle = kT \quad \forall i, \tag{3.50}$$

where $\tilde{p}_i = p_i/s$. Following the analysis as before yields,

$$\tilde{p}_i = \sqrt{2m_i kT}\cos(\omega_i t), \quad q_i = \sqrt{2kT}\sin(\omega_i t), \quad i = 1, 2, \cdots, N, \tag{3.51}$$

$$p_s = \sum_{i=0}^{N} \frac{kT\sin(2\omega_i t)}{2\omega_i}, \tag{3.52}$$

$$s = \tilde{A}\exp\left(\frac{H_0}{N_f kT} - 1\right)\prod_{i=0}^{N}\exp\left(-\frac{kT\cos(2\omega_i t)}{4Q\omega_i^2}\right), \tag{3.53}$$

where,

$$\tilde{A} = \left\langle \prod_{i=0}^{N}\exp\left(-\frac{kT\cos(2\omega_i t)}{4Q\omega_i^2}\right)\right\rangle^{-1}. \tag{3.54}$$

To estimate the optimum Nosé mass for multiple oscillators we can modify (3.47) using (3.51)-(3.53) to obtain,

$$\max(p_s) = \max\left(a\sum_{i=0}^{N}\frac{kT\sin(2\omega_i t)}{2\omega_i}\right) \leq akT\sum_{i=0}^{N}\frac{1}{2\omega_i}, \tag{3.55}$$

where $a \leq 2$ from (3.40). Solutions for p_s^*, p_s on the auxiliary variable phase-space bounding curve (3.2), when s is at an average value (3.11), are,

$$p_s^* = \sqrt{2QN_f kT}, \tag{3.56}$$

and will be the point where p_s is at its maximum. The optimum value for Q will occur when (3.55) and (3.56) are equal.

In contrast to the linearization methods found previously in the literature [50, 47], by using this new approach it is possible to estimate the Nosé mass for a system with multiple frequencies. To illustrate this we take a 3 harmonic oscillator model with arbitrarily chosen frequencies of $\omega_1 = 0.3$, $\omega_2 = 1.0$ and $\omega_3 = 2.5$, we let $kT = 1$ and integrate using the Nosé-Poincaré method for values of Q from 2 to 12. Figure 3.8 shows the auxiliary variable

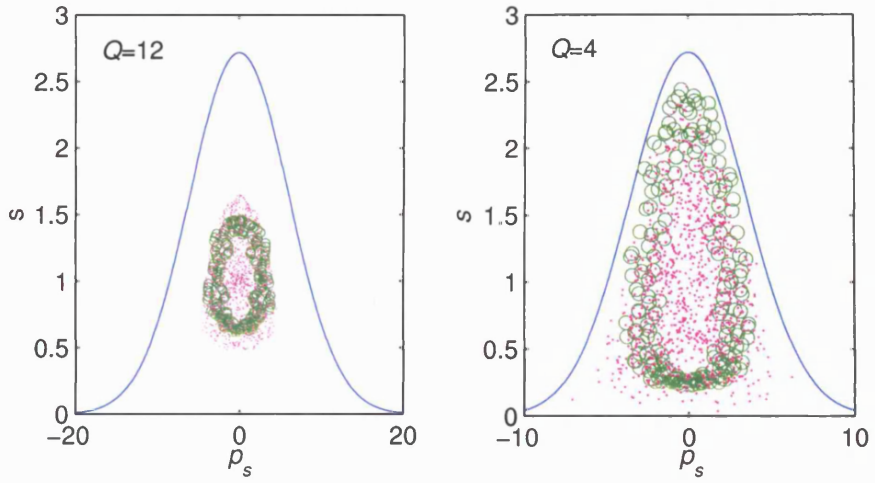

Figure 3.8: p_s,s phase-space for 3 oscillators with $\omega_1 = 0.3$, $\omega_2 = 1.0$ and $\omega_3 = 2.5$. $Q = 12$ left hand graph and $Q = 4$ right hand graph. Key: model results (circles), experimental data (dots), and the phase-space boundary (solid line).

phase-space for $Q = 12$ and $Q = 4$ where the model results are circles, experimental data are dots and the phase-space boundary is the solid line. From this we observe that there is good correlation between the experimental results and the model predictions. The optimum value of Q, from (3.55) and (3.56) with $a = 2.0$, is approximately 4, the same value which is obtained experimentally from Figure 3.9. Here values of Q from 2 to 12 are plotted against $\log(\Delta_D)$, where Δ_D is defined in (4.36) as the ℓ^2-norm of the difference between the actual and theoretical distributions, with the results showing the narrow band of possible Q values that is typical of the Nosé, Nosé-Hoover and Nosé-Poincaré methods.

For a comparison with the linearization techniques, we consider a system where all of the oscillators are of similar frequency, ω, and set $a = 2$, the upper bound for a, we have,

$$\max(p_s) \leq \frac{N_f kT}{\omega}, \tag{3.57}$$

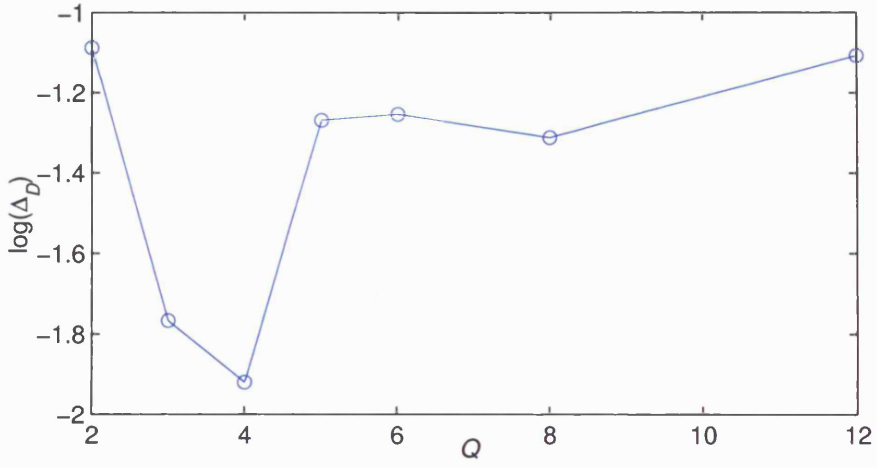

Figure 3.9: Difference between the actual and theoretical distributions, where Δ_D is defined in (4.36), with varying Q for the 3 oscillator model.

giving optimum Q,

$$Q \leq \frac{N_f kT}{2\omega^2}. \tag{3.58}$$

Compare this with Nosé's estimate $Q = 2N_f kT/\omega^2$. As before a more accurate estimate for a could be obtained, but this would only be useful for very specific cases as it is unlikely that all of the oscillators will be of exactly the same frequency.

However, if we compare the auxiliary variable phase space for 4 harmonic oscillators of different frequencies with that of the single harmonic oscillator, we see that the area of phase space used is similar in both examples, see Figure 3.10. This is expected as the probability of the entire system's energy residing in the auxiliary variables is small. It addition is shown in Section 5.1 (5.3) that if the auxiliary variables were homogeneously distributed then we would have $\langle p_s^2/Q \rangle = N_f kT$ which is contrary to both the results in Section 3.2.2 and the values predicted by the equipartition theorem (see Appendix D).

If we assume that there is no correlation between the dynamics of each body, the tra-

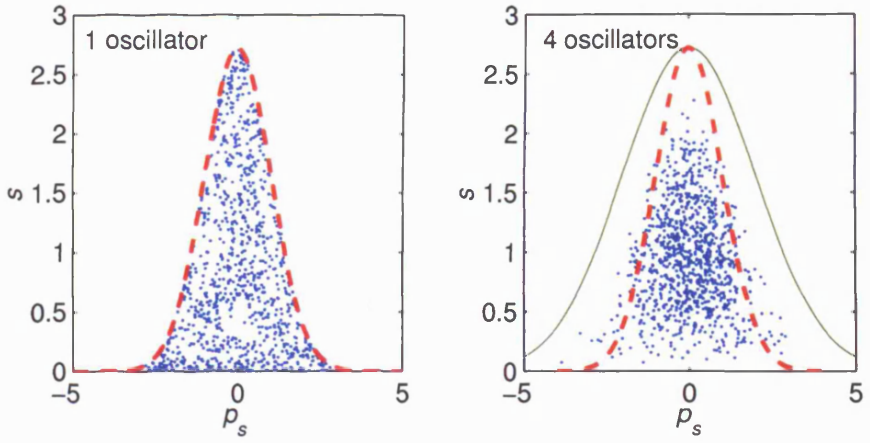

Figure 3.10: Comparison of auxiliary variable phase-space for 1 and 4 oscillators. Key: Single oscillator phase-space boundary (thick dashed line), 4 oscillator phase-space boundary (solid line).

jectories are random in relation to each other, then we can analyze this as follows. The auxiliary variable momentum, p_s is driven by the variations in the kinetic energy of the system, as we can see from its equations of motion. As the dimension, N_f, of the system increases the variations in kinetic energy will now be reduced by a factor $1/\sqrt{N_f}$ and hence the magnitude of p_s will increase by $\sqrt{N_f}$ rather than by N_f as assumed in (3.57). If we substitute $\sqrt{N_f}\tilde{p}_s = p_s$ into (3.2), where $E = \tilde{H}_0$ we get,

$$s = \exp\left(\frac{\tilde{H}_0}{N_f kT} - \frac{\tilde{p}_s^2}{2QkT}\right), \tag{3.59}$$

which coincides with both the auxiliary variable phase-space for the single harmonic oscillator, and the results obtained experimentally as shown in Figure 3.10.

For the calculation of the Nosé mass we now have, for oscillators of similar frequency close to ω,

$$\max(\tilde{p}_s) = \frac{\sqrt{N_f}kT}{\omega}, \tag{3.60}$$

and a bound on $\tilde{p}_s$ at $\langle s \rangle$ of,

$$\tilde{p}_s = \sqrt{2QkT}, \tag{3.61}$$

giving optimum $Q = N_f kT/(2\omega^2)$, the same as in (3.58). Experiments with 4-8 oscillators indicate that using the masses predicted by Nosé's linearization method do not give sampling in the canonical ensemble, the onset of this behavior occurring close to the prediction of (3.58).

Chapter 4

Hamiltonian Generalized Thermostatting Bath.

It has been observed by Hoover and others [30, 56, 24] that thermostatting small or stiff systems using Nosé and Nosé-Hoover schemes does not generally produce the correct canonical distribution. This was partially addressed by Martyna, Klein and Tuckerman [47] with the introduction of Nosé-Hoover chains. The introduction of the Nosé-Poincaré method by Bond, Laird and Leimkuhler [8], which is real-time and has a Hamiltonian, has renewed interest in Hamiltonian methods which can improve dynamical sampling. This class of methods, although applicable to small systems, has applications in large scale systems with complex chemical structure, such as protein-bath models and quantum-classical systems. As an extension to the Nosé and Nosé-Poincaré method Laird and Leimkuhler [38] have introduced the Generalized Dynamical Thermostatting Technique where a more general heat bath, produced by coupling an additional system through the thermostatting variables, is

considered. Experiments with this method, when applied to the harmonic oscillator with a box of soft spheres as the heat bath, indicate that ergodic behavior is achieved, but without reducing the dependence on the Nosé mass as is observed for the Nosé-Hoover chains method. In this chapter the Generalized Dynamical Thermostatting Technique is extended to allow multiple thermostats to interact directly with the system to be thermostatted and the Nosé-Poincaré chains method is derived.

4.1 Generalized Dynamical Thermostatting Technique.

In the Generalized Dynamical Thermostatting Technique (GDTT) [38] the Nosé Hamiltonian is coupled to an auxiliary system with position variables $\{\sigma_i\}$ and conjugate momenta $\{p_{\sigma_i}\}$, and is of the following form,

$$H_{GN} = H\left(q, \frac{p}{s}\right) + gkT \ln s + f(p_s, \{\sigma_i, p_{\sigma_i}\}),$$

where f is a continuous function that must be chosen such that it is bounded below and $\exp(-f/kT) \in L_1$. The corresponding Generalized Nosé-Poincaré Hamiltonian is then,

$$H_{GNP} = s(H_{GN} - H_0),$$

where H_0 is chosen such that $H_{GNP} = 0$ at initial conditions. It is easily shown in a manner similar to that used for the Nosé-Poincaré method, subject to the restrictions on f to insure that the integration converges, that sampling is from the canonical ensemble.

An example of this approach, when applied to a single harmonic oscillator, is to implement a box of soft spheres and use 'vertex coupling' to couple it to the thermostatted system. The addition of a box of soft spheres is motivated by the fact that ergodicity can

be proved for certain hard sphere systems, the study of which dates back to the work of Krylov [36] and Sinai [61, 62]. The extension of this work to two hard spheres in a box was undertaken by Simányi [60]. Here $\hat{H}_{GNP}$, with auxiliary system H_{BATH} and thermostat interaction H_{INT}, becomes,

$$\hat{H}_{GNP} = \left(\frac{p^2}{2s^2} + \frac{\omega^2 q^2}{2} + kT \ln s + H_{INT} + H_{BATH} - H_0 \right) s,$$

where H_0 is chosen such that $\hat{H}_{GNP} = 0$ at initial conditions and,

$$H_{INT} = \left(\sum_{i=1}^{3} |\sigma_i|^2 \right) \frac{p_s^2}{2Q},$$

$$H_{BATH} = \sum_{i=1}^{3} \frac{|p_{\sigma_i}|^2}{2Q_i} + \sum_{i=1}^{3} \left[\left(\frac{\sigma_{i,x}}{l} \right)^{12} + \left(\frac{\sigma_{i,y}}{l} \right)^{12} + \left(\frac{\sigma_{i,z}}{l} \right)^{12} \right] + \sum_{i} \sum_{j>i} |\sigma_i - \sigma_j|^{-12},$$

where l is the length of the soft cubic box, the bath positions and momenta σ_i and p_{σ_i} are vectors in $\mathbb{R}^3$ with associated scalar 'masses' Q_i, all other variables are as previously defined. Setting $Q_1 = 1$, $Q_2 = 2$, $Q_3 = 3$, $T = 1$, $\omega = 1$ and time step $\Delta t = 0.01$ gave good results, with convergence close to the canonical distribution within $2,000,000$ steps as shown in Figure 4.1. However extensive testing showed that this convergence only occurred for Q in the range $0.2 < Q < 1.2$, when re-scaled to account for the vertex coupling term. The fastest convergence occurred at $Q = 0.4$ which is close to the optimum value, derived in Section 3, of 0.3, and we note that convergence does not occur at Nosé's estimate [51] of 2.0 from (2.7). In Figure 4.1 $\log(\Delta_D)$, where Δ_D is defined in (4.36) as the ℓ^2-norm of the difference between the actual and theoretical distributions, is plotted for varying Q. From this it appears that the Generalized Dynamical Thermostatting Technique, with the this choice of heat bath, promotes ergodic behavior without reducing the dependence on the Nosé mass that is observed for the Nosé-Hoover chains method.

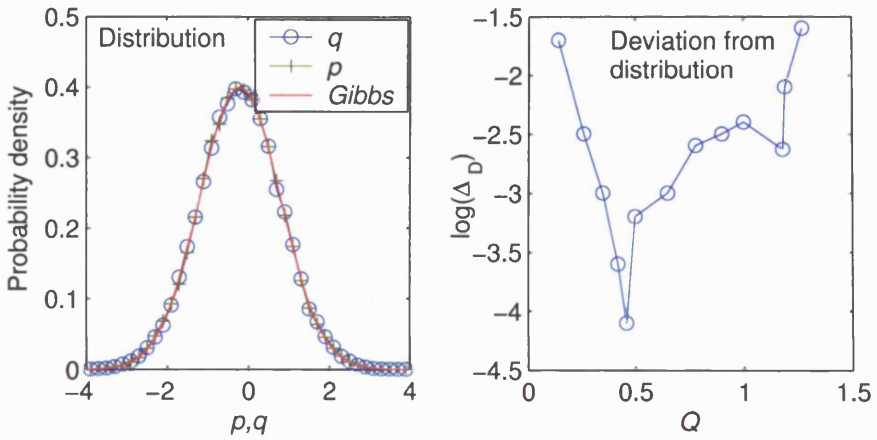

Figure 4.1: Single harmonic oscillator distributions for the GDTT method over 2,000,000 steps of 0.01 with optimum Q, and variation in the deviation from the correct distribution for varying Q where Δ_D represents difference between the actual and theoretical distributions as defined in (4.36).

4.2 Multiple Thermostat Generalized Thermostatting Bath.

Given a Hamiltonian system where $H(q,p)$ is the energy of an N-body system, $q = (q_1, q_2, \cdots, q_N)$ and $p = (p_1, p_2, \cdots, p_N)$ are the positions and momenta of the N bodies, a Hamiltonian formulation for the Multiple Thermostat Generalized Thermostatting Bath (MTGTB) class of thermostats is given by,

$$H_{GT}(q,p,s_1,s_2,\cdots,p_{s_1},p_{s_2},\cdots) = H\left(q,\frac{p}{s_{i_1}s_{i_2}\cdots}\right) + H_G(s_1,s_2,\cdots,p_{s_1},p_{s_2},\cdots), \tag{4.1}$$

where $s_1, s_2, \cdots$ are the auxiliary variables, $p_{s_1}, p_{s_2}, \cdots$ the auxiliary variables momenta, $\{s_{i_1}, s_{i_2}, \cdots\}$ is the set of auxiliary variables which scale the momenta of the original system, and H_G the part of the revised Hamiltonian which dictates the dynamics of the auxiliary variables. Since rescaling the momentum also rescales time it is appropriate to apply a time

reparametrization in the revised system using either a Sundman (as in the Nosé-Hoover formulation [30]) or Poincaré transformation as in [8] with a time reparametrization variable equal to $s_{i_1} s_{i_2} \cdots$. When there is no time rescaling, or when it is done using a Poincaré transformation, the resulting system has a Hamiltonian structure, and it is possible to show analytically that the modified system samples from the canonical ensemble subject to certain constraints. It is primarily these methods that will be considered here.

4.3 Constructing Multiple Thermostats.

It is possible to introduce additional thermostats into the Nosé and Nosé-Poincaré methods while retaining both their Hamiltonian structure and sampling from the canonical ensemble. This can be illustrated in a more general setting by rewriting the Nosé method, (2.1), to include the momenta of the thermostatting variable with the system momenta such that $\hat{p} = (p_1, p_2, \cdots, p_N, p_{N+1})$ to give,

$$\begin{aligned} H_N(q, s_1, \hat{p}) &= \hat{H}_N\left(q, \frac{p_1}{s_1}, \frac{p_2}{s_1}, \cdots, \frac{p_N}{s_1}, p_{N+1}\right) + (N_f + 1) kT \ln s_1 \\ &= \hat{H}_N(q, \hat{p}') + (N_f + 1) kT \ln s_1, \end{aligned}$$

where,

$$\hat{H}_N(q, \hat{p}) = H\left(q, p_1, p_2, \cdots, p_N\right) + \frac{p_{N+1}^2}{2Q_1},$$

and,

$$\hat{p}' = (p_1', p_2', \cdots, p_N', p_{N+1}') = \left(\frac{p_1}{s_1}, \frac{p_2}{s_1}, \cdots, \frac{p_N}{s_1}, p_{N+1}\right). \tag{4.2}$$

A second thermostat can be added as follows,

$$H_{NT}(q, s_1, s_2, \hat{p}, p_{N+2}) = \hat{H}_N\left(q, p_{j_1}', \cdots, p_{j_{N+1-M}}', \frac{p_{i_1}{}'}{s_2}, \cdots, \frac{p_{i_M}{}'}{s_2}\right)$$

$$+(N_f+1)kT\ln s_1+\frac{p_{N+2}^2}{2Q_2}+g_2kT\ln s_2+f_2(s_2),$$

where $f_2(s_2)$ is a real valued function, g_2 is a scalar and the new thermostat is applied to M of the momenta, the thermostatted set being $\{p'_{i_1},\cdots,p'_{i_M}\}$ and the non-thermostatted set being $\{p'_{j_1},\cdots,p'_{j_{N+1-M}}\}$ for some integers $i_1,\cdots,i_M$, $j_1,\cdots,j_{N+1-M}$. Note that the thermostatted set may include any of the system momenta and the thermostatting variable momenta. The partition function for this method, for energy E, is defined as,

$$Z=\frac{1}{N!h^{N_f}}\int dp_{N+2}\int ds_2\int ds_1\int d\hat{p}\int dq\;\delta\left[H_{NT}-E\right]. \tag{4.3}$$

We can substitute $p'_i=p_i/s_1\;\;1\le i\le N$, $p'_{N+1}=p_{N+1}$, the volume element then becomes $d\hat{p}=s_1^{N_f}d\hat{p}'$, where $\hat{p}'$ is defined as above. There is no upper limit in momentum space so we can change the order of integration of $d\hat{p}'$ and ds_1 giving,

$$Z\;=\;\frac{1}{N!h^{N_f}}\int dp_{N+2}\int ds_2\int d\hat{p}'\int dq\int ds_1\;s_1^{N_f}\delta\left[H_{NT}-E\right].$$

Using the equivalence relation for δ, $\delta[r(x)]=\delta[x-x_0]/|r'(x)|$, where x_0 is the zero of $r(x)=0$, for $x=s_1$, and noting that $s_1>0$ is assumed as a natural consequence of the form of the Hamiltonian, we get,

$$\begin{aligned}Z\;=\;&\frac{1}{N!h^{N_f}(N_f+1)kT}\int dp_{N+2}\int ds_2\int d\hat{p}'\\&\int dq\;\exp\left(\frac{-\left(\hat{H}_N+\frac{p_{N+2}^2}{2Q_2}+g_2kT\ln s_2+f_2(s_2)-E\right)}{kT}\right).\end{aligned}$$

We can substitute $p''_{l_1}=p'_{l_1}/s_2\;\;l_1\in\{i_1,\cdots,i_M\}$, $p''_{l_2}=p'_{l_2}\;\;l_2\in\{j_1,\cdots,j_{N+1-M}\}$ the volume element then becomes $d\hat{p}'=s_2^M d\hat{p}''$ where $\hat{p}''=(p''_1,p''_2,\cdots,p''_{N+1})$. There is no upper limit in momentum space so we can change the order of integration of $d\hat{p}''$ and ds_2

giving,

$$
\begin{aligned}
Z &= \frac{1}{N!h^{N_f}(N_f+1)kT}\int dp_{N+2}\int d\hat{p}''\int dq \\
&\qquad \int ds_2\; s_2^M \exp\left(\frac{-\left(\hat{H}_N(q,\hat{p}'')+\frac{p_{N+2}^2}{2Q_2}+g_2kT\ln s_2+f_2(s_2)-E\right)}{kT}\right), \\
&= \frac{1}{N!h^{N_f}(N_f+1)kT}\int dp_{N+2}\int d\hat{p}''\int dq\int ds_2\; s_2^{M-g_2}\exp\left(\frac{-f_2(s_2)}{kT}\right) \\
&\qquad \exp\left(\frac{-\left(\hat{H}_N(q,\hat{p}'')+\frac{p_{N+2}^2}{2Q_2}-E\right)}{kT}\right).
\end{aligned}
$$

If we chose $g_2 = M$ and suppose that,

$$\int_0^\infty \exp\left(\frac{-f_2(x)}{kT}\right)\,dx \;=\; K_2 < \infty,$$

then,

$$Z \;=\; \frac{K_2}{N!h^{N_f}(N_f+1)kT}\int dp_{N+2}\int d\hat{p}''\int dq\;\exp\left(\frac{-\left(\hat{H}_N(q,\hat{p}'')+\frac{p_{N+2}^2}{2Q_2}-E\right)}{kT}\right).$$

Integrating over both thermostat momenta, p''_{N+1} and p_{N+2}, gives,

$$Z \;=\; \frac{C}{N!h^{N_f}}\int dp''\int dq\;\exp\left(\frac{-H(q,p'')}{kT}\right),$$

where,

$$C = \frac{2\pi K_2\sqrt{Q_1Q_2}}{N_f+1}\;\exp\left(\frac{E}{kT}\right),$$

and,

$$p'' = (p_1'', p_2'', \cdots, p_N'').$$

This process can be repeated to add more thermostats, with the possibility at each stage of thermostatting the previous thermostat's momentum in addition to any of the other momenta. A similar proof can be applied to the Nosé-Poincaré variation.

4.4 Multiple Thermostat Schemes.

The general Hamiltonian for this class of methods, with M thermostats, will then be,

$$\begin{aligned} H_{NM} &= \sum_{j=1}^{N} \frac{p_j^2}{2m_j s_{k_1}^2 s_{k_2}^2 \cdots s_{k_m}^2} + V(q) + \sum_{i=1}^{M-1} \frac{p_{s_i}^2}{2Q_i \psi_i} + \frac{p_{s_M}^2}{2Q_M} \\ &\quad + gkT \ln s_1 + \sum_{i=2}^{M} (g_i kT \ln s_i + f_i(s_i)) \end{aligned} \tag{4.4}$$

where $g = N_f + 1$. The original system is thermostatted by a subset of the thermostats, $\{s_{k_1}, s_{k_2} \cdots, s_{k_m}\}$, with $\{k_1, k_2, \cdots, k_m\} \subseteq \{1, 2, \cdots, M\}$. The i^{th} thermostat is thermostatted by ψ_i defined as,

$$\psi_i = \prod_{j=1}^{n_i} s_{l_j}^2,$$

where $\{l_1, l_2, \cdots, l_{n_i}\} \subseteq \{i+1, i+2, \cdots, M\}$. g_i is the number of degrees of freedom thermostatted by the i^{th} thermostat and the auxiliary functions, $\{f_i(s_i)\}$, are real valued satisfying,

$$\int_0^\infty \exp\left(\frac{-f_i(x)}{kT}\right) dx = K_i < \infty. \tag{4.5}$$

The Nosé-Poincaré variation can be produced by applying a Poincaré time transformation to (4.4) using a time re-parametrization variable equal to $s_{k_1} s_{k_2} \cdots s_{k_m}$, and setting $g = N_f$.

We can apply this scheme to both the Nosé and Nosé-Poincaré methods, to produce thermostatting chains, by introducing additional thermostats which only control the proceeding thermostat.

4.5 Nosé chains.

Thermostatting chains, consisting of M thermostats, can be added to the Nosé equation (2.1), with some additional terms as follows,

$$\begin{aligned} H_{NC} &= H\left(q, \frac{p}{s_1}\right) + \sum_{i=1}^{M-1} \frac{p_{s_i}^2}{2Q_i s_{i+1}^2} + \frac{p_{s_M}^2}{2Q_M} + (N_f+1)kT \ln s_1 \\ &\quad + \sum_{i=2}^{M} (kT \ln s_i + f_i(s_i)), \end{aligned} \tag{4.6}$$

where the auxiliary functions $\{f_i(s_i)\}$ are real valued and satisfy (4.5).

The partition function for this ensemble, for energy E, is defined as,

$$Z = \frac{1}{N! h^{N_f}} \int dp_{s_M} \ldots \int dp_{s_1} \int ds_M \ldots \int ds_1 \int dp \int dq \; \delta\left[H_{NC} - E\right]. \tag{4.7}$$

We can substitute $p' = p/s_1$, the volume element then becomes $dp = s_1^{N_f} dp'$. There is no upper limit in momentum space so we can change the order of integration of dp' and ds_1 giving the integral over s_1 as,

$$\int ds_1 \; \delta\left(H_{NC} - E\right) = \int ds_1 \; s^{N_f} \delta \left[H\left(q, p', \hat{p}_s\right) + \sum_{i=2}^{M} F_i + (N_f+1)kT \ln s_1 - E \right],$$

where,

$$H\left(q, p', \hat{p}_s\right) = H\left(q, p'\right) + \sum_{i=1}^{M-1} \frac{p_{s_i}^2}{2Q_i s_{i+1}^2} + \frac{p_{s_M}^2}{2Q_M}, \tag{4.8}$$

$$\hat{p}_s = \left(\frac{p_{s_1}}{s_2}, \ldots, \frac{p_{s_{M-1}}}{s_M}, p_{s_M}\right), \tag{4.9}$$

and,

$$F_i = kT \ln s_i + f_i(s_i). \tag{4.10}$$

Using the equivalence relation for δ, $\delta[r(x)]) = \delta[x - x_0]/|r'(x)|$, where x_0 is the zero of $r(x) = 0$, for $x = s_1$, and noting that $s_1 > 0$ from the Hamiltonian formulation, we get,

$$\int ds_1 \; s_1^{N_f} \delta \left[H\left(q, p', \hat{p}_s\right) + \sum_{i=2}^{M} F_i + (N_f+1)kT \ln s_1 - E \right]$$

$$= \int ds_1 \frac{s^{N_f+1}}{(N_f+1)kT} \delta\left[s - \exp\left(\frac{-(H(q,p',\hat{p}_s) + \sum_{i=2}^{M} F_i - E)}{(N_f+1)kT}\right)\right]$$
$$= \frac{1}{(N_f+1)kT} \exp\left(\frac{-(H(q,p',\hat{p}_s) + \sum_{i=2}^{M} F_i - E)}{kT}\right). \quad (4.11)$$

Substituting $p'_{s_1} = p_{s_1}/s_2$, changing the order of integration, and integrating (4.11) over s_2 we get,

$$\int ds_2 \frac{s_2}{(N_f+1)kT} \exp\left(\frac{-(H(q,p',p'_{s_1},p_{s_2},\ldots,p_{s_M}) + \sum_{i=2}^{M} F_i - E)}{kT}\right)$$
$$= \frac{K_2}{(N_f+1)kT} \exp\left(\frac{-(H(q,p',p'_{s_1},p_{s_2},\ldots,p_{s_M}) + \sum_{i=3}^{M} F_i - E)}{kT}\right), \quad (4.12)$$

where K_2 is defined in (4.5). Repeating this for $s_3, \ldots, s_M$ gives,

$$\int ds_M \ldots \int ds_1 \, \delta\left[H(q,p,\hat{p}_s) + \sum_{i=2}^{M} F_i + (N_f+1)kT \ln s_1 - E\right]$$
$$= \frac{\Pi_{j=2}^{M} K_j}{(N_f+1)kT} \exp\left(\frac{-\left(H\left(q,p',p'_{s_1},p'_{s_2},\ldots,p'_{s_{M-1}},p_{s_M}\right) - E\right)}{kT}\right). \quad (4.13)$$

Changing the order of integration and integrating (4.13) over all p'_{s_i} and p_{s_M} gives,

$$\int p_{s_M} \int p'_{s_{M-1}} \cdots \int p'_{s_1} \frac{\Pi_{j=2}^{M} K_j}{(N_f+1)kT} \exp\left(\frac{-\left(H\left(q,p',p'_{s_1},\ldots,p'_{s_{M-1}},p_{s_M}\right) - E\right)}{kT}\right)$$

$$= \frac{\pi^{\frac{M}{2}} (kT)^{\frac{M}{2}-1} \Pi_{i=1}^{M} Q_i^{\frac{1}{2}} \Pi_{j=2}^{M} K_j}{(N_f+1)} \exp\left(\frac{-(H(q,p') - E)}{kT}\right)$$
$$= C_{NC} \exp\left(\frac{-H(q,p')}{kT}\right), \quad (4.14)$$

where,

$$C_{NC} = \frac{\pi^{\frac{M}{2}} (kT)^{\frac{M}{2}-1} \Pi_{i=1}^{M} Q_i^{\frac{1}{2}} \Pi_{j=2}^{M} K_j}{(N_f+1)} \exp\left(\frac{E}{kT}\right).$$

Then,

$$Z = \frac{C_{NC}}{N! h^{N_f}} \int dp' \int dq \, \exp\left(\frac{-H(q,p')}{kT}\right). \quad (4.15)$$

This means that constant energy dynamics of the extended Hamiltonian H_{NC} correspond to constant temperature dynamics of $H(q, p/s_1)$.

4.6 Nosé-Poincaré chains.

In a similar manner, thermostatting chains, consisting of M thermostats, can be added to the Nosé-Poincaré equation (2.17), with some additional terms as follows,

$$\begin{aligned} H_{NPC} &= s_1 \left(H\left(q, \frac{p}{s_1}\right) + \sum_{i=1}^{M-1} \frac{p_{s_i}^2}{2Q_i s_{i+1}^2} + \frac{p_{s_M}^2}{2Q_M} + N_f kT \ln s_1 \right. \\ &\quad \left. + \sum_{i=2}^{M} (kT \ln s_i + f_i(s_i)) - H_0 \right), \end{aligned}$$

where the auxiliary functions $\{f_i(s_i)\}$ are real valued and satisfy equation (4.5), and H_0 is equation (4.6) evaluated at the initial conditions.

The partition function for this ensemble is defined as,

$$Z = \frac{1}{N! h^{N_f}} \int dp_{s_M} \ldots \int dp_{s_1} \int ds_M \ldots \int ds_1 \int dp \int dq \; \delta \left[H_{NPC} - 0 \right]. \tag{4.16}$$

Substituting $p' = p/s_1$, the volume element then becomes $dp = s_1^{N_f} dp'$. There is no upper limit in momentum space so we can change the order of integration of dp' and ds_1 giving the integral over s_1 as,

$$\int ds_1 \; \delta \left(H_{NPC} \right) = \int ds_1 \; s_1^{N_f} \delta \left[s_1 \left(H\left(q, p', \hat{p}_s\right) + \sum_{i=2}^{M} F_i + N_f kT \ln s_1 - H_0 \right) \right],$$

where $H\left(q, p', \hat{p}_s\right)$, $\hat{p}_s$ and F_i are defined in equations (4.8)-(4.10). Using the equivalence relation for δ, $\delta[r(x)] = \delta[x - x_0]/|r'(x_0)|$, where x_0 is the zero of $r(x) = 0$, for $x = s_1$, to

get,

$$\int ds_1 \; s_1^{N_f} \delta \left[s_1 \left(H\left(q,p',\hat{p}_s\right) + \sum_{i=2}^{M} F_i + N_f kT \ln s_1 - H_0 \right) \right]$$

$$= \int ds_1 \; \frac{s_1^{N_f}}{N_f kT} \; \delta \left[s_1 - \exp\left(\frac{-(H\left(q,p',\hat{p}_s\right) + \sum_{i=2}^{M} F_i - H_0)}{N_f kT} \right) \right]$$

$$= \frac{1}{N_f kT} \exp\left(\frac{-(H\left(q,p',\hat{p}_s\right) + \sum_{i=2}^{M} F_i - H_0)}{kT} \right).$$

The remaining thermostatting variables can be integrated out as above in equations (4.12)-(4.15) to get the partition function,

$$Z = \frac{C_{NPC}}{N! h^{N_f}} \int dp' \int dq \; \exp\left(\frac{-H(q,p')}{kT} \right), \tag{4.17}$$

where,

$$C_{NPC} = \frac{\pi^{\frac{M}{2}} (kT)^{\frac{M}{2}-1} \Pi_{i=1}^{M} Q_i^{\frac{1}{2}} \Pi_{j=2}^{M} K_j}{N_f} \exp\left(\frac{H_0}{kT} \right).$$

4.7 Auxiliary Function.

For the Nosé-chains to work correctly an auxiliary function, $f_i(s_i)$, must be chosen not only to satisfy equation (4.5) but to provide a suitable modification to the thermostats. One such choice is,

$$f_i(s_i) = \frac{(a_i - s_i)^2}{2C_i}, \tag{4.18}$$

where C_i, the auxiliary function coefficient, is a constant. The value a_i is chosen as the required average value of s_i, generally 1, as the additional term will operate as a negative feedback loop to minimize $(a_i - s_i)$, as can be seen from the equations of motion. For a Hamiltonian of the form,

$$H = \sum_{i=1}^{N} \frac{p_i^2}{2m_i} + V(q),$$

the equations of motion for s_i and p_{s_i} in the equivalent Nosé-chain system will be,

$$\begin{aligned} \dot{p}_{s_i} &= \frac{p_{s_{i-1}}^2}{Q_{i-1}s_i^3} - \frac{kT}{s_i} + \frac{a_i - s_i}{C_i}, \\ \dot{s}_i &= \frac{p_{s_i}}{Q_i s_{i+1}^2}. \end{aligned}$$

If C_i is sufficiently small, if s_i increases above a_i then p_{s_i} will decrease, eventually decreasing s_i. Conversely, if s_i decreases below a_i then p_{s_i} will increase, eventually increasing s_i.

4.8 Estimation of the Auxiliary Function Coefficient.

The value of C_i, $i \geq 2$ can be estimated by considering the equation of motion for the momenta of one of the thermostats, s_i,

$$\dot{p}_{s_i} = \frac{p_{s_{i-1}}^2}{Q_{i-1}s_i^3} - \frac{kT}{s_i} + \frac{a_i - s_i}{C_i}. \tag{4.19}$$

Then the changes in s_i are driven by the changes in $p_{s_{i-1}}$. The purpose of the auxiliary function is to limit the excursions of s_i, which can be achieved if ds_i/dp_{s_i} is a maximum at $s_i = a_i$. The negative feedback loops arising in Nosé dynamics drive $\langle \dot{p}_{s_i} \rangle$ to zero, in the above equation, over a sufficiently long integration time. For the purpose of estimating the value of C_i, we will assume that $\dot{p}_{s_i}$ is small. Then, from equation (4.19),

$$p_{s_{i-1}} \approx \sqrt{Q_{i-1}\left(kTs_i^2 - \frac{a_i s_i^3}{C_i} + \frac{s_i^4}{C_i}\right)}, \tag{4.20}$$

differentiating with respect to s_i,

$$\frac{dp_{s_{i-1}}}{ds_i} \approx \frac{Q_{i-1}\left(2kTs_i - 3\frac{a_i s_i^2}{C_i} + 4\frac{s_i^3}{C_i}\right)}{2\sqrt{Q_{i-1}\left(kTs_i^2 - \frac{a_i s_i^3}{C_i} + \frac{s_i^4}{C_i}\right)}}. \tag{4.21}$$

Differentiating again to get the turning points, and substituting $s_i = a_i$,

$$\frac{d^2 p_{s_{i-1}}}{ds_i^2} \approx \frac{Q_{i-1}^{\frac{1}{2}} a_i (8kTC_i - a_i^2)}{4(kT)^{\frac{3}{2}} C_i^2}. \tag{4.22}$$

Putting $d^2 p_{s_{i-1}}/ds_i^2 = 0$ and solving for C_i gives,

$$C_i \approx \frac{a_i^2}{8kT}. \tag{4.23}$$

Evaluating $d^3 p_{s_{i-1}}/ds_i^3$ at this point gives a positive value, indicating a minimum for $dp_{s_{i-1}}/ds_i$ or a maximum for $ds_i/dp_{s_{i-1}}$ as required.

Experimental data from tests with the harmonic oscillator, with $a_i = 1$, show that Nosé chains will not work with $C_i > 1/8kT$, but will work for all $C_i < 1/8kT$. However, with very small values of C_i the additional thermostats become ineffective as s_i is restricted to a value close to 1, as shown in the second experiment of Section 4.10.

4.9 Hamiltonian Splitting Method for Nosé-Poincaré chains.

The numerical methods used for the following experiments are based on the following general Hamiltonian,

$$H = \sum_{i=1}^{N} \frac{p_i^2}{2m_i} + V(q).$$

The Nosé-chains method derived from this, with M thermostats based on the auxiliary function in equation (4.18) is then,

$$\begin{aligned} H_{NC} \;=\; & \sum_{i=1}^{N} \frac{p_i^2}{2m_i s_1^2} + V(q) + \sum_{j=1}^{M-1} \frac{p_{s_j}^2}{2Q_j s_{j+1}^2} + \frac{p_{s_M}^2}{2Q_M} \\ & + gkT \ln s_1 + \sum_{j=2}^{M} \left(kT \ln s_j + \frac{(a_j - s_j)^2}{2C_j} \right), \end{aligned}$$

giving a Nosé-Poincaré-chains method,

$$H_{NPC} = s_1 \left[H_{NC} - H_0 \right],$$

where H_0 is chosen as the initial value of H_{NC} and setting $g = N_f$. The equations of motion are,

$$\begin{aligned}
\dot{q}_i &= \frac{p_i}{m_i s_1}, & \dot{\tilde{p}}_i &= -s_1 \frac{\partial V(q)}{\partial q_i}, \\
\dot{s}_1 &= \frac{s_1 p_{s_1}}{Q_1 s_2^2}, & \dot{p}_{s_1} &= \sum_{i=1}^{N} \frac{p_i^2}{m_i s_1^2} - N_f kT \\
& & & \quad - H_{NC}(q, \tilde{p}, s, p_s) + H_0, \\
\dot{s}_j &= \frac{s_1 p_{s_j}}{Q_j s_{j+1}^2}, & \dot{p}_{s_j} &= s_1 \left(\frac{p_{s_{j-1}}^2}{Q_{j-1} s_j^3} - \frac{kT}{s_j} + \frac{a_j - s_j}{C_j} \right), \\
& & & \quad j = 2, \ldots, M-1, \\
\dot{s}_M &= \frac{s_1 p_{s_M}}{Q_M}, & \dot{p}_{s_M} &= s_1 \left(\frac{p_{s_{M-1}}^2}{Q_{M-1} s_M^3} - \frac{kT}{s_M} + \frac{a_M - s_M}{C_M} \right),
\end{aligned}$$

where $s = (s_1, \ldots, s_M)$, $p_s = (p_{s_1}, \ldots, p_{s_M})$ and $p = \tilde{p}/s_1$. The thermostats have introduced an implicit coupling into the equations of motion, but an explicit method can be formulated by splitting the Hamiltonian and corresponding Liouville operator. For an odd number of thermostats, M, this can be reduced to three Hamiltonians by employing even-odd splitting of the extended variables. Then if,

$$H = H_1 + H_2 + H_3,$$

we have,

$$H_1 = s_1 \left[\sum_{i=1}^{N} \frac{p_i^2}{2 m_i s_1^2} + \sum_{i=1}^{\frac{M-1}{2}} \frac{p_{s_{2i}}^2}{2 Q_{2i} s_{2i+1}^2} + N_f kT \ln s_1 \right.$$

$$+\sum_{i=1}^{\frac{M-1}{2}}\left(kT\ln s_{2i+1}+\frac{(a_{2i+1}-s_{2i+1})^2}{2C_{2i+1}}\right)\Bigg],$$

$$H_2 = s_1\left[\frac{p_{s_1}^2}{2Q_1 s_2^2}-H_0\right],$$

$$H_3 = s_1\Bigg[V(q)+\sum_{i=2}^{\frac{M-1}{2}}\frac{p_{s_{2i-1}}^2}{2Q_{2i-1}s_{2i}^2}+\frac{p_{s_M}^2}{2Q_M}$$
$$+\sum_{i=1}^{\frac{M-1}{2}}\left(kT\ln s_{2i}+\frac{(a_{2i}-s_{2i})^2}{2C_{2i}}\right)\Bigg].$$

Using a symmetric splitting of the Liouville operator to get a symplectic and time reversible method,

$$iL_H = \{.,H\} = \{.,H_1\}+\{.,H_2\}+\{.,H_3\}$$
$$= iL_{H_1}+iL_{H_2}+iL_{H_3}.$$

This splitting introduces an error of order Δt^3 at each step in terms of the solution operator, giving a second order method,

$$\Psi_H(\Delta t) = e^{iL_H\Delta t},$$
$$= e^{iL_{H_3}\frac{\Delta t}{2}}e^{iL_{H_2}\frac{\Delta t}{2}}e^{iL_{H_1}\Delta t}e^{iL_{H_2}\frac{\Delta t}{2}}e^{iL_{H_3}\frac{\Delta t}{2}}$$
$$+O(\Delta t^3).$$

The dynamics for H_1 and H_3 can be solved in a straightforward manner as each s_i and p_{s_i} are decoupled, leaving H_2 to be solved either analytically or by using the generalized leapfrog algorithm [8, 6].

When the time transformation is dependent on a reduced number of phase-space variables, such as s in this case, a novel approach towards developing an explicit method for H_2

appeared in the paper by Bond, Laird and Leimkuhler [8] and is reproduced in Appendix A.1.

4.10 Harmonic Oscillator experiments.

The Harmonic Oscillator is generally regarded as one of the hardest models to thermostat and as such is a good test for these methods. The Hamiltonian for the test system is,

$$H = \frac{p^2}{2m} + \frac{q^2}{2},$$

giving the Nosé-Poincaré-chains method,

$$\begin{aligned} H_{NPC} \;=\; s_1 \Bigg[& \frac{p^2}{2ms_1^2} + \frac{q^2}{2} + \sum_{j=1}^{M-1} \frac{p_{s_j}^2}{2Q_j s_{j+1}^2} \\ & + \frac{p_{s_M}^2}{2Q_M} + kT \ln s_1 \\ & + \sum_{j=2}^{M} \left(kT \ln s_j + \frac{(a_j - s_j)^2}{2C_j} \right) - H_0 \Bigg]. \end{aligned}$$

Using $\triangle t = 0.05$, $m = 1.0$, $Q_1 = 1.0$, $Q_2 = 3.0, \ldots, Q_M = 3.0$, $C_2 = 0.08 = 1/12kT, C_3 = 0.04, C_4 = 0.02, C_5 = 0.01$, $kT = 1.0$, $M = 5$, $a_2 = \cdots = a_M = 1$ produced good results with convergence close to the canonical distribution in 500,000 steps as shown in Figures 4.2 and 4.3.

To illustrate the importance of the correct selection of thermostatting parameters, and the improvements obtained using thermostatting chains, further experiments were carried out. When very small values are used for the C_i, the thermostats are forced to be close to 1, preventing them from operating and producing distributions that would normally be

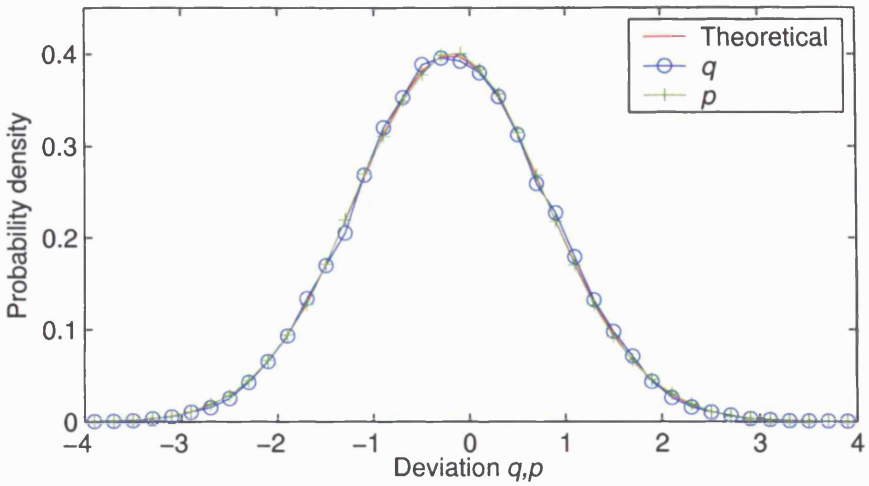

Figure 4.2: Distribution for position/momentum. Nosé-Poincaré chains with optimum auxiliary function coefficients.

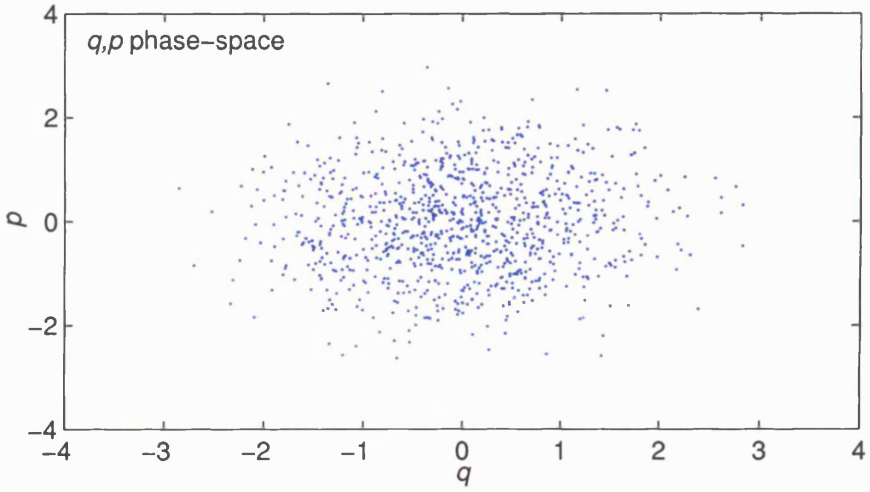

Figure 4.3: q,p phase-space. Nosé-Poincaré chains with optimum auxiliary function coefficients.

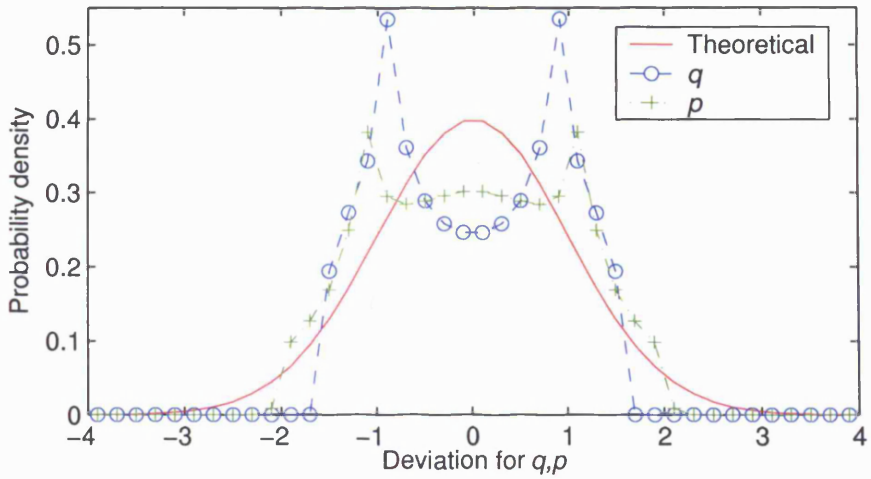

Figure 4.4: Distribution for position/momenta. Nosé-Poincaré chains, small auxiliary function coefficients.

expected from the standard Nosé or Nosé-Poincaré methods, without thermostatting chains, for the Harmonic oscillator. With the parameters the same as the above experiment except $\triangle t = 0.01, C_2 = 0.0008, C_3 = 0.0004, C_4 = 0.0002, C_5 = 0.0001$ gave the results in Figures 4.4 and 4.5.

As we can see from the first example, it is possible to implement an efficient canonical sampling with the chain technique, while using symplectic integrators.

4.11 Estimating Thermostat Self-Oscillation Frequency.

The dependence of the thermostat's self-oscillation frequencies on the thermostatting masses, Q_j, can be estimated by simplifying the equations of motion to decouple the thermostats, the resulting equations can then be linearized to evaluate their behavior near to a point of equilibrium. When calculating the masses for Nosé-Hoover chains [47] it is assumed that adjacent thermostats are slow in comparison to the thermostat of interest, average val-

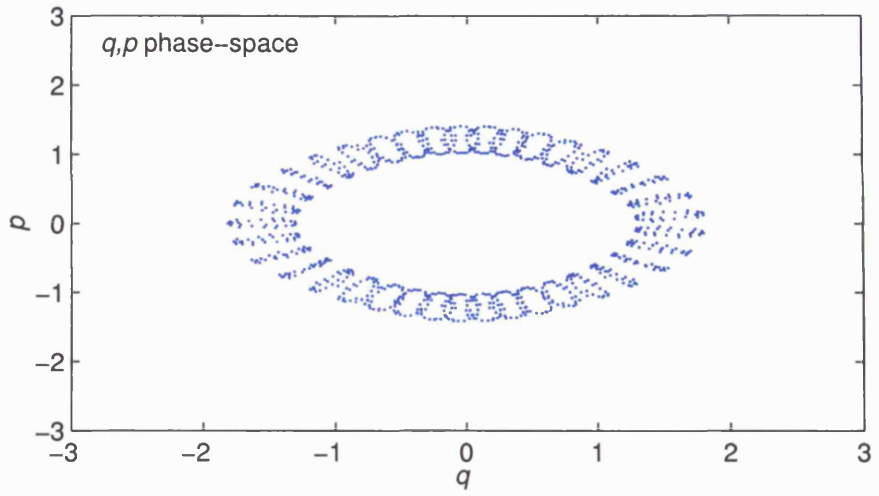

Figure 4.5: q,p phase-space. Nosé-Poincaré chains, small auxiliary function coefficients.

ues can then be used for $s_{j-1}, s_{j+1}, p_{s_{j-1}}, p_{s_{j+1}}$. Under these conditions, the analysis for the Nosé-Poincaré chains is similar to that provided by Nosé [52] *provided that we also consider the variation in* s_1 *to be slow*, in order that we can replace it with its average value, for all but the first thermostat. For Nosé-Poincaré chains the equations of motion for s_j, p_{s_j} for $1 < j \leq M$ are,

$$\dot{s}_j = \frac{s_1 p_{s_j}}{Q_j s_{j+1}^2}, \tag{4.24}$$

$$\dot{p}_{s_j} = s_1 \left(\frac{p_{s_{j-1}}^2}{Q_{j-1} s_j^3} - \frac{kT}{s_j} + \frac{a_j - s_j}{C_j} \right). \tag{4.25}$$

Rearranging and differentiating (4.24), then substituting into (4.25),

$$\frac{d(Q_j s_{j+1}^2 \dot{s}_j)}{dt} = s_1^2 \left(\frac{p_{s_{j-1}}^2}{Q_{j-1} s_j^3} - \frac{kT}{s_j} + \frac{a_j - s_j}{C_j} \right). \tag{4.26}$$

We will consider a fluctuation δs_j of s_j around an average $\langle s_j \rangle$,

$$s_j = \langle s_j \rangle + \delta s_j. \tag{4.27}$$

Linearizing (4.26) to obtain an equation for δs,

$$\begin{aligned}\frac{d}{dt}(Q_j s_{j+1}^2 \dot{\delta s_j}) &= s_1^2 \left[\frac{p_{s_{j-1}}^2}{Q_{j-1}\langle s_j \rangle^3} \left(1 - 3\frac{\delta s_j}{\langle s_j \rangle}\right) \right. \\ &\quad - \frac{kT}{\langle s_j \rangle}\left(1 - \frac{\delta s_j}{\langle s_j \rangle}\right) \\ &\quad \left. + \frac{a_j - \langle s_j \rangle - \delta s_j}{C_j} \right]. \end{aligned} \tag{4.28}$$

If the change in s_j is much faster than the rest of the system, then the change of the momentum can be ignored as the constant temperature is maintained by s_j, then,

$$\begin{aligned}\frac{p_{s_{j-1}}^2}{Q_{j-1}\langle s_j \rangle^3} &= \frac{kT}{\langle s_j \rangle} - \frac{a_j - \langle s_j \rangle}{C_j}, \\ &= \frac{kT}{\langle s_j \rangle}, \end{aligned} \tag{4.29}$$

since a_j is chosen as $\langle s_j \rangle$, as discussed in section 4.7. Substituting (4.29) into (4.28), expanding the left hand side and substituting $\langle s_j \rangle = a_j$, $\langle s_{j+1} \rangle = a_{j+1}$, $s_1 \approx \langle s_1 \rangle$, we get,

$$\ddot{\delta s_j} = -\frac{\langle s_1 \rangle^2}{Q_j a_{j+1}^2}\left(\frac{2kT}{a_j^2} + \frac{1}{C_j}\right)\delta s_j, \tag{4.30}$$

giving a self-oscillation frequency, w_j, of,

$$w_j = \left(\frac{\langle s_1 \rangle^2}{Q_j a_{j+1}^2}\left(\frac{2kT}{a_j^2} + \frac{1}{C_j}\right)\right)^{\frac{1}{2}}. \tag{4.31}$$

Since we normally choose $a_j = 1$, $j \neq 1$, (4.31) reduces to the more general form,

$$w_j = \left(\langle s_1 \rangle^2 \left(\frac{2kT}{Q_j} + \frac{1}{Q_j C_j}\right)\right)^{\frac{1}{2}}. \tag{4.32}$$

For the remaining thermostat's variables, s_1 and p_{s_1}, the equations of motion are,

$$\dot{s}_1 = \frac{s_1 p_{s_1}}{Q_1 s_2^2}, \tag{4.33}$$

$$\dot{p}_{s_1} = s_1\left(\sum_{i=1}^{N} \frac{p_i^2}{m_i s_1^3} - \frac{N_f kT}{s_1}\right). \tag{4.34}$$

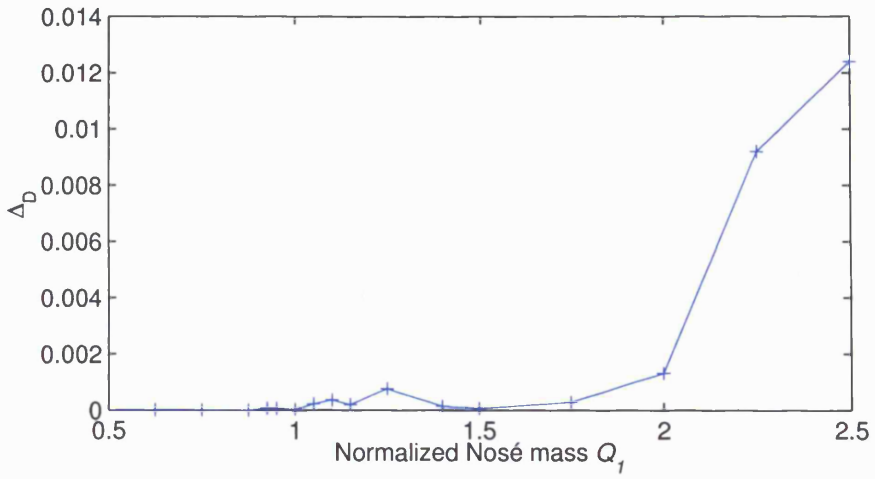

Figure 4.6: Deviation from the correct distribution, where Δ_D is defined in (4.36), with varying Nosé mass.

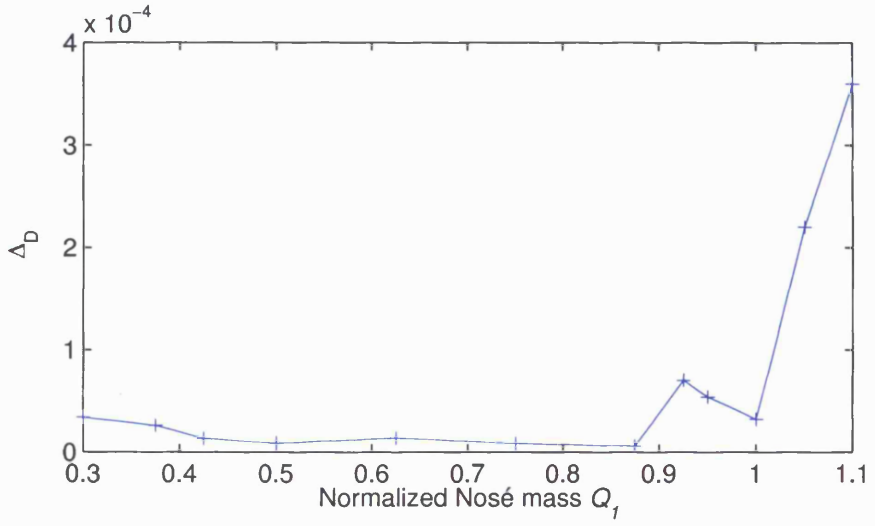

Figure 4.7: Deviation from the correct distribution, where Δ_D is defined in (4.36), with varying Nosé mass (expanded scale).

Following a similar procedure to that above gives a self-oscillation frequency, where $a_2 = 1$, of,

$$w_1 = \left(\frac{2N_f kT}{Q_1}\right)^{\frac{1}{2}}, \tag{4.35}$$

which is of the form familiar from Nosé's paper [52].

4.12 Optimum Thermostat Masses.

To evaluate the relationship between the self-oscillation frequencies and the optimum choice of the Nosé and auxiliary masses, experiments were carried out to assess the deviation from the required q distribution with varying masses. The q distribution is determined by grouping the data into 250 bins covering the range $-5 \leq q \leq 5$ and the deviation from the correct distribution is defined as the ℓ^2-norm of the difference between the measured and theoretical probability densities for each bin,

$$\Delta_D = \left(\sum_{i=1}^{250} \left(\frac{b_i}{nw} - P(x_i) \right)^2 \right)^{\frac{1}{2}}, \tag{4.36}$$

where x_i is the class mark and b_i the bin value for the i^{th} bin, n is the total number of samples, w is the class interval and $P(x_i) = (2\pi kT)^{-\frac{1}{2}} \exp(-x_i^2/(2kT))$ for the harmonic oscillator. The experiments were based on the harmonic oscillator model with frequency 1.0, auxiliary function coefficient $C_2 = 0.08$, $a_2 = 1$, and having two thermostats, the original Nosé thermostat and one auxiliary thermostat. The initial conditions were chosen such that the average value of the Nosé variable s_1 was 1.0 and the results were taken after $5,000,000$ steps, with a step size of 0.005.

In the first experiment the auxiliary thermostat mass was chosen to have a self-oscillation frequency equal to that of the harmonic oscillator and the Nosé thermostat was varied over a range of values, producing the results in figures 4.6 and 4.7. Here Q_1 has been normalized so that 1.0 is the value given by equation (4.35). These indicate that there is a broad choice of Nosé mass, in contrast to the results obtained for the auxiliary heat bath method [38], with possible values ranging from $0.01 < Q_{SO} < 2$, where Q_{SO} is the value for Q when the

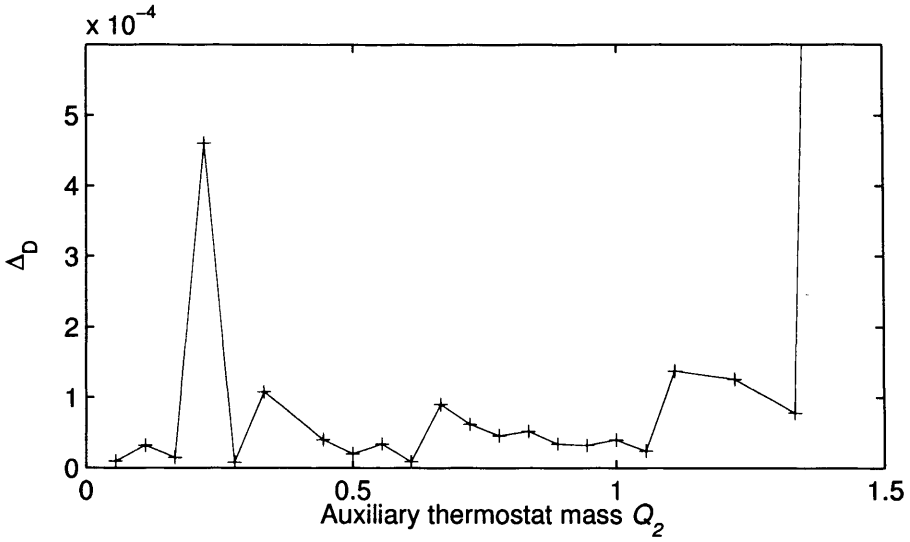

Figure 4.8: Deviation from the correct distribution, where Δ_D is defined in (4.36), with varying auxiliary thermostat mass.

thermostat's self-oscillation frequency coincides with the oscillator frequency. These results are consistent with those obtained when using Nosé-Hoover chains, both of these methods appear to suppress the thermostat oscillating as a single mode for small Q.

For the second experiment the Nosé mass was fixed at half that of its self-oscillation frequency and the mass of the auxiliary thermostat was varied, giving the results in figure 4.8. Here Q_2 has been normalized so that 1.0 is the value given by equation (4.32) and Δ_D is defined in (4.36). Again, good results are obtained over a large range of values.

Since the Nosé-Poincaré method is Hamiltonian based Theorem 3.2.1 allows the value of $\langle p_s^2/Q \rangle$ to be determined, if we assume that the system is ergodic. Comparing the ergodic value of kT with that obtained in experiments with varying values of Q gives a good indication of the range of acceptable values. In Figure 4.9, $\langle p_s^2/Q \rangle$ is plotted against Q for a Nosé-Poincaré chains integrator consisting of 5 thermostats with $Q_j = 2Q$ and $C_j = 0.08$ where $kT = 1$. From this we see that the range of Q is increased and that

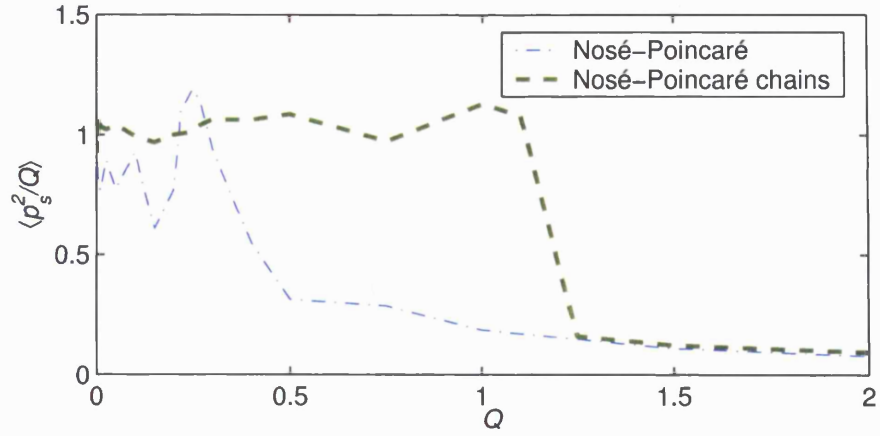

Figure 4.9: $\langle p_s^2/Q \rangle$ for Q in the range 0.001-2.

chains can also limit the activity of the auxiliary variables, preventing them from entering self-oscillation. There is also good correlation between these results and the range of Q, determined by the mean square difference between the actual and theoretical distributions, from above.

4.13 Limitations of Nosé-Poincaré chains.

Section 2.1 raises stability issues for methods without time reparamiterization for the single harmonic oscillator. The i^{th} thermostat variable s_i has a momentum term, from the Hamiltonian, of,

$$\frac{s_1 p_{s_i}^2}{2Q_i s_{i+1}^2}. \tag{4.37}$$

From this we see that for the i^{th} thermostat, time is re-scaled by $(s_{i+1})^{-1}$ in addition to the overall time transformation based on the first thermostat s_1. Studying the phase-space portrait for the $(i+1)^{th}$ thermostat shows that small values of s_{i+1} occur, which is equivalent to large time steps in the numerical method for the preceding thermostat, s_i.

To guarantee stability for integration times of over 100 million steps in the single harmonic oscillator model, with $\omega = 1$ and using the method in Appendix 4.9, requires step-sizes of $\Delta t < 0.002$. This is considerably less than $\Delta t = 0.02$, required for the same model using the Nosé-Poincaré method.

In Section 5.1 it is shown that, for an ergodic system, $\langle p_{s_i}^2/(Q_i s_{i+1}^2)\rangle = kT$, as expected. However, due the the small dimension of sub-system that each additional thermostat is required to control, this may not be achievable. Experiments utilizing a Nosé-Poincaré chains integrator consisting of 5 thermostats with $Q_i = 2Q$ and $C_i = 0.08$ where $kT = 1$, integrated over 20,000,000 steps of 0.01 gave the averages in Table 4.1, all of which should be equal to $kT = 1$. Even if the dimension of the underlying system is increased this problem persists, hence the system is not ergodic and the proof of sampling from the canonical ensemble is invalid.

In this section we have seen that the implementation of Nosé-Poincaré chains can provide significant improvements in the ergodicity of systems such as the harmonic oscillator and, in addition, this fully Hamiltonian method allows the use of symplectic integrators for improved behavior over long integration times. Limitations due to the evolution in virtual time for each thermostat, and the small dimensional subsystem that each additional thermostat controls, means that some caution should be exercised when using this method.

i	$\langle p_{s_i}^2/(Q_i s_{i+1}^2)\rangle$
1	0.987
2	0.678
3	0.543
4	0.484
5	0.525

Table 4.1: Average values for $p_{s_i}^2/(Q_i s_{i+1}^2)$ using Nosé-Poincaré Chains.

Chapter 5

Recursive Nosé/Nosé-Poincaré Thermostats.

The seminal paper by Nosé [50] established, for thermostatted systems, the thermostat self-oscillation equation $\omega_N = (2gkT/Q)^{\frac{1}{2}}$, and it is observed for harmonic systems of frequency ω that the optimum Q is proportional to gkT/ω^2, perpetuating the viewpoint that the self-oscillation frequency should coincide with some frequency within the system. From the analysis in Chapter 3 we see that the correct choice of Q occurs where the auxiliary variables approach their phase-space boundary and expected averages, with the derived equation for Q satisfying the observed proportionality from above. Since obtaining the expected ergodic averages is dependent on the choice of Q the effectiveness of the approach of Martyna, Klein and Tuckerman [47] in achieving the correct 'kinetic' averages for the first thermostat, and the method's insensitivity to the value of Q, is now understood. The Nosé-Poincaré chains method, introduced in Chapter 4, also displays these characteristics and,

as they are based on a Hamiltonian, we can now study the correct averages in an ergodic setting by direct integration. In this chapter the averages expected from the model in Chapter 3, and their ergodic equivalents, are investigated and a new scheme where the choice of Q is essentially independent of the underlying system, the Recursive Multiple Thermostat (RMT), is proposed which overcomes the limitations of the Nosé-Poincaré chains method. A comparisons of the methods, based on the ergodic averages, is provided and special features of the RMT method displayed.

5.1 Expected average values for p_s^2/Q.

Since the Hamiltonian formulation of the MTGTB methods allow the calculation of average values for the thermostat variables and their 'kinetic' terms, if the system is ergodic, we can compare these with averages predicted from both the model and phase-space geometries. If we consider the single harmonic oscillator thermostatted by the Nosé-Poincaré method, from (3.33) and (3.34) we would expect that the maximum value of p_s to occur when s is at its average value, where the phase-space boundary for p_s is given by (3.32) as $\sqrt{2QkT}$. This, together with the observation from (3.33) that $\max\left(p_s^2\right) = 2\left\langle p_s^2 \right\rangle$, gives,

$$\left\langle \frac{p_s^2}{Q} \right\rangle = kT. \tag{5.1}$$

From this we observe that the average value of p_s^2/Q, when Q is greater than the 'optimum' value, is always less than kT, which is observed in practice and illustrated in Figure 3.3.

From a different perspective, if the phase-space trajectories of the auxiliary variables were homogenously distributed we could calculate the average value from the auxiliary

variable phase-space using (3.2). Here the probability density function for p_s would be,

$$\rho_{p_s} = \frac{\exp\left(-\frac{p_s^2}{2QN_fkT}\right)}{\int_{-\infty}^{\infty}\exp\left(-\frac{p_s^2}{2QN_fkT}\right)dp_s}, \tag{5.2}$$

then,

$$\left\langle \frac{p_s^2}{Q} \right\rangle = \int_{-\infty}^{\infty} \frac{p_s^2}{Q}\rho_{p_s}dp_s = N_fkT. \tag{5.3}$$

For the single harmonic oscillator, where $N_f = 1$, this would give the same result as (3.12), but would raise some interesting questions for multiple oscillators.

If we consider the Nosé-Poincaré chains Hamiltonian (4.16) the average values for $p_{s_i}^2/(Qs_{i+1}^2)$ can be obtained, if the system is ergodic, by substituting $p_{s_i}^2/(Qs_{i+1}^2)$ for s in (3.4). In a method similar to that used in Section 3.2 we can substitute $\tilde{p}_{s_i} = p_{s_i}/s_{i+1}$ and use the equivalence relation for δ in both the denominator and numerator of the new equation. Noting that,

$$\int_0^{\infty} \frac{s_j}{a_j}\exp\left(-\frac{(a_j - s_j)^2}{C_j}\right)ds_j \approx \int_0^{\infty}\exp\left(-\frac{(a_j - s_j)^2}{C_j}\right)ds_j, \tag{5.4}$$

and that,

$$\int_{-\infty}^{\infty} \frac{\tilde{p}_{s_i}^2}{Q_i}\exp\left(-\frac{\tilde{p}_{s_i}^2}{2Q_ikT}\right)dp_{s_i} = kT\int_{-\infty}^{\infty}\exp\left(-\frac{\tilde{p}_{s_i}^2}{2Q_ikT}\right)dp_{s_i}, \tag{5.5}$$

the new equation reduces to,

$$\left\langle \frac{p_{s_i}^2}{Q_is_{i+1}^2} \right\rangle \approx kT. \tag{5.6}$$

Similarly we can show,

$$\left\langle \frac{p_{s_M}^2}{Q_M} \right\rangle \approx kT. \tag{5.7}$$

5.2 The Recursive Multiple Thermostat method.

From these discussions it is clear that controlling the thermostats to enforce their ergodic averages is the correct approach. The limitations identified for chains methods in Section 4.13 indicate that additional thermostats should control sub-systems of greater dimension than just the preceding thermostat, and time reparamiterization should take account of all thermostat variables.

One such approach is to apply a Nosé thermostat to the original Hamiltonian, then apply a second thermostat to all of the 'kinetic' terms in the new Hamiltonian, including the term for p_{s_1}, the first thermostatting variable momentum. This method can then be applied recursively to add as many thermostats as required with the dimension of the system to be thermostatted increasing for each thermostat. This leads to better stability when compared with chains, as the time reparametrization for the Nosé-Poincaré based method involves all of the thermostats, and experiments have shown that generally only one additional thermostat is required, even for low dimensional systems. The Hamiltonian for the formulation without time rescaling, with M thermostats will be,

$$\begin{aligned} H_{NR} &= \sum_{j=1}^{N} \frac{p_j^2}{2m_j s_1^2 s_2^2 \cdots s_M^2} + V(q) + \sum_{i=1}^{M-1} \frac{p_{s_i}^2}{2Q_i s_{i+1}^2 \cdots s_M^2} + \frac{p_{s_M}^2}{2Q_M} \\ &\quad + gkT \ln s_1 + \sum_{i=2}^{M} ((N_f + i - 1)kT \ln s_i + f_i(s_i)) \end{aligned} \tag{5.8}$$

where $g = N_f + 1$ and the auxiliary functions, $\{f_i(s_i)\}$, are real valued satisfying equation (4.5). Since this method belongs to the class of multiple thermostat methods presented in Section 4.3, the proof of canonical sampling from that section applies here.

The Nosé-Poincaré based method is derived from this by applying a rescaling of time

by $s_1 s_2 \cdots s_M$,

$$
\begin{aligned}
H_{NPR} \;=\; s_1 s_2 \cdots s_M \Bigg[& \sum_{j=1}^{N} \frac{p_j^2}{2 m_j s_1^2 s_2^2 \cdots s_M^2} + V(q) \\
& + \sum_{i=1}^{M-1} \frac{p_{s_i}^2}{2 Q_i s_{i+1}^2 \cdots s_M^2} + \frac{p_{s_M}^2}{2 Q_M} + g k T \ln s_1 \\
& + \sum_{i=2}^{M} ((N_f + i - 1) k T \ln s_i + f_i(s_i)) - H_0 \Bigg],
\end{aligned}
\tag{5.9}
$$

where H_0 is chosen such that $H_{NPR} = 0$ at initial conditions and setting $g = N_f$, and again the proof of canonical sampling in Section 4.3 is valid due to the method's construction.

Since the correct value of $\langle p_{s_1}^2 / Q_1 \rangle$ is obtained by thermostatting rather than the parameter Q_1 we find that Q_1 is now essentially independent of the underlying system. The parameters can instead be chosen to obtain some useful property in the numerical method, such as better numerical stability or, as in [35] a desired scale separation.

An important feature of the formalism presented here is that the method always remains within the class of Hamiltonian dynamical models, for which symplectic integrators, having superior long-term stability properties, are possible. Construction of efficient schemes suitable for molecular dynamics applications is an important task and, in Section 5.4, it is shown to be possible here, by designing an efficient Hamiltonian splitting method for RMTs.

5.3 Choice of the Auxiliary Function.

For the additional thermostats to work correctly an auxiliary function, $f_i(s_i)$, must be chosen not only to satisfy equation (4.5) but to provide a suitable modification to the thermostats as discussed in Chapter 4. One such choice is,

$$f_i(s_i) = \frac{(a_i - s_i)^2}{2C_i}, \tag{5.10}$$

where the auxiliary function coefficient C_i is a constant and, for Nosé-Poincaré chains, must satisfy $C_i \leq a_i^2/8kT$. The value a_i is chosen as the required average value of s_i, generally 1.

5.4 Hamiltonian Splitting Method for RMTs.

The numerical methods used for the following experiments are based on the following general Hamiltonian,

$$H = \sum_{i=1}^{N} \frac{p_i^2}{2m_i} + V(q),$$

where $q = (q_1, \ldots, q_N)$. The RMT method derived from this, with M thermostats based on the auxiliary function in equation (5.10) is then,

$$\begin{aligned} H_{NR} &= \sum_{i=1}^{N} \frac{p_i^2}{2m_i s_1^2 \cdots s_M^2} + V(q) + \sum_{j=1}^{M-1} \frac{p_{s_j}^2}{2Q_j s_{j+1}^2 \cdots s_M^2} + \frac{p_{s_M}^2}{2Q_M} + gkT \ln s_1 \\ &\quad + \sum_{j=2}^{M} \left((N_f + j - 1)kT \ln s_j + \frac{(a_j - s_j)^2}{2C_j} \right), \end{aligned}$$

where $g = N_f + 1$, giving a Nosé-Poincaré multiple thermostat method, with $g = N_f$,

$$H_{NPR} = s_1 s_2 \cdots s_M \left[H_{NR} - H_0 \right],$$

where H_0 is chosen as the initial value of H_{NR}. The equations of motion are,

$$\dot{q}_i = \frac{p_i}{m_i s_1 \cdots s_M},$$

$$
\begin{aligned}
\dot{p}_i &= -s_1 \cdots s_M \frac{\partial V(q)}{\partial q_i}, \\
\dot{s}_1 &= \frac{s_1 \cdots s_M p_{s_1}}{Q_1 s_2^2 \cdots s_M^2}, \\
\dot{p}_{s_1} &= s_2 \cdots s_M \left(\sum_{i=1}^{N} \frac{p_i^2}{m_i s_1^2 \cdots s_M^2} - N_f kT - H_{NR}(q,p,s,\hat{p}_s) + H_0 \right), \\
\dot{s}_j &= \frac{s_1 \cdots s_M p_{s_j}}{Q_j s_{j+1}^2 \cdots s_M^2}, \\
\dot{p}_{s_j} &= s_1 \cdots s_M \left(\sum_{i=1}^{N} \frac{p_i^2}{m_i s_1^2 \cdots s_j^3 \cdots s_M^2} + \sum_{l=1}^{j-1} \frac{p_{s_l}^2}{Q_l s_{l+1}^2 \cdots s_j^3 \cdots s_M^2} \right. \\
&\quad \left. - \frac{(N_f + j - 1)kT}{s_j} + \frac{a_j - s_j}{C_j} - \frac{H_{NR}(q,p,s,\hat{p}_s) - H_0}{s_j} \right), \quad 1 < j < M, \\
\dot{s}_M &= \frac{s_1 \cdots s_M p_{s_M}}{Q_M}, \\
\dot{p}_{s_M} &= s_1 \cdots s_M \left(\sum_{i=1}^{N} \frac{p_i^2}{m_i s_1^2 \cdots s_{M-1}^2 s_M^3} + \sum_{l=1}^{M-1} \frac{p_{s_l}^2}{Q_l s_{l+1}^2 \cdots s_{M-1}^2 s_M^3} \right. \\
&\quad \left. - \frac{(N_f + M - 1)kT}{s_M} + \frac{a_M - s_M}{C_M} - \frac{H_{NR}(q,p,s,\hat{p}_s) - H_0}{s_M} \right),
\end{aligned}
$$

where $s = (s_1, \ldots, s_M)$, $\hat{p}_s = (p_{s_1}, \ldots, p_{s_M})$ and $p = (p_1, \ldots, p_N)$. The thermostats have introduced an implicit coupling into the equations of motion, but an explicit method can be formulated by splitting the Hamiltonian and corresponding Liouville operator. For M thermostats this can be done using $2+M$ Hamiltonians by employing a separate Hamiltonian for each extended variable 'kinetic' term. Then if,

$$
H = H_1 + H_2 + H_{3_1} + \cdots + H_{3_M},
$$

we have,

$$
\begin{aligned}
H_1 &= s_1 \cdots s_M \left[\sum_{i=1}^{N} \frac{p_i^2}{2 m_i s_1^2 \cdots s_M^2} + N_f kT \ln s_1 \right], \\
H_2 &= s_1 \cdots s_M \left[V(q) + \sum_{j=2}^{M} \left((N_f + j - 1)kT \ln s_j + \frac{(a_j - s_j)^2}{2C_j} \right) \right], \\
H_{3_1} &= s_1 \cdots s_M \left[\frac{p_{s_1}^2}{2 Q_1 s_2^2 \cdots s_M^2} - H_0 \right],
\end{aligned}
$$

$$
\begin{aligned}
H_{3_j} &= s_1 \cdots s_M \left[\frac{p_{s_j}^2}{2Q_j s_{j+1}^2 \cdots s_M^2} \right], \quad 1 < j < M, \\
H_{3_M} &= s_1 \cdots s_M \left[\frac{p_{s_M}^2}{2Q_M} \right].
\end{aligned}
$$

Using a symmetric splitting of the Liouville operator to get a symplectic and time reversible method,

$$
\begin{aligned}
iL_H &= \{., H\} \\
&= \{., H_1\} + \{., H_2\} + \{., H_{3_1}\} + \cdots + \{., H_{3_M}\} \\
&= iL_{H_1} + iL_{H_2} + iL_{H_{3_1}} + \cdots + iL_{H_{3_M}}. \qquad (5.11)
\end{aligned}
$$

This splitting introduces an error of order $\triangle t^3$ at each step in terms of the solution operator, giving a second order method,

$$
\begin{aligned}
\Psi_H(\triangle t) &= e^{iL_H \triangle t}, \\
&= e^{iL_{H_2} \triangle t/2} e^{iL_{H_{3_1}} \triangle t/2} \cdots e^{iL_{H_{3_M}} \triangle t/2} e^{iL_{H_1} \triangle t} e^{iL_{H_{3_M}} \triangle t/2} \\
&\quad \cdots e^{iL_{H_{3_1}} \triangle t/2} e^{iL_{H_2} \triangle t/3} + O(\triangle t^3).
\end{aligned}
$$

The dynamics for H_1 and H_2 can be solved in a straightforward manner , leaving $H_{3_1} \cdots H_{3_M}$ to be solved either analytically or by using the generalized leapfrog algorithm as described in [8] and Appendix A.1.

5.5 Harmonic Oscillator experiments with RMTs.

Using the splitting method from Section 5.4 with two thermostats and parameters $\triangle t = 0.05$, $m = 1.0$, $Q_1 = 0.5$, $Q_2 = 1.0$, $C_2 = 0.04$, $kT = 1.0$, $M = 2$, $a_2 = 1$ produced good

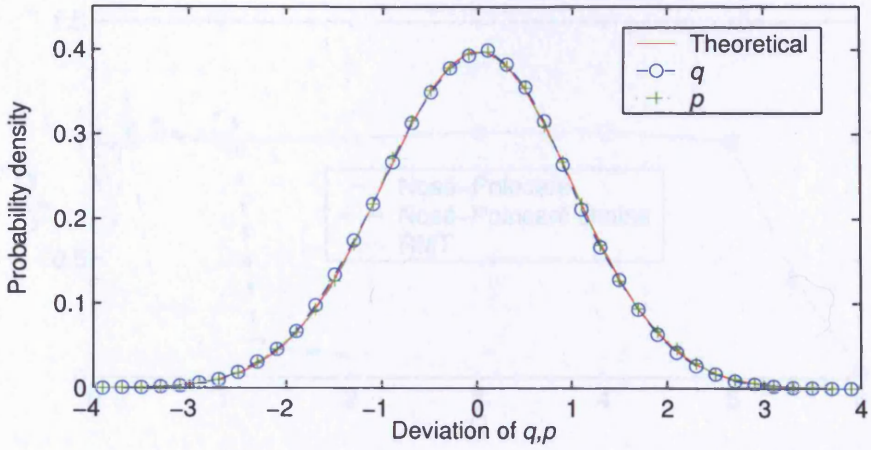

Figure 5.1: Distribution for position/momentum, RMT method with 2 thermostats.

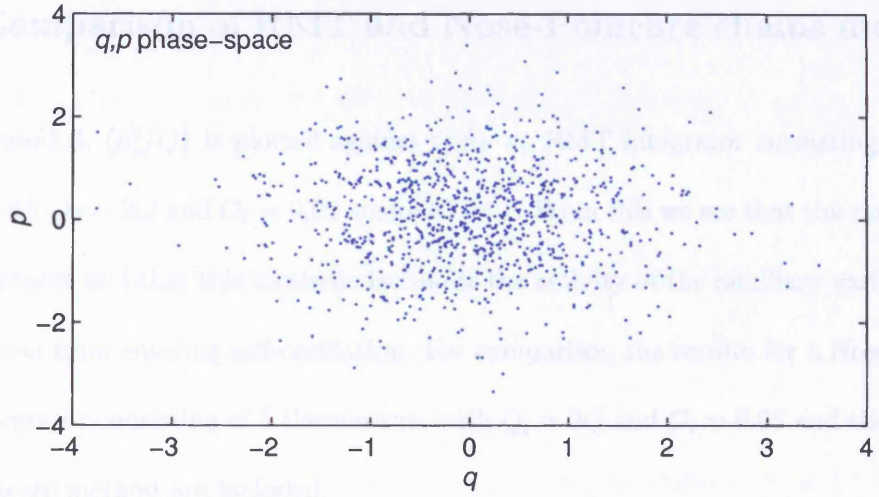

Figure 5.2: q,p phase-space, RMT method with 2 thermostats.

results with convergence close to the canonical distribution in 500,000 steps as shown in Figures 5.1 and 5.2.

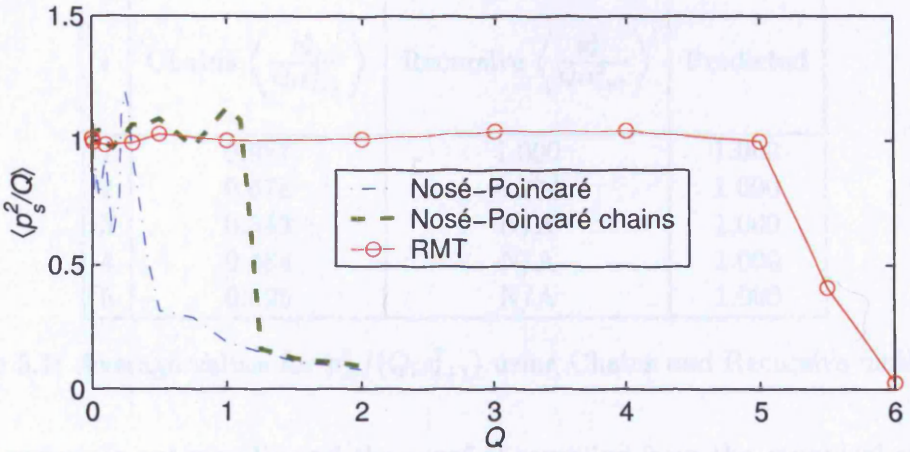

Figure 5.3: $\langle p_s^2/Q \rangle$ for Q in the range 0.001-6.

5.6 Comparison of RMT and Nosé-Poincaré chains methods.

In Figure 5.3, $\langle p_s^2/Q \rangle$ is plotted against Q for an RMT integrator consisting of 2 thermostats with $Q_2 = 2Q$ and $C_2 = 0.04$ where $kT = 1$. From this we see that the range of Q is vastly increased and that this method also limits the activity of the auxiliary variables, preventing them from entering self-oscillation. For comparison the results for a Nosé-Poincaré chains integrator consisting of 5 thermostats with $Q_i = 2Q$ and $C_i = 0.08$ and the standard Nosé-Poincaré method are included.

As discussed in Section 4.13, the required average value of $p_{s_i}^2/(Q_i s_{i+1}^2)$ for each thermostat may not be achievable for Nosé-Poincaré chains, a limitation which should not apply to the RMT method. The averages for a Nosé-Poincaré chains integrator consisting of 5 thermostats, with $Q_i = 2Q$ and $C_i = 0.08$, are compared to those from an RMT integrator consisting of 2 thermostats, with $Q_2 = 2Q$ and $C_2 = 0.04$, where $kT = 1$ and integrated over 20,000,000 steps of 0.01 are presented in Table 5.1. For the Nosé-Poincaré chains method, even if the dimension of the underlying system is increased this problem persists,

i	Chains $\left\langle \frac{p_{s_i}^2}{Q_i s_{i+1}^2} \right\rangle$	Recursive $\left\langle \frac{p_{s_i}^2}{Q_i s_{i+1}^2} \right\rangle$	Predicted
1	0.987	1.000	1.000
2	0.678	0.973	1.000
3	0.543	N/A	1.000
4	0.484	N/A	1.000
5	0.525	N/A	1.000

Table 5.1: Average values for $p_{s_i}^2/(Q_i s_{i+1}^2)$ using Chains and Recursive methods.

hence the system is not ergodic and the proof of sampling from the canonical ensemble is invalid. By contrast, with the RMT scheme each new thermostat will thermostat a system of increasing dimension and it has been found that, even for low dimensional systems, one additional thermostat is usually sufficient to provide good sampling.

5.7 Obtaining expected average values Independently of Q for Multiple Oscillators.

We have seen that $\langle p_s^2/Q \rangle = kT$, based on the model in Section 3.3, was sufficient for the auxiliary variables to interact with their phase-space boundary for a single harmonic oscillator, giving rise to the behavior required to sample from the canonical ensemble. In Section 3.7 it was shown that the volume of auxiliary variable phase-space sampled by the system is essentially independent of the number of oscillators being considered, despite the increase in the available volume from (3.2), if the system is ergodic. From this we would expect that enforcing the ergodic averages for the thermostat's 'kinetic' term would give good results for multiple oscillators, with a much reduced dependence on Q, as we saw for

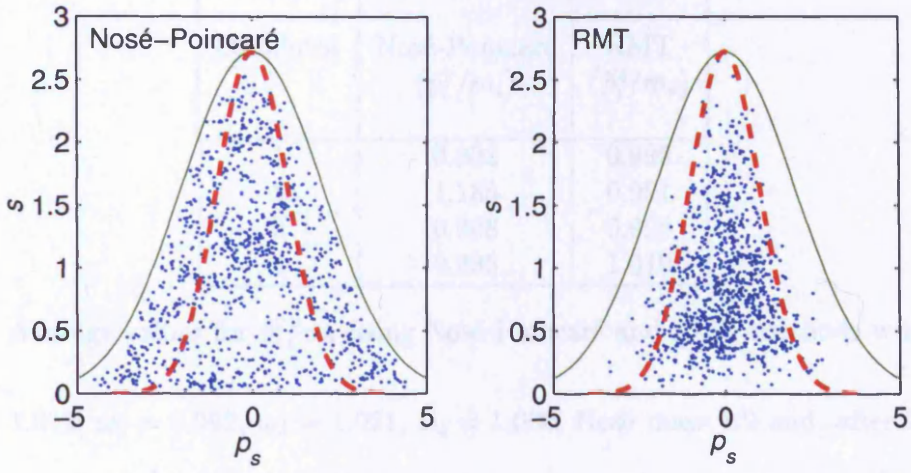

Figure 5.4: Auxiliary Variable phase-space for 4 oscillators of similar frequency for the Nosé-Poincaré and RMT methods. The dashed line is the single oscillator phase-space boundary, solid line is the 4 oscillator phase-space boundary.

the case of the single harmonic oscillator, and this can be seen in experiments. However there may be additional benefits for multiple oscillators and these can be classified for systems consisting of oscillators of similar frequency and multi-scale systems. To illustrate these observations we will remain within the class of multiple harmonic oscillators with Hamiltonian,

$$H_{ho}(q,p) = \sum_{i=1}^{N} \left(\frac{p_i^2}{2m_i} + \frac{q_i^2}{2} \right). \tag{5.12}$$

5.7.1 Multiple Oscillators of similar frequency.

The equation defining the boundary of the volume of phase-space occupied by the auxiliary variables, (3.59) in Section 3.7, assumes random interaction between the oscillators and is easily seen where the oscillators are synchronous, or where there is some correlation between the oscillators and the system is of small dimension, different results can be produced as shown in Figure 5.4, left hand side graph. In this example there are 4 oscillators

Oscillator	Nosé-Poincaré $\langle \tilde{p}_i^2/m_i \rangle$	RMT $\langle \tilde{p}_i^2/m_i \rangle$
1	0.902	0.996
2	1.185	0.991
3	0.988	0.998
4	0.935	1.010

Table 5.2: Average values for $\tilde{p}_i^2/m_i$ using Nosé-Poincaré and RMT methods with $kT = 1$.

with $\omega_1 = 1.012$, $\omega_2 = 0.992$, $\omega_3 = 1.021$, $\omega_4 = 1.000$, Nosé mass 1.2 and, after 20,000,000 steps of 0.02, we find that $\langle p_s^2/Q \rangle = 3.144$. Compare this result with the correct value $\langle p_s^2/Q \rangle = 1$ and the homogenous value predicted from (5.3) of $\langle p_s^2/Q \rangle = 4$. Clearly, in this case, thermostatting p_s should have a dramatic effect on the results, as seen in the right hand side graph of Figure 5.4 for and RMT method with $Q_2 = 2Q_1$ and $C_2 = 0.04$, where $\langle p_s^2/Q \rangle = 1.010$ leading to much faster convergence to the canonical ensemble. This can be seen from Figure 5.5 where the distribution data for each oscillator is shown (solid line) with the theoretical distribution (dotted line), the graphs along the top generated by the Nosé-Poincaré method and those along the bottom from the RMT method.

From the Equipartition theorem (see Appendix D) we expect that $\langle \tilde{p}_i^2/m_i \rangle = kT \ \forall i$, where $\tilde{p}_i = p_i/s$, $s = s_1$ for the Nosé-Poincaré method and $s = s_1 s_2$ for the RMT method with two thermostats. The average kinetic energy values for each oscillator, from the experiment above, are included in Table 5.2 where we see that the deviation from the correct results is nearly 20 times less for the RMT method than for the Nosé-Poincaré method.

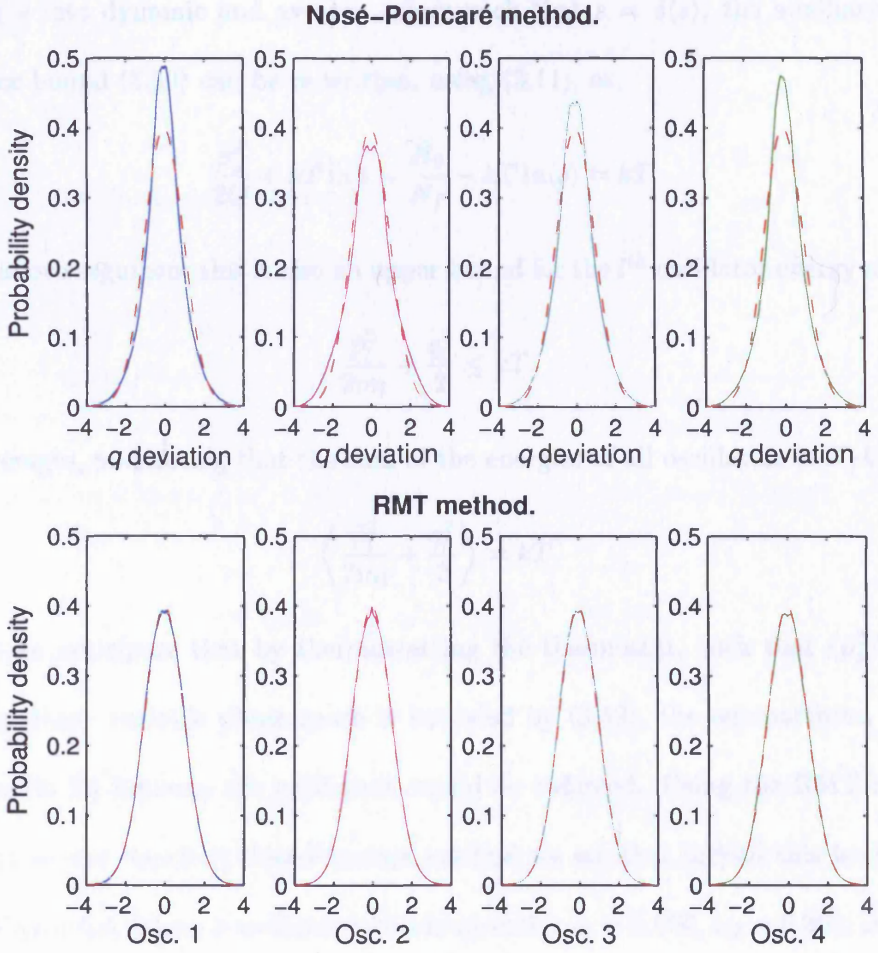

Figure 5.5: q distributions for 4 oscillator model with similar frequencies using Nosé-Poincaré method (top) and RMT method (bottom). The dotted curve represents the theoretical distribution.

5.7.2 Multiple Oscillators in Multi-Scale Systems.

In systems where there is no correlation between the oscillators, for example in a multi-scale system, we would expect the only interaction to be between the oscillators and the auxiliary variables. When sampling from the canonical ensemble the l^{th} oscillator would be expected to pass through the point $\tilde{p}_l = 0$, $q_l = 0$ at which point all of the energy for that oscillator must reside in the auxiliary variables, based on the assumption above. By

separating s into dynamic and average values such that $s = \tilde{s}\langle s \rangle$, the auxiliary variable phase-space bound (3.59) can be re-written, using (3.11), as,

$$\frac{\tilde{p}_s^2}{2Q} + kT \ln \tilde{s} = \frac{\tilde{H}_0}{N_f} - kT \ln\langle s \rangle = kT. \tag{5.13}$$

From the above argument this is also an upper bound for the l^{th} oscillator energy and hence,

$$\frac{\tilde{p}_l^2}{2m_l} + \frac{q_l^2}{2} \leq kT. \tag{5.14}$$

Taking averages, and noting that the sum of the energies of all oscillators is $N_f kT$, yields,

$$\left\langle \frac{\tilde{p}_l^2}{2m_l} + \frac{q_l^2}{2} \right\rangle = kT. \tag{5.15}$$

From this we anticipate that by thermostatting the thermostat, such that $\langle \tilde{p}_s^2/Q \rangle = kT$ and the auxiliary variable phase space is bounded by (3.59), the equipartition of energy (see Appendix D) between the oscillators would be enforced. Using the RMT method in comparison to the standard Nosé-Poincaré method we see that indeed this is the case as shown in Figure 5.6, where 3 oscillators with frequencies $\omega_1 = 1.000$, $\omega_2 = 0.308$, $\omega_3 = 0.095$, Nosé mass 8, $Q_2 = 16$ and $C_2 = 0.04$ for the RMT method, and a step size 0.05 are simulated. The kinetic energies are calculated for each oscillator using running averages of 1,000,000 steps. Since the equipartition of energy can be shown for systems of harmonic oscillators which sample from the canonical ensemble (see Appendix D), convergence to the canonical ensemble is considerably faster. This is illustrated in Figure 5.7 where the distribution data for each oscillator is shown (solid line) with the theoretical distribution (dotted line), the graphs along the top generated by the Nosé-Poincaré method and those along the bottom from the RMT method, for a simulation length of 20,000,000 steps of 0.05 . As before we expect that the average kinetic energy for the oscillators to be equal to kT

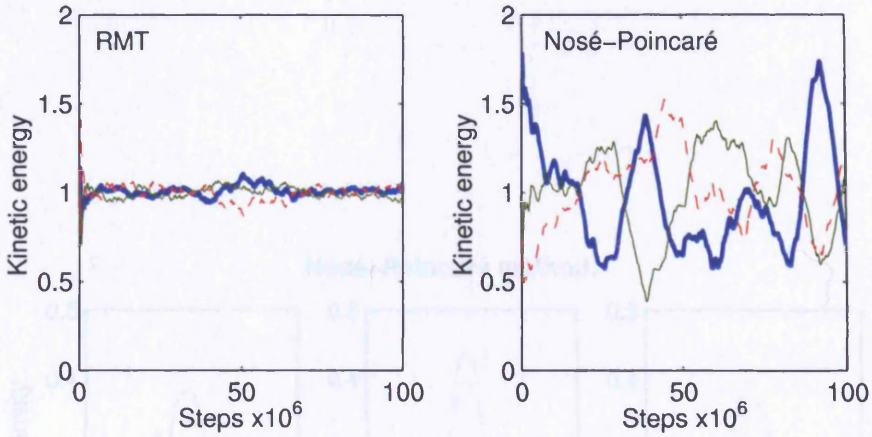

Figure 5.6: Kinetic energy for 3 oscillators using RMT and Nosé-Poincaré methods for $kT = 1$.

Oscillator	Nosé-Poincaré $\langle \tilde{p}_i^2/m_i \rangle$	RMT $\langle \tilde{p}_i^2/m_i \rangle$
1	0.946	1.000
2	1.074	0.996
3	1.101	1.002

Table 5.3: Average values for $\tilde{p}_i^2/m_i$ using Nosé-Poincaré and RMT methods with $kT = 1$ for the multi-scale model.

and the average kinetic energy values for each oscillator, from the experiment above, are included in Table 5.3.

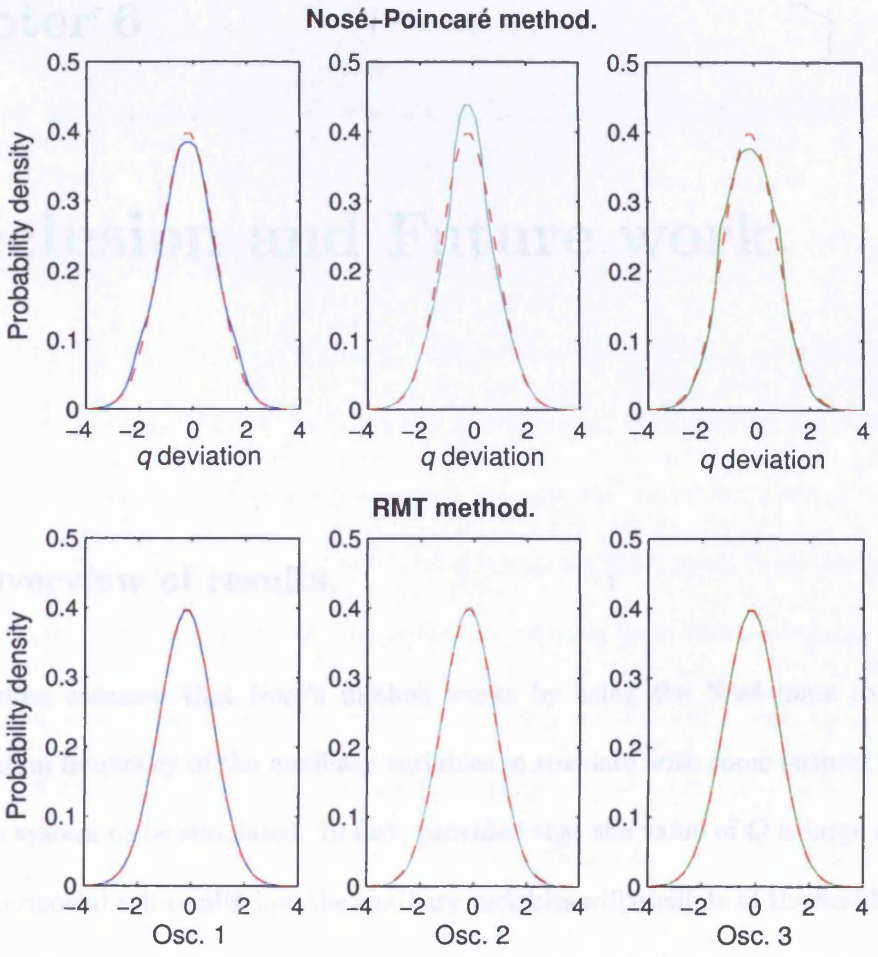

Figure 5.7: q distributions for 3 oscillator multi-scale model using Nosé-Poincaré method (top) and RMT method (bottom). The dotted curve represents the theoretical distribution.

Chapter 6

Conclusion and Future work.

6.1 Overview of results.

It is often assumed that Nosé's method works by using the Nosé mass to tune the self-oscillation frequency of the auxiliary variables to resonate with some natural frequency within the system to be simulated. In fact, provided that the value of Q is large enough to prevent thermostat self-oscillation, the auxiliary variables will oscillate at the first harmonics of any frequencies within the system, introducing a potential 2:1 resonance, as shown by the model in Section 3.3. These first harmonics persist as the system moves into the canonical ensemble (with additional oscillations at the fundamental frequencies, as seen in Figure 6.1, for an oscillator with frequency 0.167Hz showing the fourier analysis of p_s) when interactions with the auxiliary variable phase-space boundary occur and coincide with more chaotic

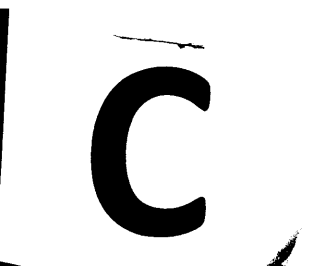

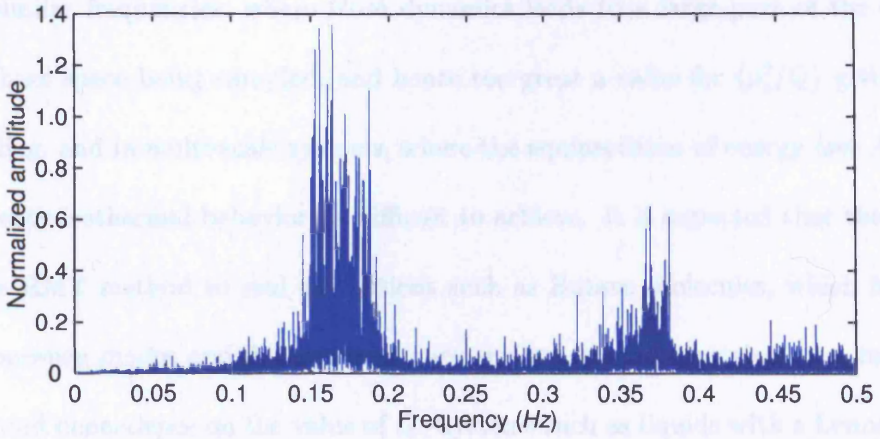

Figure 6.1: Frequency domain plot of p_s for single harmonic oscillator, with frequency 0.167Hz, sampling from the canonical ensemble.

behavior of the system. It is clear that to sample from the canonical ensemble the phase-space variables must approach their boundary and this can be induced by the correct choice of Q, or by controlling the thermostat so that its canonical ensemble average is achieved. In the latter case the Recursive Thermostatting technique has proven to overcome many of the difficulties of previous methods, and generally requires fewer thermostats.

The model presented in Chapter 3 has provided an improved insight into the mechanisms of extended system thermostatting methods, showing that the generally established belief that resonance occurs at the thermostat variable's self-oscillation frequency is flawed. For harmonic systems it is now possible to accurately predict the correct choice for the Nosé mass, even when multiple frequencies are present, in contrast to traditional linearization techniques. Of particular interest is the model's prediction that the choice of Nosé mass is dictated by the required ergodic averages for the thermostatting variable's 'kinetic' energy, explaining the effectiveness of chains methods.

Recursive Thermostatting has benefits in situations where the system consists of oscil-

lators of similar frequencies, where Nosé dynamics leads to a large part of the auxiliary variable phase space being sampled, and hence too great a value for $\langle p_s^2/Q \rangle$ giving incorrect sampling, and in multi-scale systems, where the equipartition of energy (see Appendix D), and hence isothermal behavior, is difficult to achieve. It is expected that the application of the RMT method to real simulations such as Butane molecules, which have poor coupling between modes and discreet frequency spectra, should also give good results and much reduced dependence on the value of Q. Systems such as liquids with a Lennard-Jones potential, where the coupling between different parts of the system is good and they display a broad frequency spectrum, have a wide choice of Q but the RMT method should make Q essentially independent of the system. As an additional benefit, the large range of choice for the Nosé mass allows for the use of small masses, and hence fast thermostatting, which is useful for large systems where traditionally a large Nosé mass is required, since it is proportional to the number of degrees of freedom.

One of the main objectives was to produce a Hamiltonian method so that symplectic integrators can be used, with their attendant advantages of long term stability, preservation of first integrals and the resulting simulation being from a nearby Hamiltonian due to the existence of a backward error analysis. The construction of a general family of fully Hamiltonian multiple thermostat methods has led to the implementation of Nosé and Nosé-Poincaré chains [43] as an alternative to the non-Hamiltonian Nosé-Hoover chains. This method is characterized by the existence of a proof of the correct ensemble sampling under an ergodic assumption and experimental evidence for the broader choice of Nosé mass provided by chains methods. Following on from this the extension of the multiple thermo-

stat methods, such that multiple thermostats can interact directly with the system to be thermostatted, has led to the construction of the Recursive Multiple Thermostat scheme [44]. This fully Hamiltonian method overcomes the limitations of Nosé-Poincaré and chains methods and, in addition to the advantages of Nosé-Poincaré chains, experimental evidence shows that the choice of Nosé mass is essentially independent of the underlying system and long term trajectories show excellent stability and preservation of total system energy. In implementing these methods special features of the thermostatting variable's phase-space, and their role in producing the correct sampling, have been documented.

6.2 Future work.

The aim of this work has been to gain an insight into the mechanism behind extended system thermostatting methods with a view towards producing new schemes which overcome some of the present limitations that exist. Future work can be split into the following categories:

6.2.1 Theoretical work.

The frequency domain model in Chapter 3 helps in the understanding of the role of the Nosé mass parameter, and allows the accurate prediction of the onset of ergodic behavior, for simplified harmonic systems. However there is considerably more work required to understand the chaotic regime after this point and the insight, and experimental data, gained so far will be useful when considering this task. Particularly important is the observation that, for harmonic systems, the thermostatting variable has oscillations at the first harmonic

of any frequencies within the underlying system, giving a potential 2:1 resonance.

6.2.2 Molecular dynamics simulations.

The simulations considered here have been based on harmonic oscillators, motivated by Nosé's prediction of the Nosé mass parameter based on frequency. Although the results of these simulations show great promise, the RMT method must be applied to real Molecular Dynamics simulations to confirm its many advantages. As a minimum the simple protein in solvent model, and constant pressure simulations need to be considered.

6.2.3 Fast thermostatting.

Fast Thermostatting can be accomplished use of the RMT scheme. In traditional thermostatting schemes the optimum value for Q, from (3.58), increases with the dimension of the system resulting in a dramatic increase in thermostat response time for large systems, which may be undesirable. From Figure 5.3 we see that thermostatting the thermostat gives a vastly increased range for Q which allows very small values to be used, giving a much faster response. This may have applications in Multi-scale systems where thermostatting is applied to the 'fast' part of the system and it is desirable to have thermostatting in the same timescale.

6.2.4 Molecular dynamics software packages.

There exist molecular dynamics software packages, such as CHARMM and AMBER, and implementing the RMT method for these platforms would give access to numerous

sample problems with which to test the scheme. In addition, subject to successful testing, this would allow interested parties to experiment with the RMT method.

Appendix A

Numerical methods.

A.1 A Numerical Method for the Nosé-Poincaré scheme.

In the paper by Bond, Laird and Leimkuhler [8] an explicit method was proposed for the Nosé-Poincaré method for systems where the time transformation is dependent on a reduced number of phase-space variables, such as s. This has application for both the Nosé-Poincaré chains and the RMT methods, and is reproduced here for reference.

For an underlying Hamiltonian of the form,

$$H(q,p) = \sum_{i=1}^{N} \frac{p_i^2}{2m_i} + V(q), \tag{A.1}$$

the equations of motion for the Nosé-Poincaré method are then,

$$\begin{aligned} \dot{q}_i &= \frac{p_i}{m_i s}, \\ \dot{p}_i &= -s\nabla_{q_i} V(q), \\ \dot{s} &= s\frac{p_s}{Q}, \end{aligned}$$

$$\dot{p}_s = \sum_{i=1}^{N} \frac{p_i^2}{m_i s^2} - gkT - \Delta H(q,p,s,p_s),$$

where,

$$\Delta H(q,p,s,p_s) = \sum_{i=1}^{N} \frac{p_i^2}{2m_i s^2} + V(q) + \frac{p_s^2}{2Q} + gkT \ln s - H_0,$$

with H_0 chosen such that $\Delta H = 0$ at initial conditions. The generalized leapfrog algorithm [22, 64] can then be used, resulting in the symplectic and time-reversible method [58],

$$p_i^{n+1/2} = p_i^n - \frac{\Delta t}{2} s^n \nabla_{q_i} V(q^n), \tag{A.2}$$

$$p_s^{n+1/2} = p_s^n + \frac{\Delta t}{2}\left(\sum_{i=1}^{N} \frac{1}{m_i}\left(\frac{p_i^{n+1/2}}{s^n}\right)^2 - gkT\right) - \frac{\Delta t}{2}\Delta H(q^n, p^{n+1/2}, s^n, p_s^{n+1/2}), \tag{A.3}$$

$$s^{n+1} = s^n + \frac{\Delta t}{2}(s^{n+1} + s^n)\frac{p_s^{n+1/2}}{Q}, \tag{A.4}$$

$$q_i^{n+1} = q_i^n + \frac{\Delta t}{2}\left(\frac{1}{s^{n+1}} + \frac{1}{s^n}\right)\frac{p_i^{n+1/2}}{m_i}, \tag{A.5}$$

$$p_s^{n+1} = p_s^{n+1/2} + \frac{\Delta t}{2}\left(\sum_{i=1}^{N} \frac{1}{m_i}\left(\frac{p_i^{n+1/2}}{s^{n+1}}\right)^2 - gkT\right) - \frac{\Delta t}{2}\Delta H(q^{n+1}, p^{n+1/2}, s^{n+1}, p_s^{n+1/2}), \tag{A.6}$$

$$p_i^{n+1} = p_i^{n+1/2} - \frac{\Delta t}{2} s^{n+1} \nabla_{q_i} V(q^{n+1}). \tag{A.7}$$

The resulting method is explicit. Note that (A.3) requires the solution of a scalar quadratic equation for $p_s^{n+1/2}$:

$$\frac{\Delta t}{4Q}(p_s^{n+1/2})^2 + p_s^{n+1/2} + C = 0, \tag{A.8}$$

where,

$$C = \frac{\Delta t}{2}\left(gkT(1 + \ln s^n) - \sum_{i=1}^{N} \frac{1}{2m_i}\left(\frac{p_i^{n+1/2}}{s^n}\right)^2 + V(q^n) - H_0\right) - p_s^n. \tag{A.9}$$

The equation can be solved explicitly using the quadratic formula, but the correct root should be solved for. To avoid subtractive cancellation a variant of the quadratic formula can be used to solve (A.8):

$$p_s^{n+1/2} = \frac{-2C}{1 + \sqrt{1 - C\Delta t/Q}}. \tag{A.10}$$

The remaining steps in the algorithm are completely explicit, and can be solved sequentially.

Appendix B

Symplectic and Hamiltonian splitting methods.

Most Hamiltonian systems of interest do not have an analytical solution and this has led to the development of numerical integrators which solve the equations of motion by taking discreet steps forward (and possibly backward) in time until the required integration time has elapsed. This was first seen in simple schemes such as Euler's method, but both the mathematician De Vogalaere and the physicist Ruth had postulated that if the numerical integrator possessed some of the properties of the Hamiltonian system's flow-map then simulations would display improved behavior. This idea has led to the development and classification of Geometric Integrators, where geometric properties of the original system are preserved by their use. For Hamiltonian systems the symplectic property is perhaps the most important geometrically, and can lead to efficient explicit Hamiltonian splitting methods as discussed in the book by Leimkuhler and Reich [42].

B.1 Symplectic Maps.

The term *symplectic* was first used mathematically by Hermann Weyl and is taken from the Greek word meaning "twining or plaiting together". Symplectic systems consist of a pair of d-dimensional variables, generally position q and momentum p, "intertwined" by the symplectic two form,

$$\omega = dp \wedge dq. \tag{B.1}$$

This is an antisymmetric, bilinear form acting on a pair of tangent vectors to compute the sum of areas of the parallelograms formed by projecting the vectors onto the planes defined by the pairs $(q_i, p_i), i = 1, \cdots, d$ giving,

$$\omega(v, w) = \sum_{i=1}^{d} (v_{p_i} w_{q_i} - v_{q_i} w_{p_i}). \tag{B.2}$$

A diffeomorphism $\psi : X \mapsto X$ on a $2d$-dimensional manifold X with coordinates $z = (q, p)$ is symplectic if it preserves the symplectic form [5]. If we write $\hat{z} = (\hat{q}, \hat{p}) = \psi(q, p)$ then the symplectic condition becomes,

$$[\psi_z(z)]^T J^{-1} \psi_z(z) = J^{-1}, \tag{B.3}$$

where,

$$J^{-1} = \begin{bmatrix} 0 & I \\ -I & 0 \end{bmatrix},$$

$\psi_z(z)$ is the Jacobian matrix of $\psi(z)$, J is the inverse of the Poisson matrix and I is the dxd identity matrix.

B.1.1 Symplecticness of Hamiltonian flow-maps.

To prove that the flow-map $\Phi_{t,H}$ of a Hamiltonian system H is symplectic we can use the alternative form for the Hamiltonian,

$$\dot{z} = \mathbf{J}\nabla_z H(z), \tag{B.4}$$

where $\mathbf{J}$ is an invertible skew-symmetric matrix ($\mathbf{J}^T = -\mathbf{J}$). Let,

$$F(t) = \frac{\partial}{\partial z}\Phi_{t,H}, \tag{B.5}$$

then, from (B.3) and (B.4),

$$F(t)^T \mathbf{J}^{-1} F(t) = \mathbf{J}^{-1}. \tag{B.6}$$

Since $F(0)$ is defined as the identity mapping, for which (B.6) holds, we need to show,

$$\frac{d}{dt}(F(t)^T \mathbf{J}^{-1} F(t)) = 0. \tag{B.7}$$

Then,

$$\begin{aligned}
\frac{d}{dt}(F^T \mathbf{J}^{-1} F) &= F^T \mathbf{J}^{-1} \frac{d}{dt} F + \left(\frac{d}{dt} F\right)^T \mathbf{J}^{-1} F \\
&= F^T \mathbf{J}^{-1} (\mathbf{J} H_{zz}(z(t)) F) + (F^T H_{zz}(z(t)) \mathbf{J}^T) \mathbf{J}^{-1} F \\
&= F^T H_{zz}(z(t)) F + F^T H_{zz}(z(t)) F \\
&= 0.
\end{aligned}$$

□

If a flow-map is symplectic then it possesses certain integral invariants which relate to the evolution of subsets of phase-space. One such integral invariant is the preservation of phase-space area for systems with one degree of freedom, $d = 1$, and volume for $d > 1$,

which also follows from Liouville's theorem [5]. Since the existence of integral invariants such as this restricts the possible solutions for a Hamiltonian system it is an important property for numerical integrators if good long term results are required.

B.1.2 Phase-space area preservation for $d = 1$.

A one degree of freedom symplectic map, $\psi : \mathbb{R}^2 \mapsto \mathbb{R}^2$, has a Jacobian,

$$\psi_z(z) = \begin{bmatrix} a & b \\ c & d \end{bmatrix}, \tag{B.8}$$

for some $a, b, c, d \in \mathbb{R}$. Substituting (B.8) into (B.3) yields,

$$ad - bc = 1, \tag{B.9}$$

which is equivalent to,

$$\det[\psi_z(z)] = 1. \tag{B.10}$$

If we let Λ be a bounded subset of phase-space and $\hat{\Lambda} = \psi(\Lambda)$ its image under ψ then the area $\alpha(\Lambda)$ is given by,

$$\alpha(\Lambda) = \int_{\Lambda} dqdp. \tag{B.11}$$

Similarly the area $\alpha(\hat{\Lambda})$ is given by,

$$\begin{aligned} \alpha(\hat{\Lambda}) &= \int_{\hat{\Lambda}} d\hat{q}d\hat{p} \\ &= \int_{\Lambda} \det[\psi_z(z)]dqdp \\ &= \int_{\Lambda} dqdp \\ &= \alpha(\Lambda), \end{aligned}$$

and hence a one degree of freedom symplectic map preserves the area of phase-space. The proof of the conservation of phase-space volume for $d > 1$ can be found in references such as Arnold [5].

B.2 Time-reversal symmetry.

Newtons's equations of motion possess the geometric property of time-reversibility, which manifests itself as the invariance of a Hamiltonian $H(q,p)$ under the reflection symmetry $p \mapsto -p$. The equations of motion for this Hamiltonian are,

$$\dot{q} = \nabla_p H(q,p),\ \dot{p} = -\nabla_q H(q,p). \tag{B.12}$$

If we assume $(q(t),p(t))$ is a solution of (B.12) and consider $(\hat{q}(t),\hat{p}(t)) := (q(-t),-p(-t))$ we have,

$$\frac{d}{dt}\hat{q}(t) = -\dot{q}(-t) = -\nabla_p H(q(-t),p(-t)) = \nabla_p H(\hat{q}(t),\hat{p}(t)), \tag{B.13}$$

$$\frac{d}{dt}\hat{p}(t) = \dot{p}(-t) = -\nabla_q H(q(-t),p(-t)) = \nabla_q H(\hat{q}(t),\hat{p}(t)), \tag{B.14}$$

since $H(q,p)$ is even in p for Newtonian mechanics, giving $\nabla_q H$ even in p and $\nabla_p H$ odd in p. This shows that $(\hat{q}(t),\hat{p}(t))$ is a solution of (B.12). This invariance implies that for every solution of the Hamiltonian system there is another solution whose trajectory is in the opposite direction with negated momentum.

This time-reversal invariance can be written, for $z = (q,p)$ and I_d the dxd identity matrix,

$$H(z) = H(S(z)), \tag{B.15}$$

where,

$$S = \begin{bmatrix} I_d & 0 \\ 0 & -I_d \end{bmatrix}.$$

For the vector field of a Hamiltonian of the form (B.4) this reduces to,

$$f(z) = -Sf(Sz), \tag{B.16}$$

where $f(z) = \mathbf{J}\nabla_z H(z)$, since for any flow map $\Phi_{-t,H} = [\Phi_{t,H}]^{-1}$. A mapping Ψ with the property $\Psi_{-t,H} = [\Psi_{t,H}]^{-1}$is said to be symmetric or self-adjoint.

B.3 Hamiltonian splitting methods.

Symplectic numerical integrators are desirable for the approximation of Hamiltonian flow-maps but, for complicated systems, can lead to implicit methods which are difficult to solve. From the definition of symplecticness we see that the composition of symplectic maps is again symplectic and this leads to the idea of splitting the Hamiltonian. This can be achieved if it is possible to split the Hamiltonian H into the sum of $k \geq 2$ Hamiltonians $H_i,\ i = 1, \cdots, k$,

$$H(z) = \sum_{i=1}^{k} H_i(z), \tag{B.17}$$

where each Hamiltonian vector field,

$$\dot{z} = J\nabla_z H_i(z), \tag{B.18}$$

can be solved explicitly. From this the composition method,

$$\Phi_{\Delta t} = \phi_{\Delta t,H_1} \circ \phi_{\Delta t,H_2} \circ \cdots \circ \phi_{\Delta t,H_k}, \tag{B.19}$$

is a first order symplectic integrator.

For the simulation of systems with time-reversal symmetry, in addition to the symplectic property, a symmetric method is required but methods composed in the above manner are generally not symmetric. To achieve this the same Hamiltonian splitting can be utilized but composed in a symmetric manner as follows,

$$\hat{\Phi}_{\Delta t} = \phi_{\frac{1}{2}\Delta t,H_1} \circ \phi_{\frac{1}{2}\Delta t,H_2} \circ \cdots \circ \phi_{\Delta t,H_k} \circ \cdots \circ \phi_{\frac{1}{2}\Delta t,H_2} \phi_{\frac{1}{2}\Delta t,H_1}. \tag{B.20}$$

From this we can see that,

$$[\hat{\Phi}_{-\Delta t}]^{-1} = [\phi_{-\frac{1}{2}\Delta t,H_1}]^{-1} \circ \cdots \circ [\phi_{-\Delta t,H_k}]^{-1} \circ \cdots \circ [\phi_{-\frac{1}{2}\Delta t,H_1}]^{-1}. \tag{B.21}$$

If we arrange for each $\phi_{\Delta t,H_i}$ to be symmetric then we have,

$$[\hat{\Phi}_{-\Delta t}]^{-1} = \hat{\Phi}_{\Delta t}, \tag{B.22}$$

as required. This yields a symplectic, time-reversible mapping which is suitable for Hamiltonian systems based on Newton's equations. In addition it can be shown [42] that symmetric methods necessarily have order two.

Where the condition that each Hamiltonian vector field can be solved explicitly cannot be met, these splitting methods can still be of use. Here, if the majority of the solutions are explicit, splitting leads to a reduced number of simplified vector fields which need to be solved implicitly.

Appendix C

Backward error analysis.

Another important feature associated with symplectic integrators is the possibility of *Backward Error Analysis*. Since Hamiltonian systems have the symplectic property it has been postulated that the approximate solution provided by a symplectic integrator is the exact solution of a modified Hamiltonian. To illustrate this we use an integrable model, the harmonic oscillator with Hamiltonian $H_{ho} = p^2/2 + \omega^2 q^2/2$, to compare the exact and numerical results as shown in Figure C.1 for $\omega = \pi/10$. Since the numerical trajectory is closer to the exact result for smaller step size, h, we see that the the modified Hamiltonian, $\hat{H}$, must be dependent on h. We make the *ansatz*,

$$\hat{H} = H + h\hat{H}^{(1)} + h^2\hat{H}^{(2)} + \cdots, \tag{C.1}$$

where H is the original Hamiltonian and $\hat{H}^{(i)}$ are the additional terms of the modified Hamiltonian which are calculated by the backward error analysis.

The backward error analysis can be performed on the harmonic oscillator model, for a

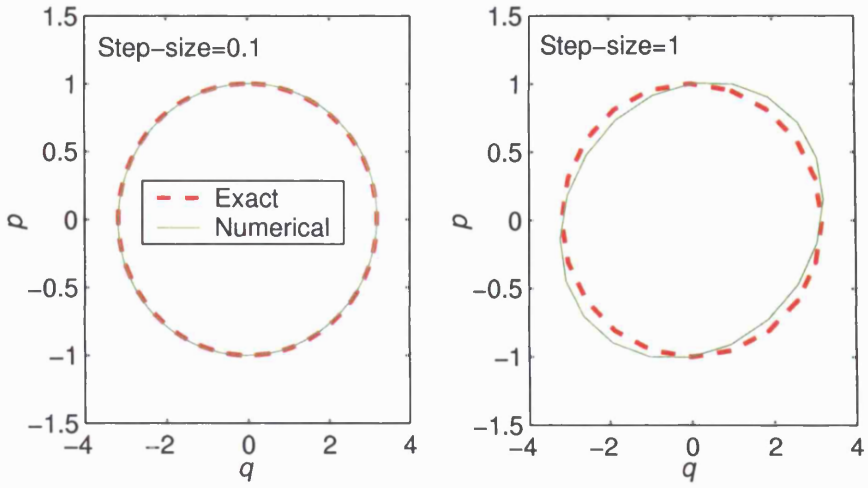

Figure C.1: Phase-space diagrams for the harmonic oscillator, with $\omega = \pi/10$, for step-sizes h=0.1 an h=1.0 compared to the exact trajectories.

given numerical method, to illustrate this technique when (C.1) is truncated after the term in h. The equations of motion for the harmonic oscillator are,

$$\dot{q} = p, \ \dot{p} = -\omega^2 q. \tag{C.2}$$

For the Euler-B numerical method, where p^n represents p at the n^{th} step, is,

$$p^{n+1} = p^n - h\omega^2 q^n, \ q^{n+1} = q^n + hp^{n+1}. \tag{C.3}$$

Then for $\hat{H}$,

$$\dot{q} = p + h\hat{H}_p^{(1)}, \ \dot{p} = -\omega^2 q - h\hat{H}_q^{(1)}, \tag{C.4}$$

where $\hat{H}_q^{(1)} = \partial\hat{H}^{(1)}/\partial q$ etc. The Taylor series for p at time t,

$$\begin{aligned} p(t) &= p(0) + tp'(0) + \frac{t^2}{2}p''(0) + \cdots \\ &= p(0) + t\left[-\omega^2 q(0) - h\hat{H}_q^{(1)}(0)\right] + \frac{t^2}{2}\left[-\omega^2\dot{q}(0) - h\left(\hat{H}_q^{(1)}(0)\right)'\right] + \cdots \\ &= p(0) + t\left[-\omega^2 q(0) - h\hat{H}_q^{(1)}(0)\right] + \end{aligned}$$

$$\frac{t^2}{2}\left[-\omega^2\left(p(0)+h\hat{H}_p^{(1)}(0)\right)-h\left(\hat{H}_q^{(1)}(0)\right)'\right]+\cdots,$$

giving,

$$p(h)=p(0)-h\omega^2q(0)-h^2\hat{H}_q^{(1)}(0)-\frac{h^2}{2}\omega^2p(0)+O(h^3). \tag{C.5}$$

Since, from the numerical solution, $p(h)=p(0)-h\omega^2q(0)$ we have solution for $\hat{H}_q^{(1)}$, for $h\neq 0$,

$$\hat{H}_q^{(1)}=-\frac{\omega^2}{2}p. \tag{C.6}$$

Similarly the Taylor series yields,

$$q(h)=q(0)+hp(0)+h^2\hat{H}_p^{(1)}(0)-\frac{h^2}{2}\omega^2q(0)+O(h^3). \tag{C.7}$$

From the numerical solution,

$$q(h)=q(0)-hp(h)=q(0)+h(p(0)-h\omega^2q(0)). \tag{C.8}$$

From (C.7) and (C.8) we have,

$$\hat{H}_p^{(1)}=-\frac{\omega^2}{2}q. \tag{C.9}$$

Equations (C.7)-(C.8) $\Rightarrow \hat{H}^{(1)}=-\frac{\omega^2}{2}qp$ yielding a modified Hamiltonian,

$$\hat{H}=\frac{p^2}{2}+\frac{\omega^2q^2}{2}-\frac{h\omega^2}{2}qp. \tag{C.10}$$

This is the equation for an ellipse and, from our knowledge of ellipses, the angle of the major axis for the modified Hamiltonian will be,

$$\tan 2\theta=\frac{-\omega^2h}{1-\omega^2}. \tag{C.11}$$

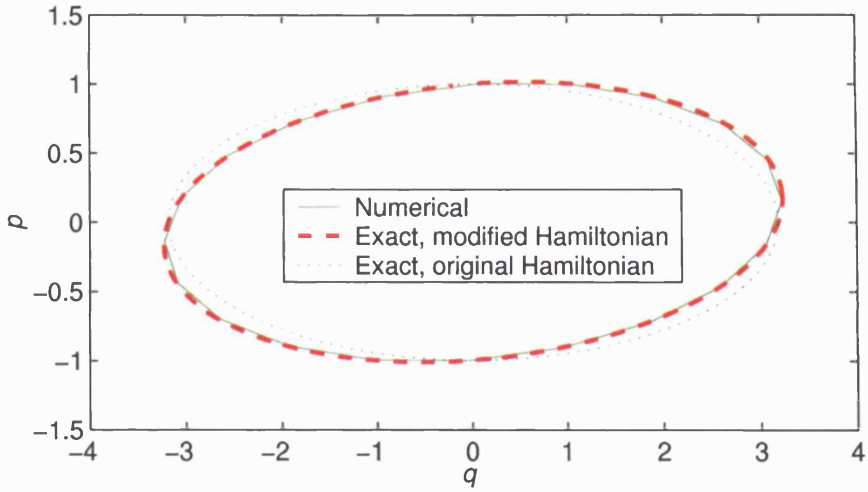

Figure C.2: Phase-space diagrams for the harmonic oscillator, with $\omega = \pi/10$, for step-size h=1.0 compared to the exact trajectories for both the modified and original Hamiltonians.

Figure C.2 shows the phase-space plot for a harmonic oscillator with $\omega = \pi/10$ and step size of 1.0 with the plot for the modified Hamiltonian, showing good correlation.

A complete treatment of the Backward Error analysis for symplectic integrators can be found in the book by Leimkuhler and Reich [42] and the paper by Hairer [22].

Appendix D

The Equipartition Theorem.

The equipartition theorem states that every degree of freedom of a body which contributes a quadratic term of a coordinate or momentum to the total energy has an average energy $kT/2$ where k is the Boltzmann constant. This can be shown as follows by examining the quantity $\langle z_k \partial H/\partial z_n \rangle$ in the canonical ensemble for Hamiltonian $H(z)$.

$$\left\langle z_k \frac{\partial H}{\partial z_n} \right\rangle = C^{-1} \int z_k \frac{\partial H}{\partial z_n} \exp\left(-\frac{H(z)}{kT}\right) dz,$$

where,

$$C = \int \exp\left(-\frac{H(z)}{kT}\right) dz.$$

Noting that,

$$\frac{\partial}{\partial z_n}\left[\exp\left(-\frac{H(z)}{kT}\right)\right] = -\frac{1}{kT}\exp\left(-\frac{H(z)}{kT}\right)\frac{\partial H}{\partial z_n},$$

then,

$$\begin{aligned}\left\langle z_k \frac{\partial H}{\partial z_n} \right\rangle &= C^{-1} \int z_k \frac{\partial}{\partial z_n}\left[-kT \exp\left(-\frac{H(z)}{kT}\right)\right] dz \\ &= C^{-1} \int \frac{\partial}{\partial z_n}\left[-kT z_k \exp\left(-\frac{H(z)}{kT}\right)\right] dz - C^{-1} \int -kT \exp\left(-\frac{H(z)}{kT}\right) \frac{\partial z_k}{\partial z_n} dz\end{aligned}$$

$$= C^{-1} \int dz' \left[-kTz_k \exp\left(-\frac{H(z)}{kT} \right) \right]_{z_n=-\infty}^{z_n=\infty} + kT\delta_{kn}.$$

For quadratic terms z_k in H,

$$\exp\left(-\frac{z_k^2}{kT} \right) \to 0, \quad z_k \to \pm\infty,$$

then,

$$\left\langle z_k \frac{\partial H}{\partial z_n} \right\rangle = kT\delta_{kn}.$$

Let $H(z) = \cdots + z_k^2/m + \cdots$ for scalar m, then,

$$\left\langle z_k \frac{\partial H}{\partial z_k} \right\rangle = \left\langle \frac{2z_k^2}{m} \right\rangle = kT,$$

giving,

$$\left\langle \frac{z_k^2}{m} \right\rangle = \frac{kT}{2},$$

as required. □

Appendix E

Higher Order Variable Step-size Methods.

This appendix provides an overview of the paper by Leimkuhler and Sweet [45], where a backward error analysis is used to develop higher order methods by the application of composition schemes to the Adaptive Verlet method.

The application of variable step-size techniques to the Verlet method generally lead to implicit schemes which can be computationally inefficient. In [32] the Adaptive Verlet method is proposed, a second order explicit integrator that is also time-reversible which, with re-parametrization function $\frac{dt}{d\tau} = G(q,p)$, is defined as,

$$p^{n+\frac{1}{2}} = p^n - \frac{\tau}{2} g^n \nabla_q V(q^n), \tag{E.1}$$

$$q^{n+\frac{1}{2}} = q^n + \frac{\tau}{2} g^n \nabla_p T(p^{n+\frac{1}{2}}), \tag{E.2}$$

$$g^{n+1} + g^n = 2G(q^{n+\frac{1}{2}}, p^{n+\frac{1}{2}}), \tag{E.3}$$

$$q^{n+1} = q^{n+\frac{1}{2}} + \frac{\tau}{2} g^{n+1} \nabla_p T(p^{n+\frac{1}{2}}), \tag{E.4}$$

$$p^{n+1} = p^{n+\frac{1}{2}} - \frac{\tau}{2} g^{n+1} \nabla_q V(q^{n+1}). \tag{E.5}$$

It has been suggested that higher order methods could be obtained by using the Adaptive Verlet method as the basic scheme in a composition framework based on the work of Yoshida [69] for separable Hamiltonian systems. Yoshida's composition scheme can be derived by expanding the method as a composition of exponentials with coefficients, we can then use the Baker-Campbell-Hausdorf (BCH) Theorem to establish constraints on the coefficients that must be satisfied to obtain a higher order method.

Given a second order symmetric method $\Psi_{\Delta t}$ with step size Δt, we can obtain a higher order method $\Psi^r_{\Delta t}$of order r and step size Δt by concatenating $\Psi_{\Delta t}$ with coefficients $w_1, w_2, \ldots, w_m$ to get:

$$\Psi^r_{\Delta t} = \Psi_{w_m \Delta t} \circ \Psi_{w_{m-1} \Delta t} \circ \cdots \circ \Psi_{w_2 \Delta t} \circ \Psi_{w_1 \Delta t}.$$

The derivation of this is based on the following assumptions: Given a system with flows $exp(tX)$, where X denotes a vector field on some space with coordinates z, time t and system initial conditions z^0 i.e

$$\dot{z} = X(z) \Rightarrow z(t) = exp(tX)z^0,$$

and, if we can write $X = A + B$, we have a map φ such that

$$\varphi : z \mapsto z' = exp(tA)exp(tB)(z) = z(t) + O(t^2),$$

then we can increase the order to r, say, by composing several stages to get

$$exp(b_m tB)exp(a_m tA) \circ \cdots \circ exp(b_1 tB)exp(a_1 tA) = z(t) + O(t^{r+1}),$$

with chosen coefficients a_i, b_i. The derivation relies heavily on the Baker-Campbell-Hausdorf (BCH) Theorem where, for two vector fields X, Y we have:

$$\begin{aligned} exp(X)exp(Y) &= exp(X+Y+\frac{1}{2}[X,Y]+\frac{1}{12}([X,X,Y]-[Y,Y,X])+ \\ &\quad \frac{1}{24}[X,Y,Y,X]+\frac{1}{720}([Y,Y,Y,Y,X]+[\cdots])+\cdots), \end{aligned}$$

where $[X,Y] = X.\nabla Y - Y.\nabla X$ is the commutator bracket of vector fields. This can be extended to a three term product and we can then define a 2^{nd} order method as:

$$\begin{aligned} S_{2^{nd}}(\tau): &= exp(\frac{\tau}{2}A)exp(\tau B)exp(\frac{\tau}{2}A) \\ &= exp(\tau\alpha_1+\tau^3\alpha_3+\tau^5\alpha_5+\tau^7\alpha_7+\cdots), \end{aligned} \tag{E.6}$$

for some A, B where $\alpha_1 := A+B, \alpha_3 := \frac{1}{12}[B,B,A]-\frac{1}{24}[A,A,B])$, etc.

The 4^{th} order method is then constructed as follows:

$$S_{4^{th}}(\tau) := S_{2^{nd}}(\tau x_1)S_{2^{nd}}(\tau x_0)S_{2^{nd}}(\tau x_1).$$

Using the BCH formula we get

$$\begin{aligned} S_{4^{th}}(\tau) &= exp(\tau(x_0+2x_1)\alpha_1+\tau^3(x_0^3+2x_1^3)\alpha_3+\tau^5(x_0^5+2x_1^5)\alpha_5+ \\ &\quad \frac{1}{6}([\tilde{B},\tilde{B},\tilde{A}]-[\tilde{A},\tilde{A},\tilde{B}])+\cdots), \end{aligned}$$

where $\tilde{A} = \tau x_1\alpha_1+\tau^3x_1^3\alpha_3+\cdots$ and $\tilde{B} = \tau x_0\alpha_1+\tau^3x_0^3\alpha_3+\cdots$. Expansion of the three term commutators in $\tilde{A}, \tilde{B}$ gives

$$[\tilde{A},\tilde{A},\tilde{B}] = O(\tau^5), [\tilde{B},\tilde{B},\tilde{A}] = O(\tau^5).$$

Hence

$$S_{4^{th}}(\tau) = exp(\tau(x_0+2x_1)\alpha_1+\tau^3(x_0^3+2x_1^3)\alpha_3+\tau^5(x_0^5+2x_1^5)\alpha_5+O(\tau^5)\cdots).$$

Coefficients	Verlet	Adaptive Verlet
Yoshida 4^{th}	4^{th}	4^{th}
Yoshida 6^{th}	6^{th}	4^{th}

Table E.1: Order of method using fixed and variable step-sizes.

To obtain the 4^{th} order method we must cancel the τ^3 term by solving $x_0 + 2x_1 = 1$, $x_0^3 + 2x_1^3 = 0$ and this yields exact values for the coefficients x_0 and x_1. Methods with orders higher than 4 can be produced by repeating the process, but using the new 4^{th} order method in place of the 2^{nd} order method. Alternatively, more economical integrators can be produced by solving a set of recursive equations numerically.

Numerical experiments to simulate both the Kepler and Arenstorf orbits, using both the Verlet and Adaptive Verlet methods composed using coefficients from [69], gave the results in Table E.1. A clue to the cause of the difficulty lies in the fact that the resolution of the time re-scaling factor g is only *second order*. By studying (E.3) we see that there is no justification to write it as $g^{n+1} = \exp(\tau\hat{X})g^n$, for some $\hat{X}$, as required by Yoshida's schemes, however examination of two time steps reveals,

$$g^n + g^{n-1} = 2G(q^{n-\frac{1}{2}}, p^{n-\frac{1}{2}}),$$

$$g^{n+1} + g^n = 2G(q^{n+\frac{1}{2}}, p^{n+\frac{1}{2}}),$$

hence,

$$g^{n+1} = g^{n-1} + 2\left(G(q^{n+\frac{1}{2}}, p^{n+\frac{1}{2}}) - G(q^{n-\frac{1}{2}}, p^{n-\frac{1}{2}})\right),$$

which is a candidate for an approximation to $g^{n+1} = \exp(2\tau\tilde{X})g^{n-1}$ for some $\tilde{X}$. Consideration of this leads to the following solutions.

E.1 Odd-even composition (OEC method)

The first solution is to compose the odd and even steps to create a new method on which to base a composition scheme i.e.

$$\Phi_\tau = \Psi_{\frac{\tau}{2},g^{n+1}} \circ \Psi_{\frac{\tau}{2},g^n}.$$

We have demonstrated this solution using the Yoshida's 6^{th} order coefficients together with 8^{th} and 10^{th} order cancellation coefficients, denoted Y8 and Y10 respectively, derived from the 6^{th} order coefficients by the 'exact' method as described in [69]. Then Y8 consist of 3 sets of the Y6 coefficients multiplied by $w_{Y8_1}, w_{Y8_0}, w_{Y8_1}$ respectively and Y10 consist of 3 sets of the Y8 coefficients multiplied by $w_{Y10_1}, w_{Y10_0}, w_{Y10_1}$. where

$$w_{Ym_0} = -\frac{2^{\frac{1}{m-1}}}{2-2^{\frac{1}{m-1}}}, \quad w_{Ym_1} = \frac{1}{2-2^{\frac{1}{m-1}}}, \quad m = 8, 10.$$

In all cases the correct order is observed for the variable step-size method.

E.2 Cancellation of even order terms (CEOT method)

For this method it is assumed that both odd and even terms in τ exist in the Adaptive Verlet method. By expanding the method using the BCH formula and solving for the cancellation of error terms using the Newton-Raphson method, the coefficients are produced for a 15 stage, 6^{th} order, method, as seen in Table E.2. The variable step-size method based on these coefficients yields 6^{th} order as expected.

order	stages	coefficients	
6	15	$w_1 = 0.17237123919774235522095$	$w_9 = w_7$
		$w_2 = 0.43916784457278231705211$	$w_{10} = w_6$
		$w_3 = 0.15751649148537327377446$	$w_{11} = w_5$
		$w_4 = 0.04987183035050663008458 4$	$w_{12} = w_4$
		$w_5 = -0.65504082716808852637175$	$w_{13} = w_3$
		$w_6 = -0.33995874304220861772593$	$w_{14} = w_2$
		$w_7 = 0.30963707464606526738266$	$w_{15} = w_1$
		$w_8 = 1 - 2\sum_{i=1}^{7} w_i$	

Table E.2: Coefficients for a 15 stage, 6^{th} order method.

E.3 Pre/post processing (MO method)

The Adaptive Verlet method is described in (E.1)-(E.5). A sequence of steps of this type can be rearranged as follows.

Pre-processing:

$$g^0 = G(q^0, p^0), \quad p^{\frac{1}{2}} = p^0 - \frac{\tau}{2} g^0 \nabla_q V(q^0), \quad q^{\frac{1}{2}} = q^0 + \frac{\tau}{2} g^0 \nabla_p T(p^{\frac{1}{2}}),$$

$$g^1 + g^0 = 2G(q^{\frac{1}{2}}, p^{\frac{1}{2}}).$$

m steps of:

$$q^{n+\frac{3}{2}} = q^{n+\frac{1}{2}} + \tau g^{n+1} \nabla_p T(p^{n+\frac{1}{2}}), \quad p^{n+\frac{3}{2}} = p^{n+\frac{1}{2}} - \tau g^{n+1} \nabla_q V(q^{n+\frac{3}{2}}), \tag{E.7}$$

$$g^{n+2} + g^{n+1} = 2G(q^{n+\frac{3}{2}}, p^{n+\frac{3}{2}}). \tag{E.8}$$

Post-processing:

$$q^{m+2} = q^{m+\frac{3}{2}} + \frac{\tau}{2} g^{m+2} \nabla_p T(p^{m+\frac{3}{2}}), \quad p^{m+2} = p^{m+\frac{3}{2}} - \frac{\tau}{2} g^{m+2} \nabla_q V(q^{m+2}).$$

In real time t we can write the evolved time t^{n+1} in terms of step-size Δt^n, where $\Delta t^n = \tau g^n$, as $t^{n+1} = t^n + \Delta t^n$. We can then re-write (E.7)-(E.8) in terms of real time as

$$\Delta t^{n+\frac{1}{2}} = \tau g^{n+1}, \tag{E.9}$$

$$q^{n+\frac{3}{2}} = q^{n+\frac{1}{2}} + \Delta t^{n+\frac{1}{2}} \nabla_p T(p^{n+\frac{1}{2}}), \tag{E.10}$$

$$p^{n+\frac{3}{2}} = p^{n+\frac{1}{2}} - \Delta t^{n+\frac{1}{2}} \nabla_q V(q^{n+\frac{3}{2}}), \tag{E.11}$$

$$t^{n+\frac{3}{2}} = t^{n+\frac{1}{2}} + \Delta t^{n+\frac{1}{2}}, \tag{E.12}$$

$$g^{n+2} + g^{n+1} = 2G(q^{n+\frac{3}{2}}, p^{n+\frac{3}{2}}). \tag{E.13}$$

If the system has a flowmap Φ, and substituting $z^n = (q^n, p^n)$, (E.10) and (E.11) can be written

$$z^{n+\frac{3}{2}} = \Phi_{\Delta t^{n+\frac{1}{2}}} z^{n+\frac{1}{2}}.$$

We can then use a composition scheme on Φ to obtain a higher order method, say r^{th} order, as follows

$$z^{n+\frac{3}{2}} = \Phi^r_{\Delta t^{n+\frac{1}{2}}} z^{n+\frac{1}{2}},$$

where

$$\Phi^r_{\Delta t} = \Phi_{w_m \Delta t} \circ \Phi_{w_{m-1} \Delta t} \circ \cdots \circ \Phi_{w_2 \Delta t} \circ \Phi_{w_1 \Delta t},$$

for some standard coefficients $w_1, \cdots w_m$.

This leads to a mixed-order method that is high order in (q,p) but second order in the re-scaling factor g. This method is fundamentally different to the OEC and CEOT methods and it's applicability is dependent on the smoothness of the re-parametrization function $G(q,p)$.

E.4 Conclusion.

Three different approaches to obtaining higher order with variable step-size have been described. It was shown that a simple application of the composition framework with the

adaptive Verlet method leads to an order reduction, but that several alternatives can be developed which provide high order.

The selection of the best approach among those presented is highly problem-specific. If the time re-scaling factor must be integrated with high accuracy, then the OEC and CEOT solutions provided in Sections E.1 and E.2 give the best results as, for a r^{th} order method, the calculation of the re-scaling factor g will also be r^{th} order. Otherwise, it may be desirable to consider MO methods, from Section E.3, which combine a low-order integration of the time re-scaling factor with a higher order method in the energy. Such schemes can be much more efficient than the full high-order alternatives as standard composition schemes may be used, leading to no increased overhead for the method.

Bibliography

[1] B.J. Alder and T.E. Wainwright. Phase transition for a hard sphere system. *J. Chem. Phys.*, 27:1208, 1957.

[2] B.J. Alder and T.E. Wainwright. Studies in molecular dynamics. i. general method. *J. Chem. Phys.*, 31:459, 1959.

[3] B.J. Alder and T.E. Wainwright. Studies in molecular dynamics. ii. behavior of a small number of elastic spheres. *J. Chem. Phys.*, 33:1439, 1960.

[4] H.C. Andersen. Molecular dynamics simulations at constant pressure and/or temperature. *J. Chem. Phys.*, 72:2384, 1980.

[5] V.I. Arnold. Mathematical methods of classical mechanics. *Springer, New York, 2nd edition*, 1988.

[6] E.J. Barth, B.B. Laird, and B.J. Leimkuhler. Generating generalized distributions from dynamical simulation. *J. Chem. Phys.*, 118:5759, 2003.

[7] S. Bond, B. Laird, and B. Leimkuhler. On the approximation of feynman-kac path integrals. *J. Comp. Phys.*, 185:473, 2003.

[8] S.D. Bond, B.B. Laird, and B.J. Leimkuhler. The nosé-poincaré method for constant temperature molecular dynamics. *J. Comp. Phys.*, 151:114, 1999.

[9] A. Bulgac and D. Kusnezov. Canonical ensemble averages from pseudomicrocanonical dynamics. *Phys. Rev. A*, 42:5045, 1990.

[10] D.M. Bylander and L. Kleinman. Energy fluctuations induced by the nosé thermostat. *Phys. Rev. B*, 46:13756, 1992.

[11] K. Cho, J.D. Joannopoulos, and L. Kleinman. Constant-temperature molecular dynamics with momentum conservation. *Phys. Rev. E*, 47:3145, 1993.

[12] K. Cho, L. Kleinman, and J.D. Joannopoulos. Ergodicity and dynamical properties of constant temperature molecular dynamics. *Phys. Rev. A*, 45:7089, 1992.

[13] G. Ciccotti and J.P. Ryckaert. Molecular dynamics simulations of rigid molecules. *Comput. Phys. Rep.*, 4:345, 1986.

[14] F.D. DiTolla and M. Ronchetti. Applicability of nosé isothermal reversible dynamics. *Phys. Rev. E*, 48:1726, 1993.

[15] L. Dupuy, R. Miller, E.B. Tadmor, and R. Phillips. Finite temperature quasicontinuum: Molecular dynamics simulations without all the atoms. *in press.*

[16] D.J. Evans. Computer experiment for nonlinear thermodynamics of couette flow. *J. Chem. Phys.*, 78:3297, 1983.

[17] D.J. Evans and B.L. Holian. Classical response theory in the heisenberg picture. *J. Chem Phys.*, 83:3560, 1985.

[18] D.J. Evans, W.G. Hoover, B.H. Failor, B. Moran, and A.J.C Ladd. Nonequilibrium molecular dynamics via gauss principle of least constraint. *Phys. Rev. A*, 28:1016, 1983.

[19] D.J. Evans and G.P. Morris. Non-newtonian molecular dynamics. *Comput. Phys. Rep.*, 1:297, 1984.

[20] D.J. Evans and G.P. Morris. Statistical mechanics of nonequilibrium liquids. *Academic Press*, 1990.

[21] G.W. Ford and M. Kac. Statistical mechanics of assemblies of coupled oscillators. *J. Math. Phys.*, 6:504, 1965.

[22] E. Hairer. Backward analysis of numerical integrators and symplectic methods. *Annals of Numerical Mathematics*, 1:107, 1994.

[23] E. Hairer, C. Lubich, and G. Wanner. Geometric numerical integration. structure-preserving algorithms for ordinary differential equations. *Springer Series in Comput. Mathematics*, 31, 2002.

[24] I. Hamilton. Nos equation for a one-dimensional oscillator: Resonance zones and the transition to large-scale irregular dynamics. *Phys. Rev. A*, 38:3120, 1988.

[25] B.L. Holian. Entropy evolution as a guide for replacing the liouville equation. *Phys. Rev. A*, 34:4238, 1986.

[26] B.L. Holian. Entropy of a nonequilibrium system. *Phys. Rev. A*, 33:1115, 1986.

[27] B.L. Holian and W.G. Hoover. Numerical test of the liouville equation. *Phys. Rev. A*, 34:4229, 1986.

[28] B.L. Holian, W.G. Hoover, and H.A. Posch. Resolution of loschmidt's paradox: The origin of irreversible behavior in reversible atomistic dynamics. *Phys. Rev. Lett.*, 59:10, 1987.

[29] B.L. Holian, H.A. Posch, and W.G. Hoover. Nonequilibrium free energy, coarse-graining, and the liouville equation. *Phys. Rev. A*, 42:3196, 1990.

[30] W.G. Hoover. Canonical dynamics: Equilibrium phase-space distributions. *Phys. Rev. A*, 31:1695, 1985.

[31] W.G. Hoover, A.J.C. Ladd, and B. Moran. High-strain-rate plastic flow via non-equilibrium molecular dynamics. *Phys. Rev. Lett.*, 48:1818, 1982.

[32] W. Huang and B.J. Leimkuhler. The adaptive verlet method. *SIAM Journal Sci. Comput.*, 18:239, 1997.

[33] S. Jang and G.A. Voth. Simple reversible molecular dynamics algorithms for nosé-hoover chain dynamics. *J. Chem. Phys.*, 107:9514, 1997.

[34] J. Jellinek and R.S. Berry. Generalisation of nosé's isothermal molecular dynamics. *Phys. Rev. A*, 38:3069, 1988.

[35] Z. Jia and B.J. Leimkuhler. Partial thermostatting molecular dynamics for slow-fast mixture problems. *in press*, 2004.

[36] N.S. Krylov. The processes of relaxation of statistical systems and the criterion of mechanical instability. *Thesis*, 1979.

[37] D. Kusnezov, A. Bulgac, and W. Bauer. Canonical ensembles from chaos. *Ann. of Phys.*, 204:155, 1990.

[38] B.B. Laird and B.J. Leimkuhler. A generalized dynamical thermostating technique. *Phys. Rev. E*, 68:16704, 2003.

[39] B.B. Laird and J.B. Sturgeon. Symplectic algorithm for constant-pressure molecular dynamics using a nosé-poincaré thermostat. *J. Chem. Phys.*, 112:3474, 2000.

[40] J.L. Lebowitz, J.K. Percus, and L. Verlet. Ensemble dependence of fluctuations with application to machine computations. *Phys. Rev.*, 153:250, 1967.

[41] B.J. Leimkuhler. A seperated form of nosé dynamics for constant temperature and pressure simulation. *Comp. Phys. Comm.*, 148:206, 2002.

[42] B.J. Leimkuhler and S. Reich. Geometric numerical methods for hamiltonian mechanics. *Cambridge University Press*, 2004.

[43] B.J. Leimkuhler and C.R. Sweet. The canonical ensemble via symplectic integrators using nosé and nosé-poincaré chains. *J. Chem. Phys.*, 121.

[44] B.J. Leimkuhler and C.R. Sweet. A hamiltonian formulation for recursive multiple thermostats in a common timescale. *in press.*

[45] B.J. Leimkuhler and C.R. Sweet. Higher order symmetric variable stepsize methods. *pre-print.*

[46] Y. Liu and M.E. Tuckerman. Generalized gaussian moment thermostatting: A new continuous dynamical approach to the canonical ensemble. *J. Chem. Phys.*, 112:1685, 2000.

[47] G.J. Martyna, M.L. Klein, and M. Tuckerman. Nosé-hoover chains: The canonical ensemble via continuous dynamics. *J. Chem. Phys.*, 97:2635, 1992.

[48] G.J. Martyna, M.E. Tuckerman, and M.L. Klein D.J. Tobias. Explicit reversible integrators for extended systems dynamics. *Mol. Phys.*, 87:1117, 1996.

[49] J.J. Morales, S. Toxvaerd, and L.F. Rull. Computer simulation of a phase transition at constant temperature and pressure. *Phys. Rev. A*, 34:1495, 1986.

[50] S. Nosé. A molecular dynamics method for simulation in the canonical ensemble. *Mol. Phys.*, 52:255, 1984.

[51] S. Nosé. A unified formulation of the constant temperature molecular dynamics methods. *J. Chem. Phys.*, 81:511, 1984.

[52] S. Nosé. Constant temperature molecular dynamics methods. *Prog. Theor. Phys. Supp.*, 103:1, 1991.

[53] S. Nosé. An improved symplectic integrator for nosé-poincaré thermostat. *J. Phys. Soc. Jpn*, 70:75, 2001.

[54] S. Nosé and F. Yonezawa. Isothermalisobaric computer simulations of melting and crystallization of a lennard-jones system. *J. Chem. Phys.*, 84:1803, 1986.

[55] E.M. Pearson, T. Halicioglu, and W.A. Tiller. Laplace-transform technique for deriving thermodynamic equations from the classical microcanonical ensemble. *Phys. Rev. A*, 32:3030, 1985.

[56] H.A. Posch, W.G. Hoover, and F.J. Vesely. Canonical dynamics of the nos oscillator: Stability, order, and chaos. *Phys. Rev. A*, 34:4253, 1986.

[57] J.R. Ray and A. Rahman. Statistical ensembles and molecular dynamics studies of anisotropic solids. ii. *J. Chem. Phys.*, 82:4243, 1985.

[58] J.M. Sanz-Serna and M.P. Calvo. Numerical hamiltonian problems. *Chapman and Hall, New York*, 1995.

[59] T. Schneider and E. Stoll. Molecular-dynamics study of a three-dimensional one-component model for distortive phase transitions. *Phys. Rev. B*, 17:1302, 1978.

[60] N. Simányi. Ergodicity of hard spheres in a box. *math.DS/9703213.*, 1, 1997.

[61] Y.G. Sinai. On the foundation of the ergodic hypothesis for a dynamical system of statistical mechanics. *Soviet Math. Dokl.*, 4:1818, 1963.

[62] Y.G. Sinai. Dynamical systems with elastic reflections. *Russian Math. Surveys.*, 25:137, 1970.

[63] A.M. Stuart and J.O. Warren. Analysis and experiments for a computational model of a heat bath. *J. Stat. Phys.*, 1999.

[64] G. Sun. Symplectic partitioned runge-kutta methods. *J. Comput. Math.*, 11:365, 1993.

[65] H. Tanaka, K. Nakanishi, and N. Watanabe. Constant temperature molecular dynamics calculation on lennard-jones fluid and its application to water. *J. Chem. Phys.*, 78:2626, 1983.

[66] M. Tuckerman and B.J. Berne. Reversible multiple time scale molecular dynamics. *J. Chem. Phys.*, 97:1990, 1992.

[67] R.G. Winkler. Extended-phase-space isothermal molecular dynamics: Canonical harmonic oscillator. *Phys. Rev. A*, 45:2250, 1992.

[68] L.V. Woodcock. Isothermal molecular dynamics calculations for liquid salts. *Chem. Phys. Lett.*, 10:257, 1971.

[69] H. Yoshida. Construction of higher order symplectic integrators. *Phys. Lett. A*, 150:262, 1990.